CRANFIELD UNIVERSITY

JASPREET KAUR MANN

ON-LINE HEALTH MONITORING OF PASSIVE ELECTRONIC COMPONENTS USING DIGITALLY CONTROLLED POWER CONVERTER

SCHOOL OF AEROSPACE, TRANSPORT AND MANUFACTURING

Doctor of Philosophy
Academic Year: 2015 - 2016

Supervisor: Dr Suresh Perinpanayagam
July 2016

CRANFIELD UNIVERSITY

SCHOOL OF AEROSPACE, TRANSPORT AND MANUFACTURING

Doctor of Philosophy

Academic Year 2015 - 2016

JASPREET KAUR MANN

ON-LINE HEALTH MONITORING OF PASSIVE ELECTRONIC COMPONENTS USING DIGITALLY CONTROLLED POWER CONVERTER

Supervisor: Dr Suresh Perinpanayagam
July 2016

This thesis is submitted in partial fulfilment of the requirements for the degree of Doctor of Philosophy

ABSTRACT

This thesis presents System Identification based On-Line Health Monitoring to analyse the dynamic behaviour of the Switch-Mode Power Converter (SMPC), detect, and diagnose anomalies in passive electronic components. The anomaly detection in this research is determined by examining the change in passive component values due to degradation. Degradation, which is a long-term process, however, is characterised by inserting different component values in the power converter. The novel health-monitoring capability enables accurate detection of passive electronic components despite component variations and uncertainties and is valid for different topologies of the switch-mode power converter.

The need for a novel on-line health-monitoring capability is driven by the need to improve unscheduled in-service, logistics, and engineering costs, including the requirement of Integrated Vehicle Health Management (IVHM) for electronic systems and components. The detection and diagnosis of degradations and failures within power converters is of great importance for aircraft electronic manufacturers, such as Thales, where component failures result in equipment downtime and large maintenance costs. The fact that existing techniques, including built-in-self test, use of dedicated sensors, physics-of-failure, and data-driven based health-monitoring, have yet to deliver extensive application in IVHM, provides the motivation for this research.

The anomaly detection in passive electronic components described in this work is performed on a digitally-controlled Buck Power Converter, with verification and validation conducted via theoretical and experimental results. The methodology develops a parametric identification of a DC-DC converter in frequency domain using a Recursive Weighted Least Square (WLS) estimator. The Recursive WLS estimator provides accurate parametric estimation with a fast convergence rate and a small prediction error. In addition, the research develops a non-parametric identification of the power converter by perturbing a user-defined multi-tone

sinusoidal excitation and performing IQ (in-phase and quadrature) demodulation to extract a system model. The use of multi-tone perturbation with an optimised amplitude spectrum and user-defined frequency resolution enables addressing the characteristics of the power converter at desired frequencies of interest. The synchronous/coherent demodulation of characteristic system parameters provides accurate non-parametric Frequency Response Function (FRF) measurements using only ten perturbation frequencies, saving a lot of computational time and involving reduced complexity. The effectiveness of the capability for anomaly detection is validated theoretically and experimentally by inserting different component values in the system. Moreover, the methodology has been substantiated by analysing uncertainty on the measured system response and the extracted component values. The simulation and experimental results reveal that the proposed health-monitoring capability can be used to detect anomalies in the passive electronic components of the SMPC.

Keywords:

IVHM, System Identification, Switch-Mode Power Converter, Digital Control, Multi-tone Excitation, IQ Demodulation, Uncertainty Management.

ACKNOWLEDGEMENTS

“Engineering is an ocean of treasure and an engineer drives in the ocean in search of that treasure.”

I pay my profound gratitude to the Almighty with whose grace I have been able to add a new dimension to my life by achieving my chosen ambition.

Diction is not enough to express my deep sense of gratitude and wish to place on record my sincere and heartfelt regards to Dr Suresh Perinpanayagam and Professor Ian Jennions for their sagacious, ceaseless encouragement, constant moral support, and whole-hearted, untiring help and sense of forgiveness throughout my association with them.

I express my sincere gratitude to Stephanie Peyrat and Christophe Taurand for their valuable suggestions, guidance, and encouragement. It was a great learning experience and my profound privilege to be guided by a genius of the calibre, whose blessings bring my best in every one of the endeavours. Without their invaluable guidance, it was not possible to complete the present work.

I am indeed grateful to staff members of IVHM Centre and Industrial partners for their invaluable feedback during Quarterly Review Meetings. I am thankful to my fellow researchers Piotr Sydor, Daniel Gagar, Ryan Walker, Manuel Esperon, and Octavian Niculita for their cooperation and valuable observations during the course of my research.

I am grateful to the IVHM Centre, Cranfield University for granting me a Research Studentship and financial support to pursue this research and attend conferences across the globe.

Finally, I express my deepest gratitude, sincerest reverence, and profound respect for my loving husband, parents, and family whose perseverance provided me the strength and inspiration to complete this project in the present form.

PUBLICATIONS

Bhambra, J.K, Perinpanayagam, S., Taurand, C., and Peyrat, S. (2011) “Health Monitoring of POL Converters using Digital PWM Controller”, *Proc. IEEE International Symp. Diagnostics for Electric Machines, Power Electronics & Drives (SDEMPED)*, 5-8 Sept., Bologna, Itlay, pp. 133-138.

Mann, J.K, Perinpanayagam, S., and Jennions, I. (2016), “Aging Detection Capability for Switch-Mode Power Converters”, *IEEE Trans. Industrial Electron.*, vol. 63, no. 5, pp. 3216-3227.

TABLE OF CONTENTS

LIST OF FIGURES

LIST OF TABLES

LIST OF EQUATIONS

ABBREVATIONS

ADC	Analog-to-Digital Converter
ARX	Auto Regressive with External Input
ATE	Automatic Test Equipment
ATC	Accelerated Temperature Cycling
ASIC	Application Specific Integrated Circuit
AWGN	Additive White Gaussian Noise
BGA	Ball Grid Arrays
BIT	Built-in Test
BL	Band-Limited
CALCE	Center for Advanced Life Cycle Engineering
CCM	Continuous Conduction Mode
CCS	Code Composer Studio
CDF	Cumulative Distribution Function
CMOS	Complementary MOSFET
CND	Cannot Duplicate
COTS	Commercial-off-the-Shelf
DCM	Discontinuous Conduction Mode
DFT	Discrete Fourier Transform
DIBS	Discrete Interval Binary Signal
DPA	Distributed Power Architecture
DPWM	Digital Pulse-Width Modulator
DSP	Digital Signal Processing
ECDF	Empirical Cumulative Distribution Function
EEPROM	Electrically Erasable Programmable Read-Only Memory
ESR	Equivalent Series Resistance
ETTF	Estimated Time to Failure
FFT	Fast Fourier Transform
FMMEA	Failure Mode, Mechanism and Effect Analysis
FPGA	Field Programmable Gate Array
FRA	Frequency Response Analyser
FRF	Frequency Response Function

GUI	Graphical User Interface
HALT	Highly Accelerated Life Test
HAST	Highly Accelerated Stress Testing
HCI	Hot Channel Injection
HDB	Hard Breakdown
IBA	Intermediate Bus Architecture
IDE	Integrated Development Environment
IEA	Integrated Electronic Assemblies
IEC	International Electrotechnical Commission
IEEE	Institute of Electrical and Electronics Engineers
IGBT	Insulated-Gate Bipolar Transistor
IIR	Infinite Impulse Response
IRS	Inverse-Repeat Binary Sequence
IVHM	Integrated Vehicle Health Management
IQ	In-phase and Quadrature
LCM	Life Consumption Monitoring
LRU	Line Replaceable Unit
LSB	Least Significant Bit
Mathcad	Engineering Math Software
MEP	Micro Edge Positioning
MCUs	Microcontrollers
ML	Machine Learning
MLS	Multi Length Sequence
MOSFET	Metal–Oxide–Semiconductor Field-Effect Transistor
MSET	Multivariate State Estimation Techniques
NBTI	Negative Bias Temperature Instability
NFF	No Fault Found
NMOS	N-channel MOSFET
NVRAM	Non-volatile Random Access Memory
OEM	Original Equipment Manufacturer
OOR	Ordered Overall Range
PCA	Principal Component Analysis
PDF	Probability Density function

PF	Particle Filter
PHM	Prognostic and Health Management
PID	Proportional-Integral-Derivative
PLD	Programmable Logic Device
PMOS	P-channel MOSFET
Pof	Physics-of-Failure
POL	Point-of-Load
POP	Periodic Operating Point
p-p	Probability-Probability
PRBS	Pseudo Random Binary Sequence
PSU	Power Supply Unit
PWM	Pulse-Width Modulator
Q-Q	Quantile-Quantile
RAM	Random Access Memory
RMS	Root Mean Square
ROI	Return on Investment
RPN	Risk Priority Number
RTOK	Retest OK
RTL	Register-Transfer-Level
RUL	Remaining Useful Life
SAR	Successive Approximation Register
SEPIC	Single-Ended Primary-Inductor Converter
SI	System Identification
SIMetrix/SIMPLIS	Mixed-mode circuit simulation package
SMPC	Switch-Mode Power Converter
SMPS	Switch-Mode Power Supply
SNR	Signal-to-Noise Ratio
SPM	Seat-back processor module
SRB	Solid Rocket Booster
SVM	Support Vector Machine
TDDB	Time-Dependent Dielectric Breakdown
VPWL	Piecewise Linear Voltage Source
WLS	Weighted Least Square

ZOH	Zero-Order-Hold

NOMENCLATURE

s	Laplace transform variable
s_k	Laplace transform variable evaluated along the imaginary axis at DFT frequency k: $s_k = j\,\omega_k$
$\omega = 2\pi f$	Angular frequency
f	Frequency
$H(s)$	Transfer function
$x(t), y(t)$	Input and output time signals
$X(k), Y(k)$	Discrete Fourier transform of the samples $x(tT_S), y(tT_S)$, t = 0, 1, 2, N-1
$X(s), Y(s)$	One-sided Laplace transform of $x(t), y(t)$
F	Number of frequency domain data samples
$\lvert x\rvert = \sqrt{(Re(x))^2 + (Im(x))^2}$	Magnitude of complex number x
$\varphi(x)$	Phase (argument) of complex number x
F_{SP}	Sampling frequency
T_S	Sampling period
F	Switching frequency
F_{OF}	Cut-off frequency of the Output filter
F_{ESR}	ESR frequency of the output filter capacitor
F_X	Crossover frequency of the power converter
F_P	Frequency of the multi-tone sinusoid signal
A_p	Amplitude of the multi-tone sinusoid signal
θ_p	Phases of the multi-tone sinusoid signal
M	Number of repeated experiments
N	Number of time domain data samples
L	Inductor in the output filter
C	Capacitor in the output filter

C_{EXT}	External Capacitor added in the output filter
rC_{EXT}	ESR of the capacitor C_{EXT}
r_C	ESR of the capacitor C
r_{L+S}	Series resistance of the inductor L and the Switch S_1 and S_2
R_{Load}	Load Resistance
Δ	Quantisation Step
μ_x	Mean value of x
σ_x	Standard Deviation of x
Subscript T	Matrix transpose

1 Introduction

1.1 Research Background

Integrated Vehicle Health Management (IVHM) is emerging as an indispensable technology for the transportation industry. It addresses the development of integrated systems to monitor all aspects of the vehicle, including structural, propulsion, and electronics [1].

It involves the implementation of Prognostic and Health Management (PHM) strategy to monitor the health of the entire vehicle by detecting, diagnosing, and predicting the extent of deviation or degradation from its normal operational conditions. The extent of deviation refers to Remaining Useful Life (RUL) [2], Estimated Time to Failure (ETTF) or probability that the system continues to operate properly up to a certain future time. The RUL is the useful/functional life of the vehicle before its actual field failure.

The importance of PHM has grown steadily for over two decades. The concept of prognostics, widely known in the field of medicine, involves diagnostic indicators to foretell the likely outcome of a patient's illness that aid in decision-making, such as blood pressure and cholesterol levels. PHM gained momentum in engineering disciplines such as aerospace, defense, nuclear, and automotive when increased vulnerability of engineering systems to failure was anticipated with ageing and adverse environmental conditions.

PHM has been studied and successfully implemented for various safety-critical mechanical structures and systems, such as roads, pressure vessels, propulsion engines, aircraft structures, gears, bridges, buildings and, rotary equipment [3-6].

However, the evolution and execution of PHM for electronic systems has been challenging due to continuous miniaturisation of electronic components and circuits. The imperceptible multitude of degradations and failures in these electronic circuits and components further obscures the quantification of estimating the RUL [7].

Since modern engineering transport systems are completely dependent on electronic systems for functions such as communication, navigation, engine control and fuel management, environmental control and collision avoidance, there is a strict need for developing PHM for electronics.

1.1.1 Benefits of PHM

The benefits that PHM can bring to customers and manufacturers alike are well-known and stakeholders are now focussing on integrating PHM systems into their systems and maintenance operations. Benefits of implementing such systems are enormous and valuable. Availability can be achieved to a higher extent, ultimately providing manufacturers the capability to deliver high-value products to their customers. The benefits of PHM include:

End-of-Life Prediction: By monitoring and diagnosing the current health of the system, deviations in original component values can be evaluated for RUL predictions [8].

Increased Airworthiness: If prognostic information is used appropriately in maintenance operations such as predictive maintenance, the probability of unscheduled maintenance operations will fall. PHM will consecutively establish safety measures for any future impending failures.

Improved Knowledge for Original Equipment Manufacturer (OEM): Systems equipped with PHM provide real-time health information including failure/degradation history for future design and root cause analysis. This allows the manufacturers to recognise any design flaws and areas of improvement.

Reduced Life-cycle Costs: Reduction in logistics footprint including inspection costs, downtime, and inventory of spares can significantly reduce operational life cycle costs [9].

1.1.2 Requirements for Health Monitoring

The implementation of PHM technology facilitates several requirements at different levels of the system. Saxena et al. [10] (as shown in

Figure 1-1)

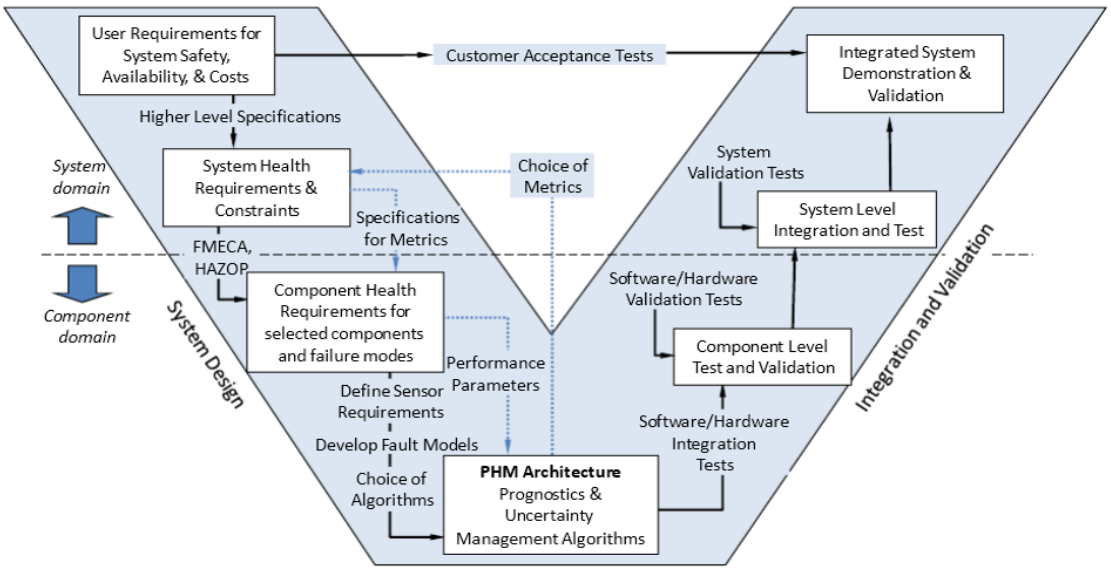

Figure 1-1 V Model for PHM system development- Choice of metrics and requirements specification is an iterative process [10]

articulate a standard V-Model approach from a systems engineering perspective wherein the customer requirements, including safety, availability, and cost, are transformed into system-level requirements. The system performance parameters, such as voltage and current thresholds, and faults, then govern the choice of components, which includes knowledge of failures, failure modes and mechanisms, and their degradation with respect of adverse environmental conditions. The above information also incorporates study of component failure and stress analysis and their implications for the system.

Taking into consideration the above requirements and their constraints, the PHM requirements model outlines the selection of sensors, performance metrics, diagnostic and prognostic tools that are robust and rugged to system stimulus and provide minimum uncertainty to diagnostic and prediction analysis.

Lastly, the verification and the validation, including component and system-level hardware/software integration tests against a healthy baseline, provide confidence in the PHM implementation.

The selection of key system metrics and prognostic tools is an iterative process as the overall requirements change and evolve during the life cycle of the system.

For instance, during the initial years of the system, in-service statistical and historical knowledge of the components govern the system and component-level requirements. However, the customer and system requirements modify as the components evolve from the preliminary burn-in period to ageing dominated life. Consequently, the obligation to use different sensors and prognostic tools necessitates adjustments and alterations in the verification and validation procedures, in addition to performance metrics and the monitoring tools.

1.2 Research Focus

The research herein focuses on exploring the performance of system-level metrics to acknowledge the failures and degradations of electronic systems and electronic components. The electronic system taken into consideration is the DC-DC power converters found in power supply boards.

Before recognising the importance of system-level health monitoring, in particular, for DC-DC converters, it is necessary to comprehend the definition of such terms as failure, failure mechanism, and degradation developed by the various standardisation bodies. In addition, it is important to understand how electronic systems and/or components fail or degrade during their operating life cycles as this information helps in selecting the best diagnostic and prognostic tools for PHM.

1.2.1 Definition of Failure and Degradation

Different organisations and authors express a variety of meanings to define the terms degradation, failure, and failure mechanism. The interpretation of the definitions is different for various fields of study based on the use and application.

Nevertheless, engineering standardising bodies define the terms focussed on product/component/system. The US Military Standard [11] descriptions are as follows:

> *Failure: The event, or inoperable state, in which any item or part of an item does not, or would not, perform as previously specified.*

Degradation: A gradual impairment in ability to perform.

Failure Mechanism: The physical, chemical, electrical, thermal or other process which results in failure.

The International Electrotechnical Commission (IEC) [12] definitions are as follows:

Failure: Termination of the ability of an item to perform a required function.

Degradation Failure: A failure which is both a gradual failure and a partial failure.

Failure Mechanism: The physical, chemical or other process which has led to a failure.

Ageing Failure/Wear-out Failure: A failure whose probability of occurrence increases with the passage of time, as a result of processes inherent in the item.

The Institute of Electrical and Electronics Engineers (IEEE) [13] describe a failure as

> "the inability of a system or component to perform its required functions within specified performance requirements".

In addition, Pecht [2] defines failure mechanisms as the physical, chemical, thermodynamic, or other processes that result in the failure.

Degradation refers to deviation in some of the characteristic properties of a component/system that affects its performance in the near future. Correspondingly, a failure mechanism is the underlying cause and effect of a failure rather than the behaviour of the overall performance of the component/system. A failure mechanism initiates by the application of a single load condition causing overstress failures or from a combination of loading conditions over an extended period resulting in wear-out failures.

1.2.2 Failure Progression in Electronics

The degradation or ageing in every electronic component is a long-term progression typically explained by a distinctive Bathtub curve. The Bathtub curve in Figure 1-2 explains the characteristic statistical component failure rate in three stages of its life period: burn in, useful life, and ageing dominated region.

The failure progression of a component starts emerging as burn in failures mainly due to defects during the manufacturing processes, damage during testing, and assembly. This also includes testing under accelerated temperature, vibration, and humidity environments which baseline the initial limits of the failure condition.

The useful life region is a constant failure rate progression where the component operates for the majority of its lifetime. The constant failure rate remains significantly low for a number of years for a component, and is generally expected to be 10 years.

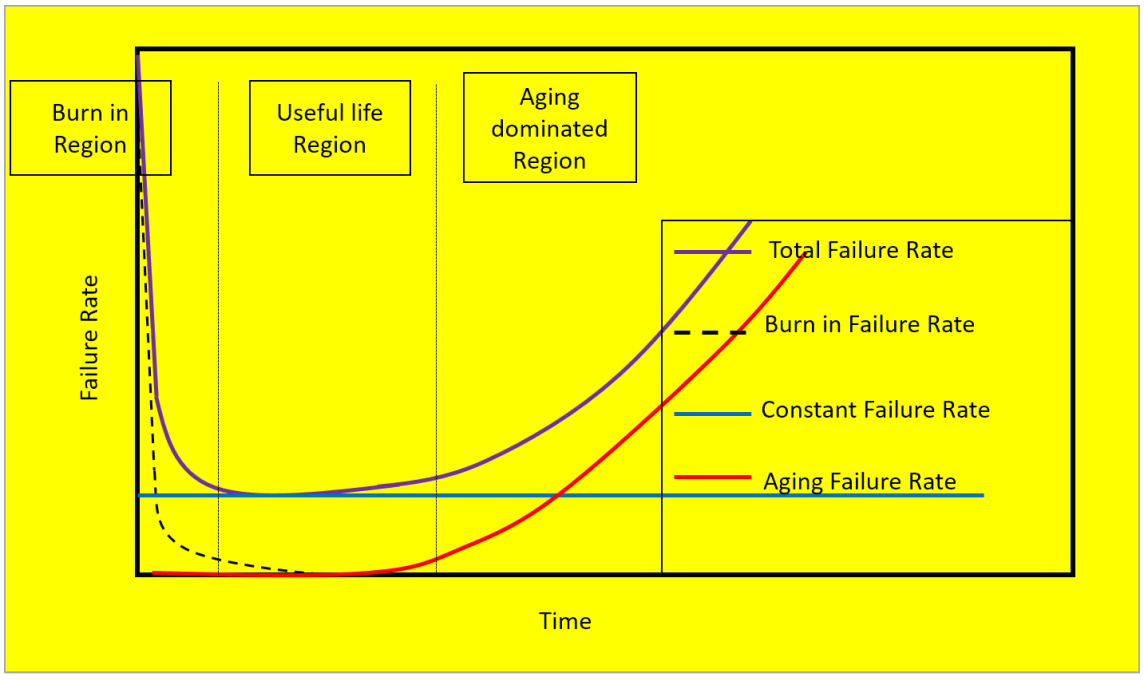

Figure 1-2 Failure Bathtub Curve [2]

Once the useful life period of a component progresses into the ageing dominated region, the constant failure rate escalates into the ageing failure rate that lasts for

a small duration of the component lifetime. The majority of the ageing-related failures occur due to long-term environmental stress, such as high temperature, operational stress and voltage stress on a particular component. Some of the ageing failures include increase in Equivalent Series Resistance (ESR) of an electrolytic capacitor, dielectric breakdown in Metal-Oxide Field Effect Transistor (MOSFET), amongst others.

1.2.3 Importance of Health Monitoring in Power Converters

The electronic systems on-board an aircraft provides communication, navigation, control (including stability augmentation), engine control and fuel management, environmental control, and collision avoidance. Each of these electronic systems, commonly known as Line Replaceable Unit (LRU), consists of a Power Supply Unit (PSU) and User Electronics, as depicted in Figure 1-3. The PSU includes circuitry for power conversion, control, and conditioning. The User Electronics, also known as Complex Electronic Hardware, includes highly-integrated digital circuits, such as Programmable Logic Devices (PLD), memory, input/output units, and CPU for controlling the vehicle operations.

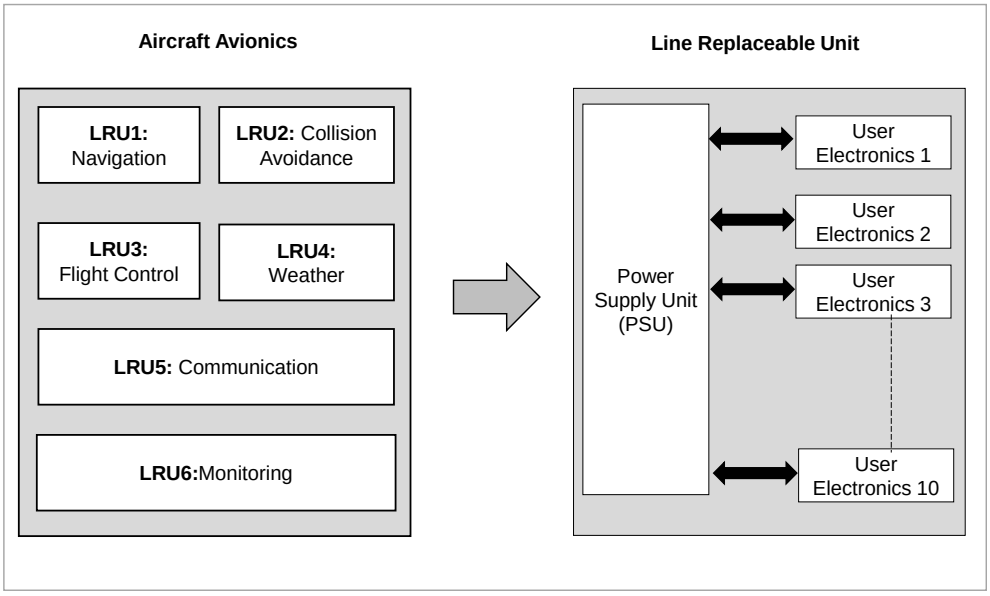

Figure 1-3 Concept of LRU in an Aircraft Avionics

The Switch-Mode Power Supplies (SMPS) form an integral part of the PSU. The high efficiency, low power consumption, and rapid response to line and load

variations has made SMPS as the ideal choice for voltage regulation across the majority of electronic products. The DC-DC power converter is one of the SMPS topologies that convert unregulated DC input voltage to regulated DC output voltage besides DC-AC, AC-AC, and AC-DC conversion [14]. The DC-DC voltage conversion could be step-up, step-down or inverted depending on the load requirements of the system. The DC-DC converters are categorised into isolated and non-isolated converters, as shown in Figure 1-4.

The isolated DC-DC converters segregate the input and output using switching transformers, whereas non-isolated converters do not incorporate any isolation between input and output ports. Furthermore, the non-isolated DC-DC converters classify in two different configurations, based on the number of energy-storing devices, typically the inductor: single inductor or dual inductor. Step-up, step-down, and step-up/step-down are single inductor topologies, while Cuk, Single-Ended Primary-Inductor Converter (SEPIC) and, ZETA are dual inductor topologies.

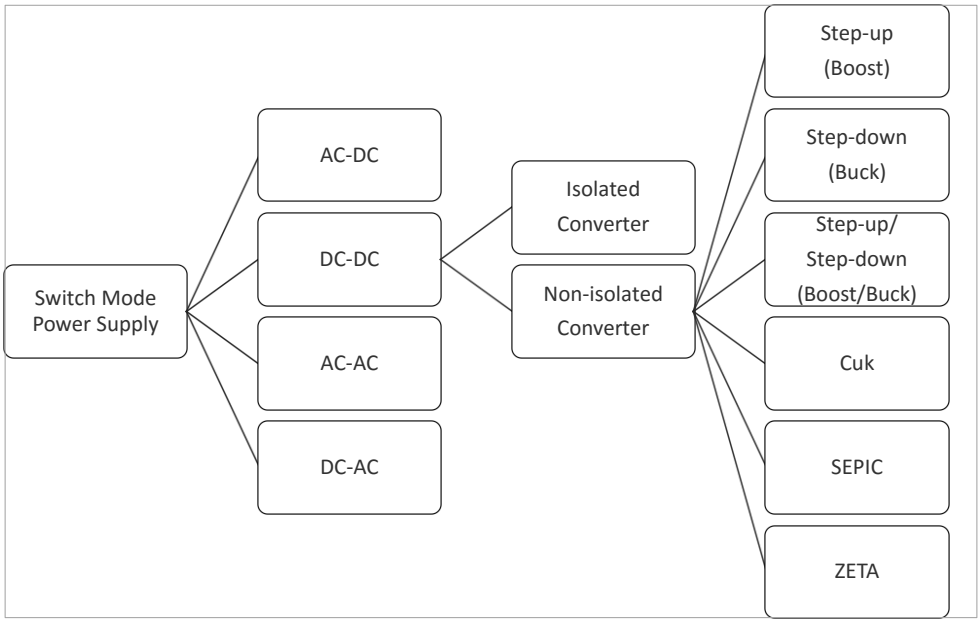

Figure 1-4: Switch-Mode Power Supply Topologies [17]

The power distribution architecture for electronic systems has evolved dramatically over two decades with advancements in user electronics or the

highly-integrated digital circuits. The architecture has emerged from the centralised power distribution to Distributed Power Architecture (DPA) and Intermediate Bus Architecture (IBA) in recent years [15; 16].

The SMPS topologies integrate into a Distributed Power Architecture (DPA) incorporating an Intermediate Bus Architecture (IBA) on an aircraft electronic system, as illustrated in Figure 1-5. Particularly, the front-end isolated power converter steps down 115 V AC or 28 V DC to medium supply rail, typically 28 V. An isolated flyback DC-DC power, buck-boost converter, reduces the medium voltage supply rail further to 12 V, while a non-isolated buck converter bucks the 12 V supply to low-voltage supply rails, such as 3.3 V, to power highly-integrated user electronics [18].

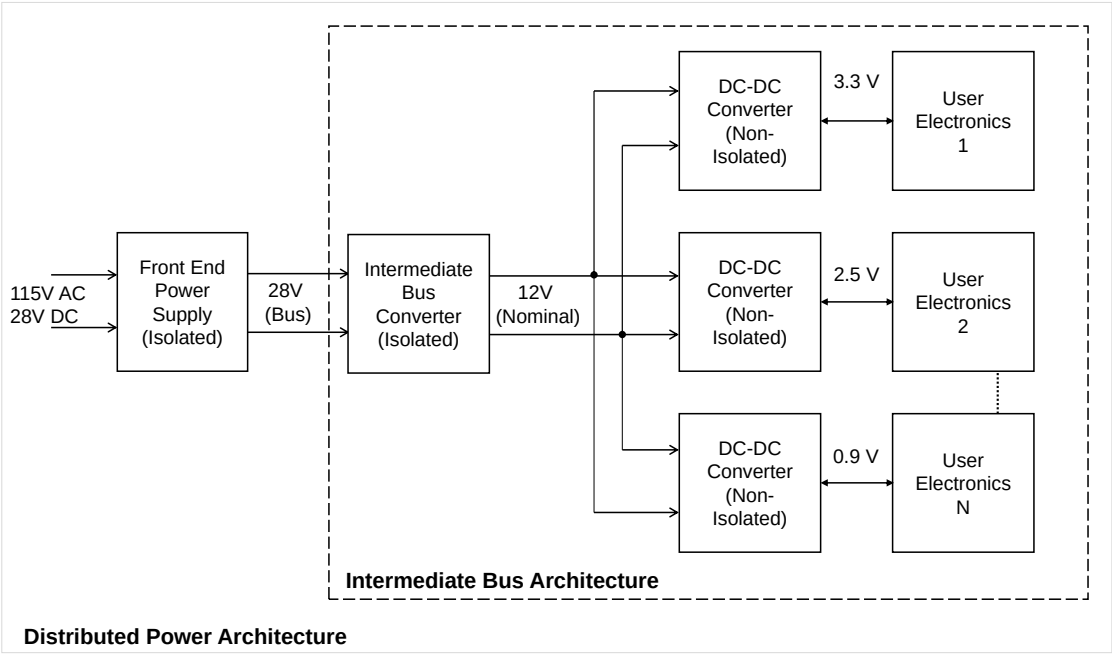

Figure 1-5 Distributed Power Architecture Integrating Intermediate Bus Architecture on Aircraft Avionics

In recent years, the high current and increased performance demands of user electronics have led to miniaturisation of these PLDs down to nanometer and sub-micron scale [19]. Consequently, these advancements in the semiconductor

industry have commanded the input voltage of these devices to reduce from 5 V and 3.3 V to below 3.3 V. These technological advances in PLD and networking microprocessors empowered the power supply industry to advance from a basic four output voltage (12.0 V, 9.0 V, 5.0 V, 3.3 V) DC-DC power converter to more than twenty output voltage (3.3 V, 2.5 V, 1.8 V,1.5 V, 1.2 V, 1.0 V, 0.9 V, 0.8 V etc.) converters [20]. This led to the use of Point-of-Load (POL) converters in distributed power architecture to minimise power losses and increase efficiency.

The POL converter is a non-isolated buck converter that provides low-voltage DC power to the proximity loads [16]. The typical output voltage of the POL converter is 3.3 V and below. The location of POL converters in propinquity to the concerned load provides efficient voltage regulation and resolves the challenge of high-peak current demands and low noise margins required by high-performance semiconductors, such as Field Programmable Gate Array (FPGA) and Application Specific Integrated Circuit (ASIC).

The tolerance on the low-voltage user electronic power supplies is dependent on the load or the user electronics. In traditional power supplies, the tolerance requirement on a typical low-voltage power converter is ±5%. However, with the advent of sub-micron technology as mentioned, the tight tolerance requirement on POL converters has become even tighter to ±3% [21]. This prerequisite inadvertently results in increased stress on the power converter and contributes towards degradation of the components and failure of the system. Moreover, the output voltage deviation outside the defined tolerance also initiates wear-out degradations in the user electronics [22; 23]. Some of the wear-out failure mechanisms include Time Dependent Dielectric Breakdown (TDDB) and Hot Channel Injection (HCI), to name a few.

Essentially, it is important to understand key factors that cause the supply rail to deviate outside the defined tolerance band. The voltage tolerance on the power rail largely diverge due to output voltage ripple, static deviations, such as component drift and temperature, and dynamic deviations, such as transient load condition besides a line transient, amongst others. The de-rating analysis of all the components during the design phase over a wide temperature range -55°C

to 125°C – assure that the power supply rail is within voltage tolerance under several degrees of temperature. Secondly, a load transient is only present for a short time period and can be minimised by adding external capacitance. However, the supply rail deviation due to component drifts is unknown until a failure has occurred.

From a system-level failure perspective, degradation in any of the power supply components due to uncertainties in the component tolerances or ageing of components with time will affect the performance of the entire electronic system. For instance, change in electrical characteristics of Commercial-off-the-Shelf (COTS) discrete components, such as capacitors, diodes, or MOSFETs, will modify the transient response and can change the voltage regulation of the converter.

Therefore, this research aims to acknowledge system-level health monitoring of DC-DC power converters to detect these anomalies and mitigate long-term failures in the operation of aircraft avionics.

From the above discussion, the health monitoring of the entire avionics system can be hypothesised as a three-stage process illustrated in Figure 1-6. The concept monitors, detects, diagnoses, and predicts the health of both the user electronics and the power supply unit itself.

The first stage incorporates continuous health monitoring of the entire avionics, entailing N user electronic blocks powered by N DC-DC power converters centrally controlled via a digital power controller. This involves continuous monitoring/measurement of failure precursors or system parameters, typically the current consumption of the user electronics with respect to different

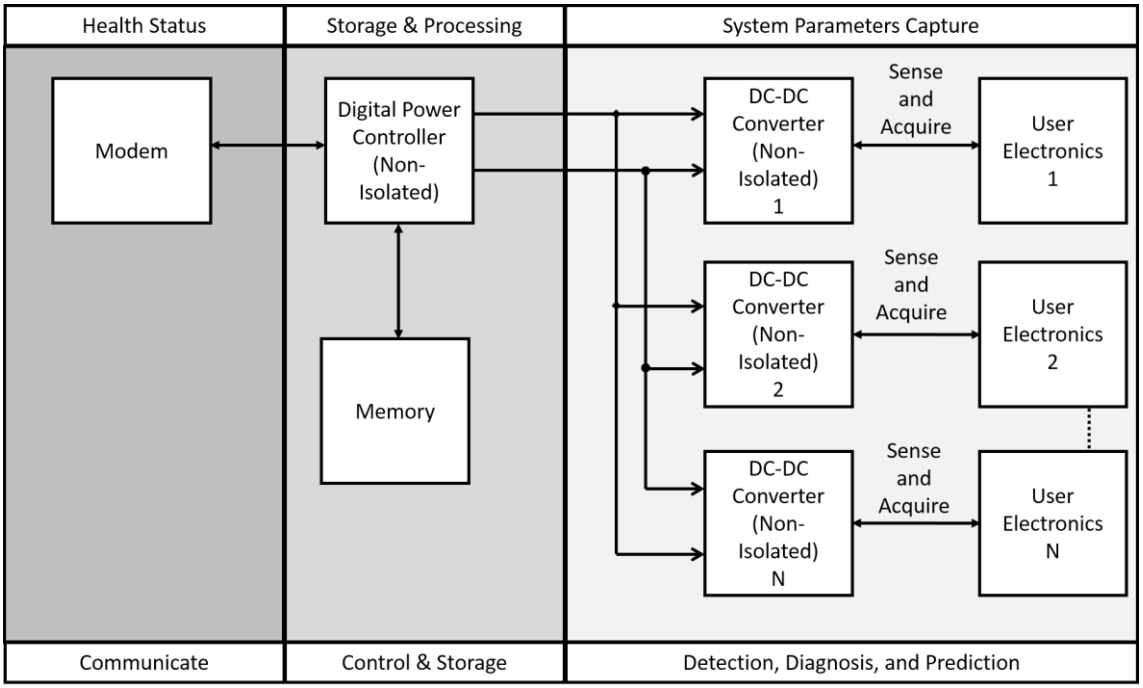

Figure 1-6 Health Management Concept

environmental and operational conditions. Typically, temperature is a significant contributor towards degradation and failure in electronic devices. For user electronics particularly, the knowledge of power consumption variability with temperature and the input supply, which is the output voltage of the power converter, provides significant knowledge of the impending failure mechanisms within the user electronics.

The second stage involves a software-configurable digital controller that not only controls the N DC-DC power converters but also provides additional capabilities, such as sequencing, soft-start, margining, and dynamic adjustment of the output voltage. Herein, the measured data set is stored in a memory device for further signal processing and analysis. This processed data representative of anomalies in either the power supply unit or the user electronics is analysed for trends or outliers against the healthy status of the circuits.

The third and final stage of the concept interfaces equipment health statistics to the OEM or the product manufacturer. Herein, the analytical information from the second stage, compared against the historical healthy baseline or a simulated

model, prognosticates the health of the equipment in terms of any requirement for proactive steps, such as preventive maintenance.

1.2.4 Need for PHM in Electronics

The detection of degradations and resulting failures in electronic components/systems is of paramount importance for mission-critical applications, including nuclear power reactors, aerospace, automotive, and space. From an economic perspective, it is recognised that with the advent of sophisticated and advanced electronic systems, every product manufacturer wants to increase the lifetime of the product with an objective to reduce unscheduled maintenance, in-service costs and improve the availability of the product [1]. More importantly, addressing the issues of how to detect, diagnose, and predict degradation and failures has been identified as a potential requirement by many industrial organisations [24; 25].

It has been elucidated by various researchers, including Saha et al. [26], Kulkarni et al. [27], and Yang et al. [28], that there is an increasing acceptance of the importance of detection of failures and degradations in electronic components and that health monitoring has the prospect of making a key contribution to detecting and predicting any impending failures. Goodman et al. [29] and Bagul et al. [30] further emphasise that health monitoring is essential to track degradations at an early stage as it prevents unscheduled maintenance and further reduces life-cycle costs.

Huang et al. [31] recognise that there is a need for system-level health monitoring in the present complex and dynamic automotive electrical and electronic control systems. Additionally, experts from the nuclear industry have experienced an iterative need to implement health-monitoring capabilities to capture ageing degradations in nuclear power plant electronic components [32].

1.3 State-of-the-Art Health-Monitoring Frameworks

A health-monitoring framework describes various tools and techniques for monitoring the overall performance of a system including detection, diagnosis,

and prognosis. The framework also includes sensor selection, historical knowledge of the system, if available, and data acquisition and synchronisation procedures.

In early avionics systems, Automatic Test Equipment (ATE) developed basic diagnostic capability to verify the reliability of a system, as even the smallest snag can lead to a disaster. ATE is an automated test procedure for evaluating the operational functionality of the system using test instruments, such as analysers, oscilloscopes, amongst others. However, the use of accurate and high-resolution test hardware made ATE an expensive solution. In addition, space and weight constraints due to increased test equipment and pitfalls in the design of Graphical User Interface (GUI) [33] significantly affected system efficiency and the highlighted the need for new health-monitoring techniques for avionic systems.

1.3.1 BIST

The earliest health-monitoring technique, which is still in use, is the Built-in Self-Test (BIST). Also known as the Built-in Test (BIT), it is an effective diagnostic technique to verify the functionality of electronic circuits. A built-in test is defined as an on-board hardware-software diagnostic means to identify and locate faults and includes error detection and correction circuits, totally self-checking circuits, and self-verification circuits [34].

The implementation of a BIT framework depends on the nature of the equipment used for monitoring, and the overall size of the system. These procedures incorporate the following:

- **Functional-level testing**: This testing may be of individual components, integrated circuits, board assemblies and complete systems, etc.
- **Purpose:** This can include fault detection, localisation, correction or prediction.
- **Active against passive:** In active BIT, separate input signals (not required for normal operation) are generated for testing the system whereas in passive BIT, the use of normal system inputs significantly affects the system’s functionality.

- **Online against offline:** Online BIT is characterised by continuous operation, whereas the test has to be initiated for the offline mode.
- **Centralised and decentralised:** BIT can be designed as a centralised approach controlling all the modules from a central processing unit or a decentralised approach where different BIT centres communicating with one another report to a master processing unit [35].

Similarly, the architecture plan for performing built-in tests depends upon the application (avionic, automotive, semiconductor, etc.) and the scale of the system (small, large). Stroud [36] introduces a simple representative of BIST architecture that facilitates self-testing and reporting to the system controller.

The architecture (as shown in Figure 1-7) consists of two significant blocks: a test pattern generator feeds different test patterns into the circuit under test and an output response analyser indicates the pass/fail condition. The architecture also involves features for controlling the test procedure from start to end (test/BIT controller) and for preventing coupling between the circuit and the pattern generator (Input Isolation Circuitry). Apart from normal I/O pins of the BIT

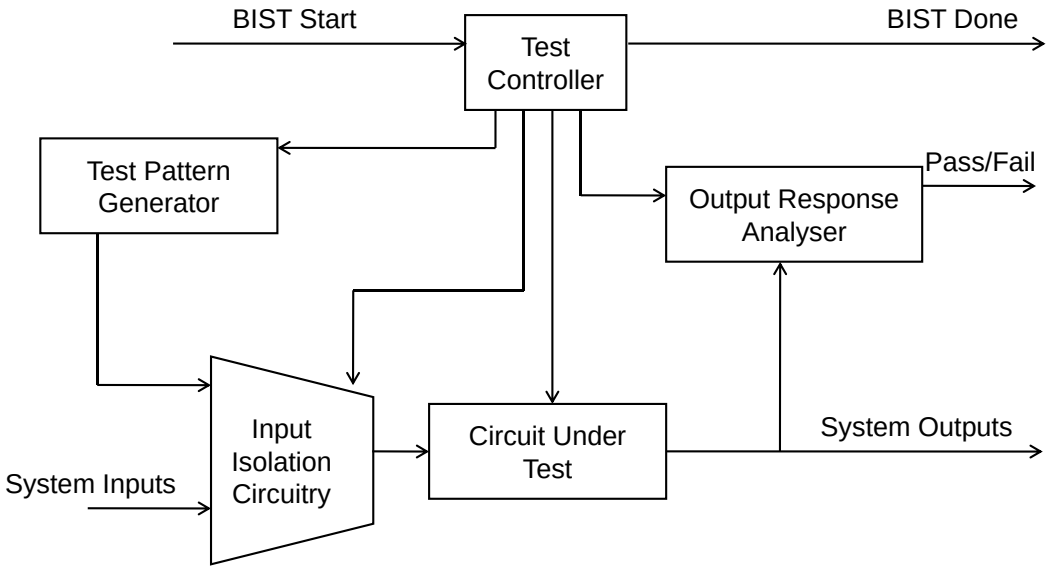

Figure 1-7 BIST Architecture

controller, additional pins may be required for initiating the BIT sequence, reporting the results to the response analyser and an optional indication that the BIT is complete and that the results are valid and no fault is found in the circuit.

BIT has been developed and demonstrated in diverse industries, including semiconductor chip testing, avionic and automotive system reliability, manufacturing for system monitoring, self-diagnosis, and process optimisation [37].

In electronic systems, two methods have been developed for monitoring the health of the system: Continuous BIT (C-BIT) and Interruptive BIT (I-BIT) [38]. The rationale behind C-BIT includes continuous and automatic monitoring of the test equipment without interruption of its normal operational conditions, whereas the concept of I-BIT involves interruption/suspension of the test equipment during the normal BIT operation. In addition to I-BIT, there is another built-in test technique, Power-on BIT (P-BIT), where the test equipment is interrupted periodically for carrying out a pseudo-continuous monitoring function [39].

The semiconductor industry describes the use of BIT for detecting faults in digital integrated circuits [40], memories [41], and Analog-to-Digital Converters (ADC) [42]. For instance, Rosenthal and Wadell [43] investigate the performance of AVLSI (Analog Very Large Scale Integration) using the C-BIT technique. Their results reveal that 2.7% of the built-in tests account for a potential source of false alarms in Digital-to-Analog converters (DAC), input resistance tests, and frequency response analysis. The researchers understood the potential sources of error through statistical inference. However, the study concludes that besides appropriate written test procedures and taking into consideration the variations in the measurement, BIT is an effective method for initial system performance evaluation.

A false alarm describes the condition when the built-in test process indicates a failure although no failure occurred in the actual system. This is similar to Cannot Duplicate (CND)/No Fault Found (NFF) and Retest OK (RTOK) behaviour.

Furthermore, researchers report that the inclusion of BIT has a detrimental effect on overall reliability and maintainability by providing misleading information. Pecht et al. [44] detail that while fault warning is detectable using BIT, the origin of actual failure mechanisms might not be accurately identified. The verification of the statement was supported by conducting built-in test strategies for seat-back processor modules (SPM), which comprise the in-flight entertainment system for Boeing 777. The SPM boards were subjected to accelerated stress by Highly Accelerated Life Test (HALT) to determine operational and destruction limits of the test modules. Soft-failure was observed on all the EEPROMs around 100°C degrees, which disappeared subsequently by lowering the temperature to a few degrees. Similarly, the programmable interrupt controller began to fail around 130°C indicating a cannot-not-duplicate (CND) failure.

Finding 1

The Built-in test PHM technique is a diagnostic capability with particular focus on fault detection and isolation rather than on prediction of continuous degradation.

1.3.2 Dedicated Sensors

Dedicated in-built sensors, also known as canaries or prognostic cells, are widely used to capture degradation information. The PHM industry borrows the word ‘canary’ from the mining industry where the canary bird provides warning for any leakage of hazardous gas in the mines. Researchers implement the same methodology, representing early indication of failure across the electronic industry.

The canary approach or in-situ sensors are pre-calibrated cells mounted on the actual device, wherein the exact manufacturing process fabricates the actual device and the sensors. The prognostic cells or canaries are co-located with the actual circuit on an IC, to act as an early-warning for upcoming device failures. The researchers predict degradation signatures by applying identical environmental stress to both the device and the prognostic cell while increasing the current density or the applied voltage only to the cell. This deliberately

degrades the performance of the cell and led to early time to failure of the actual device.

As an illustration, Goodman et al. [45] develop an in-built sensor to monitor TDDB ageing in MOSFET. Under accelerated stress established by applying higher voltage than the supply voltage, the prognostic canary experiences a high electric field across the oxide layer of the MOSFET. The canary cell fails before the actual lifetime of the circuit due to over voltage and statistical observation of failure distribution provide a predictive estimate of TDDB ageing. Kim et al. [46] propose an on-chip ageing sensor to monitor performance degradation of nanometer digital integrated circuits. They developed a sensor circuit to detect degradation of threshold voltage during a long-term NBTI and HCI stress. In a similar context, Nan and Choi [47] suggest integrated monitoring circuits for TDDB using 32-nm CMOS technology.

However, the implementation of prognostic cells in the system-level environment offers an expensive solution. Furthermore, the prognostic cells possess limitations in their implementation in legacy systems. For instance, the original canary cells may not predict degradation in the system for newer versions of the device. Thus, the health monitoring of the system using canaries presents a reliability issue for the manufacturer. Moreover, the prognostic cell designed for a particular failure mechanism may not be able to predict a combination of failure mechanisms instigating inside the cell. This interaction of failure mechanisms may cause the cell to fail earlier in its lifetime and give false indications of failure.

Finding 2

Dedicated in-built sensors or canaries enable diagnosing degradation of wear-out failure mechanisms, such as TDDB, NBTI, HCI, etc. The canary approach is not suitable for system-level health monitoring and anomaly detection for COTS electronic components.

1.3.3 Physics-of-Failure (Pof) Based Health Monitoring

Physics-of-failure based health monitoring existed before the advent of in-built sensor frameworks. Health monitoring based on physical models evaluate system health by identifying potential defects and failure mechanisms, performing life-cycle loading and stress analysis through robust design and manufacturing procedures [2].

The physics-of-failure based model involves i) identifying potential imperfections in the chemical, electrical, physical, mechanical, structural, and thermal processes leading to failures and, ii) identifying appropriate failure sites, failure modes and mechanisms related to material characteristics, damage properties, relevant geometries at failure sites, manufacturing flaws and defects, and environmental and operational loading conditions.

The physics-of-failure based reliability approach initiates by defining the system requirements, including specifications in terms of functional architecture, mechanical and material properties, testability and maintainability characteristics, application environmental (automotive, aerospace, telecommunication, etc.) and operational parameters (temperature, vibration, humidity, current, voltage, power, etc.). Depending on the life-cycle loading conditions, a database for failure site and failure mode/mechanisms prior to actual field failure is constructed. This knowledge helps to identify definite physics-based failure/damage models corresponding to each failure. The damage accumulation and stress analysis investigates the reliability of the system and its components [48]. The validation of these damage models is carried out through accelerated ageing tests like Highly Accelerated Stress Testing (HAST) and HALT.

The above-mentioned physics-of-failure based reliability approach has been comprehensively extended in determining the remaining useful life of the product towards prognostics. Using the concept of physics-of-failure, the Center for Advanced Life Cycle Engineering (CALCE) has developed the methodology of Life Consumption Monitoring (LCM) for estimating the RUL of electronic products.

Life consumption monitoring is a prognostic method for evaluating the RUL of a product in its actual life-cycle environment by continuously monitoring the product's performance parameters and environmental conditions. The life-cycle environment represents the manufacturing, storage, handling, operating and non-operating conditions of a product. The application of a life-cycle load or a combination of loads degrades the performance of the product, thereby reducing its in-service lifetime [49].

Mishra et al. [50] define the LCM concept in 6 steps (Figure 1-8) involving i) the analysis of Failure Mode, Mechanism and Effect Analysis (FMMEA), ii) virtual reliability assessment, iii) critical parameter monitoring, iv) data simplification, v) stress and damage accumulation analysis, and vi) remaining life estimation.

Step 1: Failure Mode, Mechanism and Effect Analysis (FMMEA)

A failure mode defines how a component, subsystem, or system fails to deliver its intended function. In other words, a failure mode is the effect by which failure is observed to occur [51]. Gu et al. [52] outline that a failure mode must be observable through visual inspection, electrical or thermal measurement tests or other tests. If this is not the case, potential failure modes must be identified by performing numerical stress analysis, accelerated tests to failure (e.g. HALT) or from past experience.

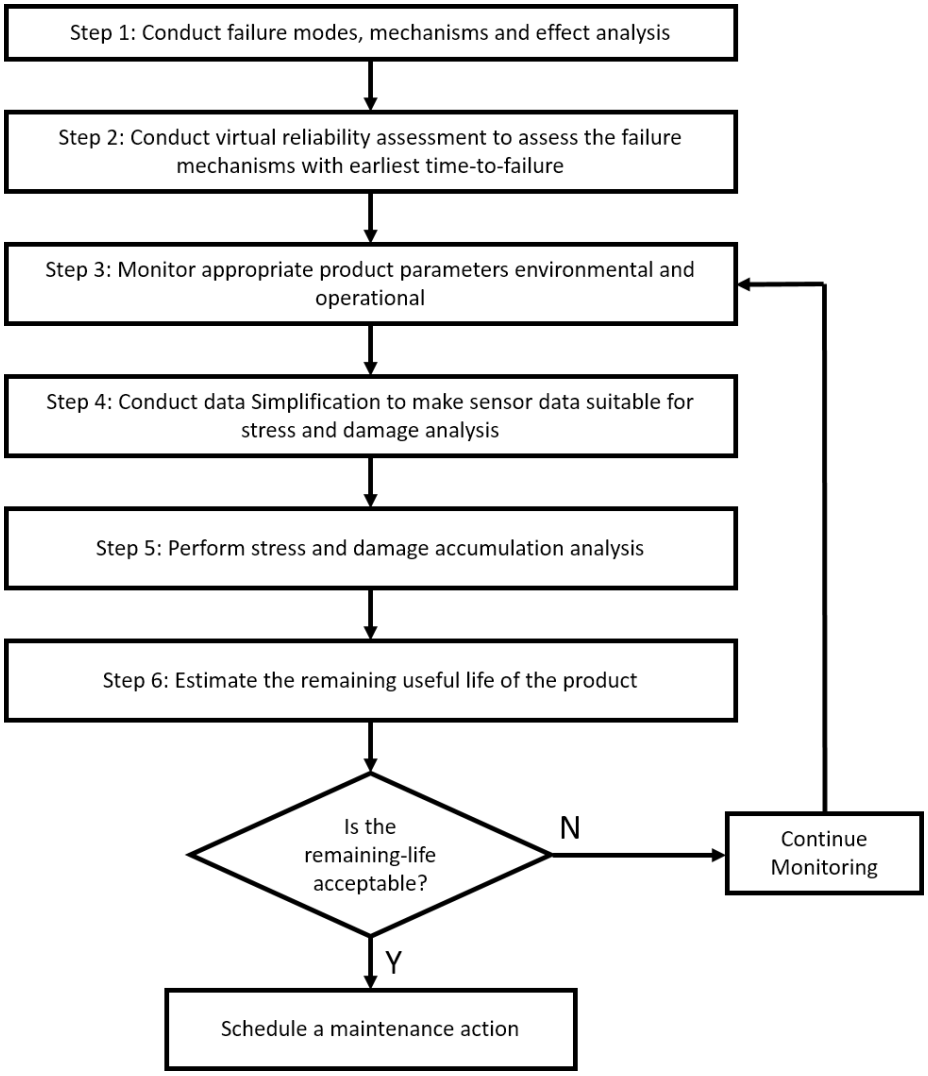

Figure 1-8 CALCE Methodology for Life Consumption Monitoring

A failure cause describes a specific process, design and/or environmental conditions that initiated the failure. Understanding the potential causes of failure further facilitates the identification of failure mechanisms driving the failure modes for a given element. Failure mechanisms are the physical, chemical, thermal, electrical or other processes that lead to the failure of a component, subsystem or a system. A failure mechanism initiates either by the application of a single

Load	Load Conditions
Electrical	Current, Voltage, Power, Frequency
Physical	Radiation, Electromagnetic Interference, Altitude
Chemical	Humidity, Pollution, Contamination, Fuel Spills
Mechanical	Pressure, Vibration, Shock, Strain, Stress
Thermal	Temperature, Heat Dissipation

Table 1-1 Examples of Load and Load Condition

load condition causing overstress failures or from a combination of loading conditions over an extended period of time (described in Table 1-1) resulting in wear-out failures.

Step 2: Virtual Reliability Assessment

Virtual reliability assessment is performed to assess the potential failure mechanisms derived from the failure analysis. The objective of virtual reliability assessment is to identify the critical failure mechanisms and the corresponding environmental and operational conditions causing the failure.

The process involves ranking of potential failure mechanisms based on Risk Priority Number (RPN). The risk priority number is defined as the product of occurrence and the severity of each failure mechanism [53]. The critical failure mechanisms are identified by ranking potential failure mechanisms; with the highest RPN being the critical failure mechanisms experienced by the product. However, when the time-to-failure due to the occurrence of a combination of failures is less than the time-to-failure due to the occurrence of a single failure, only the failure mechanisms with time-to-failure less than actual product failure time are considered as the critical failure mechanisms.

Step 3: Monitoring of Appropriate Parameters

Following the identification of critical failure mechanisms, including environmental and operational loading parameters, monitoring of these parameters is carried out using appropriate sensors. Li et al. [54] propose that the selection procedure

for appropriate sensors in terms of their size, location and sensor technology for monitoring and recording accurate information must be decided to avoid any false results. For example, the sensor should have small response time and self-correction capabilities; it should be small, easy to install with low power consumption.

Step 4: Data Reduction/Simplification for Stress and Damage Models

The objective of data reduction and simplification techniques is to extract useful features out of a large set of monitored data. The principle of data reduction techniques is to:

- condense the load histories without sacrificing important damage characteristics,
- preserve the sequence of the most damaging reversals (i.e. peaks and valleys) in the original data,
- to keep down the test precision, reducing the sampling speed.

Generally, two types of methods are used for data reduction: Haye's method and Ordered Overall Range (OOR). Fast Fourier Transform (FFT), Principal Component Analysis (PCA), Hotelling T-squared and, Student T-squared can also be used for data reduction purposes.

Step 5: Damage and Stress Accumulation Analysis

Damage is defined as the amount of deviation or degradation of the product parameters from a defect-free state. Damage and stress accumulation analysis calculates the cumulative damage due to a particular failure or combination of failures under specific loading conditions. The theory behind stress estimation is that operation of the product at a given cyclic stress amplitude will produce damage, the severity of which will be related to the number of cycles of operation at that stress amplitude and the total number of cycles that would be required to create a failure of undamaged sample at that stress amplitude. Damage, once incurred, is permanent. The operation of the product at different stress amplitudes

in sequence results in accumulated damage that is the sum of damage due to all the different stress amplitudes [54].

Step 6: Estimation of Remaining Useful Life

Estimation of remaining useful life is calculated from the accumulated damage incurred by the product over time. If the evaluated damage is within the acceptable window, the product is monitored for further damage analysis. However, if the damage is within unacceptable levels, maintenance is scheduled to repair or replace the product.

Numerous researchers implement physics-based monitoring to identify failures and failure mechanisms in electronic power supply system [25; 55-57]. For instance, Kulkarni et al. [56] develop a predictive technique to estimate failures in electrolytic capacitors. They model thermal characteristics of ripple current using bond graph techniques and physics-of-failure based thermal models. The researchers then evaluate the effect of capacitor ESR degradation for a given ripple current under ambient temperature and as a function of time. The simulated results forecast capacitor performance degradation with time, i.e. decrease in the output voltage with corresponding increase in ESR over a period of operating time.

Nasser and Curtin [57] prognosticate the reliability of power supply by focussing on specific aspects of fracture and fatigue growth on interconnects. The authors prototype the real behaviour of the interconnect material from a series of computational fatigue models. The prognosis approach involves the development of a prognosis software framework for prediction of power supply system failure based on material fatigue accounting for individual interconnect and overall product reliability. The prognosis software (VPS-MICRO) was based on a series of computational fatigue models, which allowed the simulation of real material behaviour. The simulation of the model on two separate aircrafts, Aircraft 1 that flew a less aggressive mission profile (i.e. bomber) and Aircraft 2 that flew a more aggressive mission profile (i.e. fighter), predicts the probability of component failure for each mission up to the 9,000th flight. The forecast for future mission

success by predicting expectations for missions 9,000th to 10,000th exhibits probability of mission success for Aircraft 1 and Aircraft 2 is 93.3% and 88%, respectively at the 10,000th flight.

Finding 3

PoF-based health monitoring provides confidence in the detection of an individual failure mechanism. However, the detection of different failure mechanisms developing concurrently is a challenge for the physical methods. Therefore, the detection of combination of failure mechanisms becomes more complicated than an individual failure mechanism.

1.3.4 Data-Driven Prognostics

The data-driven prognostic models follow a statistical approach to estimate and predict signatures of degradation and failure in the system. The research community considers this method as a black box operation with no need for understanding the system in terms of its material properties and structural geometries. Rather, data from continuous monitoring of the operational parameters (e.g. calibration calorimetric data, spectrometric data, power vibration, temperature, pressure, current, voltage) or assembled from the failure history during its field operation decides the state of the system. The numerical patterns or relationships, such as correlation, covariance, residuals, and inference patterns that exist in this data then approximate the dependencies between the system/component variables and operating/environmental loads. Data-driven prognostics are studied using known concepts of machine learning and statistical models.

Machine learning is a subfield of artificial intelligence concerned with the design and development of algorithms and techniques that allow a machine to “learn”. In recent years, machine learning has gained extensive applications in various fields of science, such as speech recognition, computer vision and, bio-surveillance, amongst others. The concept of Machine Leaning (ML) based on categorising meaningful information by reasoning, classification, and clustering has become major field of empirical studies. ML focuses on extracting information from data

through computational and statistical methods and then applying supervised and unsupervised learning algorithms to estimate the degradations, etc. Bayesian Techniques [2], Support Vector Machine (SVM) [58], Particle Filter (PF) [26], Monte Carlo simulations and, Hidden Markov Models (HMM) are some of the learning methodologies that assist in predicting the state of the system.

The second class of empirical algorithms effectively used by researchers across the scientific community include the application of statistical methods for estimating degradation. Statistical algorithms focus on understanding the data in terms of models, parameter selection, fitting curves and, density estimation. Two types of statistical techniques, parametric and non-parametric, exist to differentiate the behaviour/trend of the unhealthy system from the healthy system.

The parametric methods assume the input data is deterministic and fits a certain distribution profile, for example Gaussian distribution, Weibull distribution, etc. The performance parameters of the distribution, typically mean, standard deviation, and variance, govern the classification of the data based on these parameters. The non-parametric method assumes no distribution profile of the input data and classifies the unhealthy system using techniques, such as Multivariate State Estimation Techniques (MSET) and kernel regression.

For instance, Cheng and Pecht [59] estimate the remaining useful life of six electronic components using the MSET technique. The authors collect failure data by subjecting accelerated stress on the components where the mean and standard deviation of failed components govern the failure criteria for prediction of the actual component failure. The researchers acknowledge that the improper selection of training data by exclusion of some of the operational states of the product or by inclusion of abnormal states of the product could lead to false or missed alarms. Secondly, they propose that unacceptable selection of memory matrix could influence the performance of the model. Moreover, less data in the memory matrix, i.e. less information for the model itself, can lead to poor performance of the estimation. Similarly, too many vectors in the memory matrix can result in slow and reduced predictive performance.

Similarly, Pecht and Chen [60] emphasise that conventional data-driven methods, such as machine learning algorithms, cannot be used to detect degradation in natural ageing systems due to unavailability of sufficient training data. They conceive that even though the training data is available at an early stage of the healthy system, it is fixed and never updated. Moreover, the training data does not contain the entire health information of the system and can lead to false alarms for a new event. Therefore, they suggest another prognostic and health-monitoring method for naturally ageing systems, wherein both a conventional data-driven method and a moving window technique estimate the anomalies due to natural ageing or other ageing processes. The single-sided and a double-sided moving window, which can be fixed or flexible, based on the specific application update the training matrix. If both the conventional and moving-window methods indicate anomalies in the system, then the system has incurred ageing due to other failure mechanisms in the system rather than natural ageing.

Finding 4

The data-driven based health-monitoring approach requires pre-processing training data. It is an essential step in the data-driven method as errors, scaling, redundancy, masking, and other data-specific problems influence the predictions. Pre-processing of data is also specific to the type and size of the data, which limits the applicability of pre-processing techniques to certain systems.

1.3.5 Accelerated Testing

The acceleration life tests, typically Highly Accelerated Stress Test (HAST) and Highly Accelerated Life Test (HALT), stress the system environmentally (including increased temperature profile and vibration) to monitor and analyse the reliability of the system and/or its components.

In industry, each electronic system under product development is tested under HALT and HAST to identify the initial manufacturing defects and reliability of the components to operate within the defined operating parameters. For instance, if the results of the HAST reveal component failure under a certain temperature

profile, the reliability of the component is under question and reported to the component engineers for further qualification.

The research community, in contrast, use accelerating testing techniques to predict and validate the ageing progression of the electronic components and systems by observing their failure progression for initial defects and failures. Jaai et al. [61] employ Accelerated Temperature Cycling (ATC) to detect the onset of failures in Ball Grid Arrays (BGA). Mathew et al. [62] apply a vibration and shock load profile to analyse damage accumulated of an aluminium bracket of one of the Printed Circuit Boards contained in the Integrated Electronic Assemblies (IEA) of a Solid Rocket Booster (SRB).

Likewise, some researchers predict failure signatures under operational stress environments where the system parameters, such as input voltage and load current, are increased outside the minimum and maximum limits. Kulkarni et al. [27] study the effect of high voltage on the degradation of capacitors. A batch of six capacitors of 2200µF capacitance with a rated voltage of 10V, current rating of 1A, and maximum operating temperature of 105°C were subjected to high-voltage stress through an external supply source. Similarly, Orsagh et al. [63] in their research project validate the models for fault detection and failure progression by observing the results of accelerated electrical and thermal stress in SMPS.

Finding 5

Importantly, all the predictions based on accelerated stress tests are defined while the system is functioning outside its normal operating conditions. Knowledge of degradation of a system and its components when the system is functioning within its operating conditions is not available.

1.3.6 System Identification Based Health Monitoring

System identification is an interdisciplinary practice used to characterise the behaviour of a dynamic system in the form of a mathematical model. The user excites/perturbs the system with a deterministic or random excitation signal to

measure the transient or frequency response of the system. Subsequently, the application of different model estimators, such as least squares, Kalman filters, etc., to the measured data set is then used to estimate a model of the system.

Due to the complexity and multitude of electronic components on an electronic system, it is difficult to capture the characteristic parameters of a component that signify degradation. For instance, the ESR and output voltage ripple of a capacitor provide extensive information about the degradation properties of the capacitor. However, it is a challenge to measure these parameters in a complex system. Morroni et al. [64] advocate the concept of SI to monitor the performance of SMPS and propose that the method can be used to detect failures in the PSU. The online monitoring of the system parameters for instance, stability margin is used to validate the said assumption. The method is implemented on a 90W, 50V – 15V forward converter, wherein the output filter capacitance is modified to study the change in the stability margin.

Correspondingly, various researchers employ SI techniques to simulate a digital control system or control the analog system using digital control techniques. They include Miao et al. [65], Roinila et al. [66] and Shirazi et al. [67].

Finding 6

The use of system identification techniques to characterise anomalous behaviour of the system and its components enables the detection and diagnosis of degradation in electronic systems. Nevertheless, system diagnosis based on monitoring characteristic parameters is at the infant stage of its development. Though some research work has initiated system identification based monitoring in power supplies, more work is required to explore and understand the full potential of these methods.

1.3.7 Summary

Acknowledging the issues concerning degradations or failures in electronic systems, the literature review has identified several health-monitoring frameworks suitable for electronic systems as shown in Table 1-2.

Method	Applicability	Rationale for applying a method			Limitation
		Anomaly detection	Diagnostic	Prognostic	
BIST	These methods involve on-board hardware-software diagnostic tools to identify and locate faults	x			Diagnostic capability with particular focus on fault detection and isolation instead of continuous degradation
Dedicated Sensors	These methods enable diagnose of wear-out failure mechanisms such as TDDB, NBTI, HCI, etc. in digital circuits			x	Not suitable for system-level health monitoring and anomaly detection for COTS electronic components
Physics of failure	These methods evaluate system health by identifying potential defects and failure mechanisms by performing life-cycle loading and stress analysis		x	x	Require expert knowledge of physical, material and thermal properties of the components. Difficult to diagnose multiple failures.
Data-driven	These methods follow machine learning and statistical approaches to estimate and predict signatures of degradation and failure in the system			x	Pre-processing of data is specific to the type and size of the data, which limits the applicability of pre-processing techniques to certain systems
Accelerated testing	These method stress the system environmentally (including increased temperature profile and vibration) to monitor and analyse the reliability of the system and/or its components.			x	All the predictions based on accelerated stress tests are defined while the system is functioning outside its normal operating conditions. Knowledge of degradation of a system and its components when the system is functioning within its operating conditions is not available.
System Identification	Interdisciplinary practice used to characterise the behaviour of a dynamic system in the form of a mathematical model.	x	x	x	Selection of appropriate methods

Table 1-2 Summary of Health monitoring frameworks

Besides, numerous health monitoring techniques employed by the research, community highlights the challenges that confront further research in this field. Moreover, despite the availability of various methods and tools, there is lack of uniformity, and inconsistency in the demonstration of results. The findings of the review have been tabulated in

The concept of and the business case for system-level health monitoring acknowledge OEM needs. However, considering the above challenges, the researcher has to formulate diagnostic and prognostic tools and techniques that

can provide knowledge of degradation and failure from global online performance health monitoring.

1.4 Challenges in Health Monitoring

The growing complexity of systems due, to some extent, to their size, and to the integration of new technologies, combined with the economic requisite of improved operational availability and safety, drive practitioners and researchers to look for innovative prognostic tools and methods. However, health monitoring of electronic systems is challenging as it is difficult to identify the suitable tools for global health monitoring of key system metrics to recognise hidden degradation and failure patterns. Vichare and Pecht [8] emphasise that decisions specific to the system in question, such as which system parameters to monitor, the appropriate selection of sensors, suitable measurement and data-acquisition equipment/instruments, and on-board memory for data storage hinder the implementation of health monitoring.

Uncertainty

The process of detecting ageing characteristics in systems is perplexing because uncertainty in component tolerances and change in ambient conditions propagate uncertainty on the system parameters. These uncertainties influence the interpretation of degradation occurring in the components. Therefore, there will always be a percentage of uncertainty associated with the estimation of degradation. Moreover, the sources of uncertainty in system-level health monitoring, including noise from the sensors, measurements, and the system model, augment the overall quantification of uncertainty [68].

Assumptions

The development of every model or technique is based on certain assumptions. The assumptions are made to understand the dynamics of the system or the component. However, these assumptions introduce uncertainties in the model that supplement inherent system probabilities. This leads to difficulty in evaluating

the effects of these assumptions on the robustness and ruggedness of the monitoring technique.

Data Acquisition

The use of BIT, dedicated sensors, and PoF-based condition monitoring frameworks rely on data acquisition via automated methods and without any human interference. Herein, the characteristic behaviour of an impending failure input in the model is based on the performance of the system parameters rather than the actual series of events that cause the failure. For instance, the monitoring of TDDB failure mechanism using the canary approach requires the performance data to be input in the monitoring tool rather than the actual degradation events. Therefore, the tools might not capture and reveal the nature and the source of degradation or the failure.

Data-driven based monitoring relies significantly on historical data to interpret the RUL of the system. In the aerospace industry, the availability of this maintenance data is restricted due to certain organisational reasons. Now, the RUL predictions are formulated based on the available sparse data. Therefore, in most instances, the Line Replaceable Units tends to be replaced when the first indications of fault or a failure are known even though they are not faulty. Importantly, the monitoring tool based on the above data set provides no knowledge of degradation of either the system or the components.

Performance Metrics

An important factor in health monitoring for electronic systems is the selection of key performance metrics that can describe the degradation in the system itself and the components within.

Although the Remaining Useful Life and estimated time-to-failure describes the lifetime of a system or a component, these parameters are not sufficient to comprehend the degradations in the system. Zhang et al. [69] propose identifying precursors in SMPS from historical database and failure analysis. In contrast,

Vichare and Pecht [70] advise a prognostic solution to extract precursors to failure from in-situ monitoring of system parameters.

Saxena et al. [10] describe a comprehensive list of performance metrics for monitoring techniques based on both customer requirements and at the algorithm level. However, they emphasise that the metrics are the result of an initial feasibility study and need to be accepted across the PHM community.

Certification

The existing system requires certain modifications to accommodate the health-monitoring platforms. The certification of the monitoring tool, including both hardware and software platforms, comes under extensive scrutiny against airworthiness regulations [71].

The certification of components, including hardware and software that are already implemented on the existing products, is straightforward. However, the case for new components is challenging as modifications include quality and performance certification of the components and their interface to the other system. This process is time-consuming and incurs an additional cost to the development of the system.

Return on Investment

An important aspect of successful PHM implementation includes cost-benefit analysis [72]. This includes the development cost, including the cost of implementing sensors, data acquisition systems, diagnostics, and prognostics; costs associated with manufacturing, and maintaining the infrastructure. As the complexity of developing the PHM system increases, overall implementation costs begin to escalate to unmanageable proportions. Any additional investments depend on Return on Investment (ROI) and are appropriately accepted subject to a positive ROI. Therefore, there is always a trade-off between the cost of implementing health-monitoring systems and the complexity involved in developing the prognostic capability [73].

Verification and Validation

Finally, the verification and validation of a health-monitoring technique is a known and complex problem for the protagonists [74]. The unavailability of a healthy baseline of the system is a major concern. However, some researchers benchmark the failure or fault in a system against a simulated model of the system while others standardise worst-case system analysis to detect outliers in the data and hence predict any anomalies in the system. The validation of a health-monitoring method for legacy products is a bigger challenge as there is lack of data and not enough resources to capture the data.

Sensors and Their Resolution

The performance of the health-monitoring tool is highly influenced by the choice of sensors. Importantly, any deviations, non-linearity, accuracy, repeatability, and sensitivity of the sensor can question the quality of the data [75]. In addition, the quality of the data captured by the sensors depends on the characteristic features and resolution of the sensor. For instance, the measurement of tight-tolerance low-voltage power rail using a low-resolution ADC can result in insufficient acquisition of the signal characteristics, add uncertainties, and lead to ambiguous interpretation of the signal.

Furthermore, the electrical characteristics of the sensors need clear understanding before their implementation on the aircraft [76]. The information about the source of power to the sensors is vital. The majority of transducers are battery-powered and require proper power management to extend their operating life. On the contrary, an internal AC or DC power source provides power to the non-battery-powered sensors. Additionally, the electronic manufacturers provide embedded sensors in the equipment. For instance, the highly-integrated user electronics include embedded temperature sensors to monitor the operating temperature of the integrated circuit during different load conditions.

Data Storage

The common sensor systems, microcontrollers, FPGA, and Digital Signal Processor (DSP) available in the industry include on-board memory, such as Non-volatile Random Access Memory (NVRAM) or Electrically Erasable Programmable Read-Only Memory (EEPROM) to store the acquired data. The data acquisition either continuous or periodic and the sampling restrict the storage requirements of the memory. If the available storage is not sufficient, then the stored data has to be transmitted for further analysis.

Data Pre-processing

The availability of signal processing within the majority of sensor systems provides the capability to monitor system performance under different environmental conditions and provide real-time system health updates. However, the complex mathematical and computational calculations of the monitoring algorithm can consume more power than available. This restricts the use of complex monitoring algorithms on board the sensor systems.

Finding 7

There is lack of standard tools and techniques for health monitoring as the developed methods and requirements diverge from system to system. Moreover, it is necessary to comprehend the limitations and other constraints that affect the diagnostic and prognostic decisions of the monitoring tool.

1.5 Gaps in Knowledge

The literature discussed in the previous chapter addresses two key features of PHM technology: i) state-of-the-art health-monitoring frameworks ii) challenges in health monitoring.

PHM in electronic systems has evolved during the past few years with the focus on monitoring, detecting, diagnosing, and predicting failures and degradation due to environmental and operational loads and finally, on approximating RUL, improving reliability and/or predictive maintenance.

The research from authors in this field of study clearly outlines a multitude of health-monitoring frameworks but not all these techniques are mature enough to develop a prognostic capability that involves detection, diagnosis, and prognosis in electronic systems. Moreover, the various capabilities focus on different aspects of degradation and failure detection. The BIT technique discussed in the literature review is suitable for system-level health monitoring. However, the inability to provide knowledge of component degradation in the system does not support the focus of the research (Finding 1).

Similarly, other techniques presented in Table 1-2 provide partial PHM capabilities for system and component-level degradations without minimal human intervention. Physics-of-failure based health monitoring requires detailed knowledge of physics-of-failure mechanisms for degradation and failure models. This includes prototyping complex damage models that are associated to the degradation and failure of the components (Findings 3 and 5). In addition, the verification and validation of PoF tools integrate accelerating life test tools, increasing the percentage of uncertainties and complexity of the problem.

The data-driven monitoring tool based on historical maintenance or training data incorporates entirely different methods which are prone to more errors and uncertainties. The extraction of usable information from collected data, clustering into different data sets, regression analysis, etc. provides concrete knowledge of the system’s RUL. However, there is no explanation of component failures without further analysis and qualification testing (Finding 4).

Moreover, the so-called IVHM solutions developed by various organisations and academics focus on diverse tools and techniques based on specific applications. Problematically, since the development of prediction tools and importantly their integration is at the initial stage, proactive actions meant to save cost and provide availability of the aircraft result in increasing complexity of the system (Finding 7).

The PHM community, including structural health monitoring, engine health monitoring, etc., acknowledge system health monitoring or global performance monitoring of key system metrics as a potential technique for accurate

interpretation of the system and its associated components. Nevertheless, they highlight significant challenges in the implementation of system-level methodology and interpretation of system parameters to recognise initiating degradation and failures in components. Some of the challenges include modelling dynamic complex system models that associate system parameters, such as voltage or current, to detect degradation and failure of the components (Finding 6).

This analysis contributes to the gap in health monitoring of electronic systems:

The PHM community needs to determine the best combination of methods and techniques to monitor and evaluate the degradation or failure patterns in systems and/or components from global key performance parameters.

The first challenge faced in designing a system-level health-monitoring model is identifying the global performance key parameters that can underpin the degradation of the system and the inherent electronic components. The selection of key system parameters in electronic systems might seem easy as it only involves voltages, currents, duty, EMC etc. However, in SMPS, other metrics, such as switching frequency and duty cycle, can also describe the dynamics of the system. Nevertheless, in system health monitoring, performance parameters are not measureable unless external sensors are inserted in the system. Therefore,

It is important to determine global system parameters that incorporate system and/or component anomaly detection.

In order to develop an effective health-monitoring tool there is a need to minimise the effect of various constraints discussed in the previous chapter. From the list of limitations, uncertainty is one of the factors that largely influences the effectiveness of the health-monitoring tool. The uncertainty is inadvertently introduced at every step of the development process, including the sensor resolution, measurements, data storing and corruption, complex signal processing, data transmission, and certainty in modelling the dynamic system.

The health-monitoring frameworks lack extensive understanding of uncertainties in the monitoring tool and the system under question. There is a need to recognise the effect of these uncertainties on the overall effectiveness of the health-monitoring tool.

1.6 Aim and Objectives

The knowledge gaps outlined in the previous section demonstrate the motivation and importance of this research project to the PHM research community. Taking into consideration all the aspects of PHM research, including detection, diagnosis, and prognosis, the main aim of this research is to

Develop a health-monitoring capability that monitors and evaluates system parameters/metrics to detect system and/or component anomalies taking into account the uncertainties.

In order to address and acknowledge the aim of the research, the following objectives have been identified:

- Develop a health-monitoring tool on a basic DC-DC power converter topology;
- Validate the developed capability for anomaly detection;
- Examine robustness and ruggedness of the tool despite uncertainties in the system and the monitoring tool.

The objectives were fulfilled through project planning during three years of research. The above objectives were broken into tasks and deliverables that guided the research.

1.7 Research Hypothesis

The outlined aim and objectives define the research questions which need to be answered in the thesis. The four research questions include:

- How can health monitoring of system performance metrics provide detection of anomalies in the system and/or the components?

In order to understand the technical details of the monitoring tool,

- What are the best-suited techniques that can correlate system performance metrics to component degradations?

Regarding the validation of the monitoring tool:

- How can the developed health-monitoring method be validated for anomaly detection?

Finally, to substantiate the effectiveness of the tool,

- How can the ruggedness and robustness of the tool be verified against different uncertainties?

1.8 Thesis Structure

The thesis structure outline in Figure 1-9 defines a systematic approach to undertake the research project. Chapter 1 provides the reader with the subject background besides review of various health-monitoring frameworks used by the PHM community. The following sections discusses the gaps in knowledge and defines the aim and objectives of this research, along with the research questions which will be answered in the subsequent chapters.

The main research question is to investigate how health monitoring of system performance metrics can provide detection of anomalies in the system and/or the components. From the review in Chapter 1, it is recognised that the concept of system identification (SI) provides knowledge of system dynamics by monitoring system parameters. Therefore, the best approach to understand the capabilities of SI is to study the concept and its various techniques. The next chapter attempts to study and evaluate system identification methods implemented on power converters.

The second research question focuses on identifying the best-suited quantitative SI techniques for system and/or component anomaly detection in power converters. From the understanding of various methods in SI-based health monitoring in Chapter 2, Chapter 3 develops a health-monitoring tool to achieve the main aim of the research. The chapter presents a detailed study of the various algorithms that are robust and rugged enough to provide degradation signatures. This includes the rationale behind the selection and application of particular algorithms and procedures.

Every theoretical method is one-sided without its practical implementation as a Proof of Concept. Conversely, it is imperative to know the performance of the monitoring tool through simulation or experimental results. Therefore, Chapter 4 focuses on executing the developed monitoring tool on a basic DC-DC power converter. The experimental test circuit is integrated using a COTS power converter and a COTS digital controller.

The third research question targets validating the developed monitoring tool for anomaly detection in the system and/or the components. This research question is answered in Chapter 5 through simulation and experimental results. Compared to validation methods discussed in the literature review, the tool is validated by introducing component value change which is indicative of anomalies in the system.

Finally, the last research question of examining the ruggedness and robustness with respect to external stimulus is investigated in Chapter 6. This includes the examination of uncertainty on the system parameters and their effect on detecting degradations in the components.

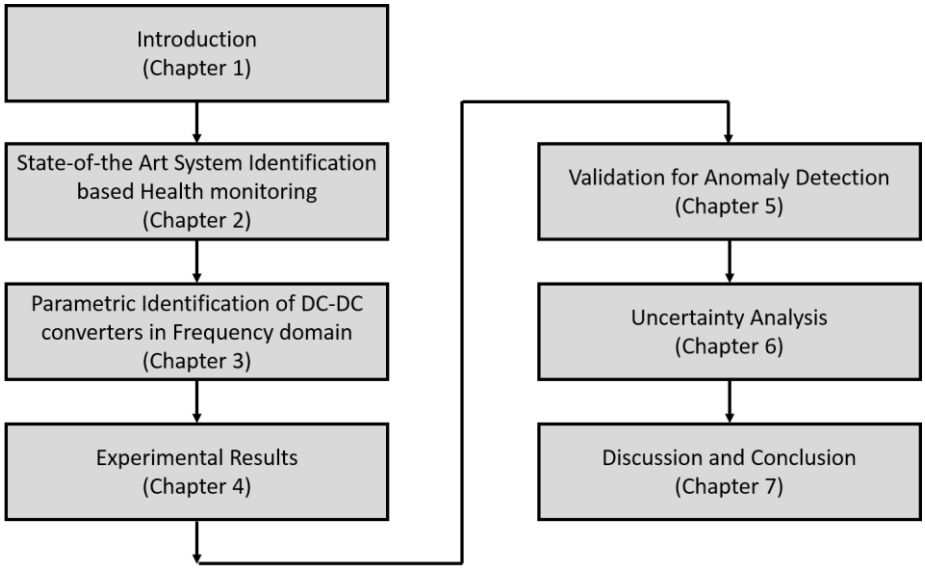

Figure 1-9 Thesis Outline

2 System Identification Based Health Monitoring

This chapter outlines the concept of system identification for health monitoring of electronic systems. Section 2.1 introduces the reader to the principles of system identification, describing various steps in its implementation.

The subsequent sections attempt to understand the following steps:

- Choice of Experimental setup in Section 2.2
- Design of Experiment in Section 2.3
- Choice of Noise Model in Section 2.4
- Data Pre-processing in Section 2.5
- Model Identification in Section 2.6
- Validation Procedure in Section 2.7

The above stages are discussed with the intention to answer the first research question of how to develop a monitoring tool for anomaly detection.

2.1 Principles of System Identification

System identification is an interdisciplinary practice used to characterise the behaviour of a dynamic system, usually in the form of a mathematical model [77]. The structural health monitoring research community extensively uses the fundamentals of system identification to model and identify the performance of structures against several stimuli. The typical stimulus includes single/multiple impact, other vehicles, traffic, etc. However, the progress of system identification centred health monitoring is at an infant stage for electronic systems.

Before explaining the concepts of system identification, the reader is referred to the definition of relevant terms.

For an unknown system depicted in Figure 2-1, the transfer-function of the system is defined as the ratio of output $Y(s)$ to the input $X(s)$ such that

$$H(s) = \frac{Y(s)}{X(s)} = \frac{n_0 + n_1 s + n_2 s^2 + \cdots}{d_0 + d_1 s + d_2 s^2 + \cdots} \quad (2\text{-}1)$$

where n_0, n_1, n_2, d_0, d_1, d_2 are model parameters while $Y(s)$ and $X(s)$ are the global system parameters.

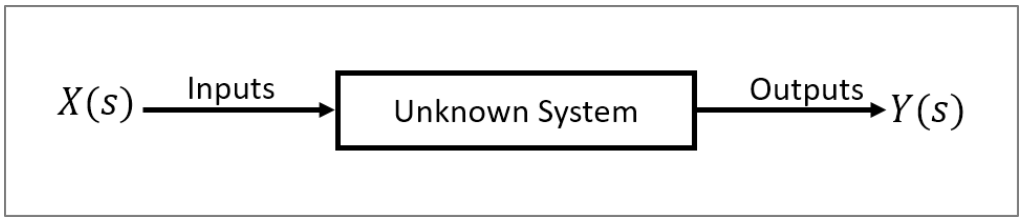

Figure 2-1 Unknown System

In system identification, two questions outline the entire identification scheme: the application/purpose for system identification and the stochastic/noise characteristics of the system.

1) Application

   In recent years, digital control systems have been used to accomplish the majority of the system identification process. Therefore, for power converters, system identification has one of two applications:

   - To model characteristics of an analog system or components into a digital control system or
   - To model system dynamics for physical interpretation of the system.

   From the basic configuration and understanding of a power converter discussed in Appendix A, the above-mentioned analog components describe the feedback compensation network and not the actual power stage network. In contrast, the model of system dynamics refers to the characteristics of the actual power stage network and not the compensation network.

The majority of the research on system identification in power converters has been to model the compensation network in digital controllers and to identify the input-output characteristics of the system.

However, the model of system dynamics to comprehend the physical characteristics of the system, such as degradation or failures in the power stage components and the system as a whole, has not been researched in depth. Therefore, this research attempts to model the system dynamics to understand the physical features of the system that allow detection of degradation in the power stage elements and the system.

2) Stochastic Framework

The stochastic framework examines the potential noise sources in the system and the identification process. Conversely, it studies how noise enters the system. Are these noise characteristics known and can they be modelled?

Consequently, the above criteria guide the selection of methods in the entire identification through six different stages illustrated in Figure 2-2.

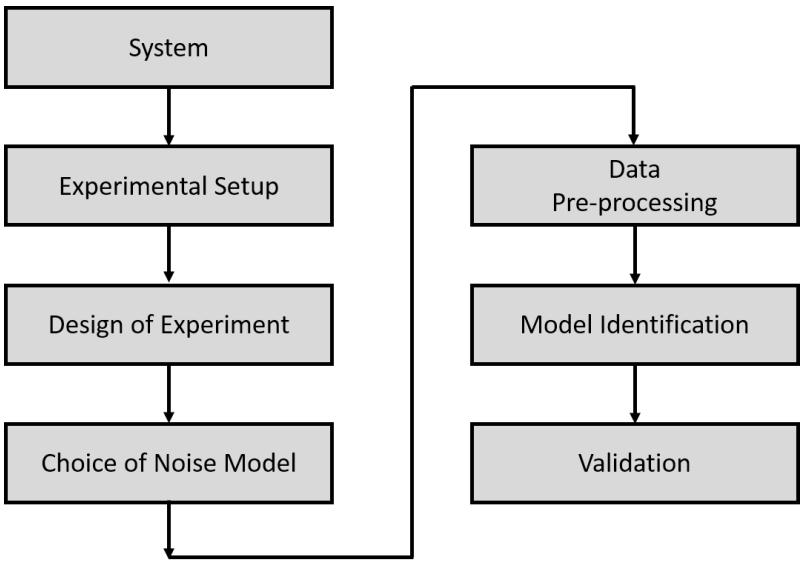

Figure 2-2 System Identification Methodology

2.2 Choice of Experimental Setup

The choice of experimental setup involves knowledge of sensors or data acquisition systems, system synchronisation, and assumptions about the sampled signal.

Firstly, the use of suitable sensors or acquisition equipment that performs filtering, attenuation, amplification, sampling, and quantisation defines the quality of the measurements. For instance, a high sampling rate with low quantisation noise ensures high Signal to Noise Ratio (SNR) of the sampled signal. Therefore, the selection of data acquisition or digital control systems is important during the experimental setup. In system identification of power converters, researchers have used various acquisition systems. For instance, Morroni et al. [64] prototype FPGA to model the compensation network and control the power stage network. Algreer et al. [78] demonstrate the use of DSP, and Patella et al. [79] design an integrated circuit that incorporates the functionality of the ADC, digital compensator, and the Pulse Width Modulator (PWM) controller.

Secondly, proper synchronisation between the acquisition device and the system clock helps reduce the majority of the leakage errors and avoids unobserved uncertainty in the sampled signal. For instance, synchronisation between the sampling frequency of the ADC and the switching frequency of the converter assures a consistent estimate of all the measurements. In addition, stability of the system clock is important because the presence of nonlinearities, such as jitter, introduces uncertainty and decreases the SNR of the measurements.

Subsequently, the characteristic of the sampled signal between the consecutive sampling instants, i.e. inter-sample behaviour largely influences the selection of the identification model. The researchers across the system identification community formulate two assumptions:

i) Zero-Order Hold (ZOH)

The ZOH criterion assumes that the sampled signal is constant between the consecutive samples. Consider that $x(kT_S)$ is a discrete-time signal with sampling period T_S and sampling instant kT_S, the reconstruction of the signal

$$x_{ZOH}(t) = \sum_{k=-\infty}^{+\infty} x(kT_S).ZOH(t - kT_S) \tag{2-2}$$

where $ZOH(t) = 1$ for $0 \leq t < T_S$ and zero elsewhere, projects a spectrum

$$X_{ZOH}(j\omega) = X(j\omega).ZOH(\frac{\omega}{\omega_s}) \tag{2-3}$$

with

$$ZOH(x) = T_S\, e^{-j\pi x} \frac{\sin(\pi x)}{\pi x} \tag{2-4}$$

The spectra of the reconstructed signal, sinc function, generate dominant frequency component at the sampling frequency F_{SP} along with its harmonics at the higher frequencies $2F_{SP}, 3F_{SP}$ ... and so on.

ii) Band-Limited (BL)

When the inter-sample behaviour of the sampled signal is band-limited, i.e. the power spectrum of the reconstructed signal $x(t)$ is zero above a frequency ω_{max}, usually half the sampling frequency. Mathematically,

$$\Phi(\omega) = 0\ for\ \forall\ |\omega| > \omega_{max} \tag{2-5}$$

the spectra of the reconstructed band-limited signal only produce a fundamental sampling frequency without any harmonics.

The difference between the signal and its reconstructed counterpart for the ZOH assumption conveys to the user that the reconstructed signal may not be the exact replica of the signal itself. This doubt is eliminated in the band-limited assumption where only the exact replica of the signal is reconstructed.

Moreover, the inter-sample behaviour influences the type of the system model, as mentioned earlier. Pintelon and Schoukens [80] show that the ZOH assumption best describes the discrete-time model of the system while the BL assumption leads to a continuous-time model of the system. The user can use a BL assumption and describe the model in discrete-time or vice versa. However, Ljung [77] emphasises that this leads to a complex model of the system and complicates the identification of the model.

2.3 Design of Experiment

The second step incorporates the experiment design that defines the characteristics of the excitation, including amplitude spectrum, frequency resolution, and periodicity.

The performance of the identification model largely depends on the experimental design and the design of the excitation signal. Additionally, the presence of uncertainties due to component tolerances significantly affects the measurements and subsequently, the estimation of the identification model and the model parameters. Therefore, the design of experiments requires careful design of the measurement matrix. This involves the selection of global system parameters, the perturbation/excitation signal, and specific timing and memory considerations.

In system identification based health monitoring, perturbing the system with an excitation linearises the non-linear dynamic system and provides a transfer

function of the system. From an electronic control engineering perspective, exciting the system with a perturbation signal linearises and provides a small-signal model of the power converter or an electrical circuit where the input and output response represents the small-signal model or the transfer function.

Several methods exist to linearise and obtain a small-signal model or global system parameters of the power converter, for example, state-space averaging and circuit averaging, etc. The small-signal analysis approximates the behaviour of non-linear devices with linear equations. This linearisation obtains a DC bias point by taking a partial derivative of the formula (non-linear device model) with respect to all governing variables. In circuit averaging, the equivalent dependent voltage and current sources replace the non-linear switching elements, such as MOSFET and diodes, to find the DC operating point. Subsequently, the average of all the circuit waveforms over one switching period provides the small-signal AC model of the converter. In contrast, state-space averaging uses differential equations in matrix notation to represent different states of the non-linear circuit. The average of the state-space equations and the state matrices representing different states of the circuit provides a small-signal low-frequency model of the converter.

In system identification, exciting the system with a perturbation signal linearises and provides a small-signal model of the power converter or an electrical circuit where the input and output response represents the small-signal model.

A possible source of excitation in the system is the inherent noise of the system, such as analog noise. This ambient system noise is best for real-time health monitoring as it eliminates the impact of initial conditions (time-domain) and leakage errors (frequency-domain), and reduces the burden of designing external perturbation. Nevertheless, different load conditions affect the behaviour of the inherent noise and lead to low SNR of the extracted system response. Therefore, the majority of researchers prefer external perturbation signals, such as an impulse signal, chirp, pink noise, random noise, and single sinusoidal. The user knows the energy of the external perturbation signal previously and can select the signal according to their intended application.

Schoukens et al. [81] classify three types of perturbation signals that can be used in system identification: i) general-purpose signals that can be applied without any optimisation, such as impulse signal, pink noise, etc.; ii) optimised test signals that allow the user to decide the power spectrum of the perturbation; and iii) dedicated signals that are optimised for specific environments as described in Table 2-1.

The general-purpose sine-sweep signal incorporated in the Frequency Response Analyser (FRA) and described by Gonzalez-Espin et al. [82] provides small-signal response of the power converter. A single sinusoid of specific frequency perturbs the system and extracts accurate dynamics at that frequency. Similarly, the excitation of the system at a sequence of desired frequencies provides the corresponding frequency response over the excited band of frequencies. The sine-sweep excitation is accurate and provides high SNR on the measured frequency response. However, it is constrained by long measurement time to capture the response at each perturbation frequency. Moreover, in order to extract significant SNR from the ambient system noise dynamics and to remove the effects of transients at each perturbed frequency, signal averaging is an additional computational burden on the design of the experiment.

Recent studies of Roinila et al. [83], Shirazi et al. [67], Miao et al. [84] and Barkley and Santi [85] describe the use of broadband excitation to extract small-signal response of the converter. The typical broadband excitation, the Pseudo Random Binary Sequence (PRBS) generated from Multi Length Sequence, (MLS) extracts the response of the converter in reduced measurement time.

PRBS is a periodic, binary, and random sequence with maximum and minimum values bound between $0,1$, and $\pm e$, where e defines the voltage level of the input analog signal. The signal is easily available as a direct function in the majority of the control software packages, such as MATLAB control toolbox, or can be generated using shift registers. However, in extracting the frequency response using a random sequence, the researchers assume that the input signal resembles a white noise with zero mean and a flat power spectral density across

Signal	User-defined power spectrum	Crest factor	Leakage
General Purpose			
Swept Sine	No	1.45	No
Impulse	No	$\sqrt{(T/T_1)}$	No
MLBS	No	1.5	No
PRBS	No	1.0	No
Random noise	No	2.0-3.0	Yes
Optimised			
DIBS	Yes	small*	No
Multi-Sine	Yes	1.4 - 2.0*	No
* Depends on the complexity of the signal T = measurement period, T_1 = pulse width			

Table 2-1 Summary of Excitaiton signals

the entire bandwidth of interest. That is, the sequence reflects all the features of the assumed input noise with auto-correlation a delta function and no cross-correlation with inherent system noise. Thus, the cross-correlation of input and output signal gives the impulse response of the system and the Discrete Fourier Transform (DFT) to the impulse response provides control to output small-signal transfer function of the power converter.

Correspondingly, Miao et al. [84] and in their associated paper [65] propose using a multiple period PRBS excitation and then averaging over several periods to increase the SNR or reduce the effects of inherent noise sources, including switching noise, analog noise and digital quantisation noise on the extraction of the frequency response. The technique significantly reduces the noise, compared to single period PRBS, and extracts accurate frequency response in the presence of switching noise, and digital delays. However, the researchers formulate an open-loop identification.

Barkley and Santi [85-87] demonstrate an improved closed-loop scenario by windowing the measured frequency response, delaying the sampled output voltage, and compensating for a non-ideal spectrum of the multiple period PRBS.

Further, Shirazi et al. [67] describe fully automated system identification by proposing the use of pre-emphasis/post-emphasis filter, fractional-decade smoothing, etc. to improve the SNR of the frequency response. Besides, Roinila et al. describe the use of other binary excitation signals such as Discrete Interval Binary Signal (DIBS) [88] and Inverse-Repeat Binary Sequence (IRS) [89] to improve the performance of frequency response.

It can be summarised that PRBS, DIBS and IRS provide good estimates of Frequency Response Function (FRF) measurements and the small-signal transfer function. Importantly, all the above studies simulate the compensator/feedback network in the digital controller assuming a ZOH inter-sample behaviour and characterise the system in discrete-time domain.

The choice of periodicity of the perturbation signal is dependent on the user and the application. Generally, it is recommended to use periodic signals against random excitation signals to minimise aliasing and prevent leakage errors during the measurements.

2.4 Choice of Noise Model

The choice of noise model in the system identification process governs the complexity of estimating the system model. A parametric model describes the behaviour of the system with a limited number of system parameters or circuit components. The non-parametric model, in contrast, estimates the system characteristics from a large number of measurements.

Generally, noise characteristics of the system are unknown until prior knowledge of the system and the acquisition systems, etc. is available. Therefore, the majority of the research does not consider noise models and focuses on identification of the system model only.

2.5 Data Pre-Processing

Pre-processing the data for model identification is imperative when raw measurements are available in either the time domain or frequency domain. The choice of time or frequency domain identification is user-specific.

The majority of the researchers prefer time-domain system identification using correlation analysis, as discussed above. They assume that the input signal resembles a piecewise constant excitation signal with characteristics of zero mean and flat power spectral density across the bandwidth of interest. The cross-correlation of input and output signal yields an impulse response of the system and applying DFT to the impulse response gives the frequency response of the system. The correlation method provides accurate estimate of system response, but require large data sets to extrapolate ageing degradation.

Similarly, transient-response analysis is an effective method to capture time-domain characteristics of the power converter. The large-signal model is perturbed with an impulse or a step input to linearise the system and attain small-signal behaviour of the converter. The transient response analysis is less time-consuming. However, the accuracy of the transient response analysis is questionable because the limited time step and short-duration of the impulse response does not provide sufficient information of the dynamic nature of the power converter. The increased time duration of the Heaviside step input can measure the entire dynamic system response. Nevertheless, this inadvertently induces instability in the system and without noticing instability or marginal stability the system can be interpreted as a stable system.

For closed-loop system identification, where present outputs depend largely on previous inputs, the inherent noise in the step response can mask the degrading features of the components and cause difficulty in extracting the output response. Thus, the identification of an unstable and noisy step response becomes difficult and often challenging due to propagation of noise in the calculations. Importantly, the time-domain identification is not always valid with the ZOH assumption and can provide large errors if the assumption is not met [90].

On the contrary, frequency-domain identification provides an accurate estimate of the dynamic response of the system. For periodic excitations, the time-domain identification with the BL framework and the ZOH assumption are still valid [77]. However, frequency-domain identification with periodic excitation enables the access of certain characteristics of the system that are not available in time-domain identification. For example, exciting the system at only the required frequencies of interest eliminates noise from the non-excited frequencies. A finite set of spectral frequencies describes the frequency response from a large number of time samples. Furthermore, it is easy to extract and recognise the non-linear distortions in frequency-domain identification with the BL framework while perturbing the system with periodic excitation.

2.6 Model Identification

In system identification, parametric or non-parametric methods outline the identification of the system characteristics. The identification from a large number of FRF measurements constitutes non-parametric system identification as discussed above.

Parametric identification, in contrast, illustrates the system model by a mathematical function with a limited number of parameters or circuit components in a power converter. Conversely, parametric identification combines the response of the system available from some measurements in only a few parameters. These model parameters or coefficients, expressed as Laplace rational fraction in continuous-time domain, define the order of the system and depict its physical characteristics:

$$H_P(\mathrm{s}) = \frac{\mathrm{N(s)}}{\mathrm{D(s)}} = \frac{\sum_{n=0}^{\mathrm{n}} \mathrm{n}_n \mathrm{s}^n}{\sum_{d=0}^{\mathrm{d}} \mathrm{d}_d \mathrm{s}^d} = \frac{\mathrm{n}_0 + \mathrm{n}_1\mathrm{s} + \mathrm{n}_2\mathrm{s}^2 + \cdots}{\mathrm{d}_0 + \mathrm{d}_1\mathrm{s} + \mathrm{d}_2\mathrm{s}^2 + \cdots} \tag{2-6}$$

where $\mathrm{N}(\mathrm{s_k})$ and $\mathrm{D}(\mathrm{s_k})$ represent the numerator and denominator polynomials and represent the order. n_0, n_1, n_2 …n_n and d_0, d_1, d_2, d_d represent the numerator and denominator coefficients of the model $H_P(\mathrm{s_k})$.

In parametric identification, the user assumes the system model, such as a black-box model, a grey-box model, or a transfer function model, and refines this model from the non-parametric measurements. Generally, the non-parametric measurements are captured from either simulation [91; 92] or the experimental data [65; 78; 93]. Conversely, parametric model identification starts from non-parametric identification. This non-parametric identification from FRF measurements provides an initial estimate of the system characteristics, complexity, and the order of the system. These FRF estimates reveal any trends, outliers, or noise in the system that can be analysed before parametric identification.

For instance, Huynh and Cho [91] demonstrate the use of a black box model to identify the parametric model of the buck converter. Firstly, the researchers obtain non-parametric FRF measurements from a simulation model of the buck converter in PSpice. Since the model structure and the order of the model are unknown at the initial stage, the efficiency of the parametric model is low. The assumptions of the first-order model of the system lead to a large prediction Root Mean Square (RMS) error between the estimated and simulated models. Further experiments and a revised model order approximates low error on the model parameters; however, the actual order of the model was unidentified. Therefore, two different power converters were modelled to validate the effectiveness of the parametric model.

The main objective of the model estimator or the identification model is to minimise the predicted error/cost function between the non-parametric model $H_{NP}(\mathrm{s_k})$and the parametric model $H_P(\mathrm{s_k})$. By defining the model order and the number of coefficients in numerator and denominator from the initial approximate of the model from FRF measurements, the model estimator best estimates the parametric system model minimising the cost function. The choice of the model optimiser, such as simple Non-Linear Least Squares, Weighted Recursive Least Square and the complex ARX, Kalman filter, etc., is application-specific and based on the stochastic framework.

2.7 Validation

The final step in the identification procedure is to validate the identified system parametric model. A basic validation test is to compare the estimated parametric model against the non-parametric frequency response measurements. Based on the error between both the models, the user may revise the parametric model by changing the model complexity and if required, the amplitude or frequency resolution of the FRF measurements. Even though the close match between the parametric model and non-parametric model provides confidence in the system identification process, the quantification of the uncertainty in the system, i.e. quantifying uncertainty on the system response measurements and the estimated model parameters, provides enhanced understanding of the system and the associated noise sources to achieve the best estimate of the system characteristics.

2.8 Chapter Summary

Health monitoring based on system identification tools and techniques reveal that the choice of the identification scheme is highly dependent on the application and the underlying noise characteristics. A clear understanding of the application provides a direct answer to some of the methods the user should take into consideration.

This chapter provides the following conclusions about system identification based monitoring.

- Sensors are essential for system identification process, which not only enables real-time health monitoring but can also be used to control the system.
- The band-limited assumption of the sampled signals, compared to ZOH, contains energy up to half the defined switching frequency minimising uncertainty in the measurements.
- The choice of optimised perturbation, compared to other random excitations, provides the flexibility to inject specific energy at defined

frequencies of interest to understand certain characteristics of the power converter.

- The non-parametric identification obtained from a large set of measurements is easy and provides basic understanding of the system characteristics. However, the parametric identification of the system, described in the form of system parameters, provides insight of the dynamic nature of the system and the noise present in the system.

3 Parametric Identification of DC-DC Converters in Frequency Domain

The development of every tool requires a systematic outline of different techniques and methods. Conversely, a logical methodology is required to define an effective tool. The first section of this chapter describes the sequence of processes to develop the health-monitoring tool.

The first stage in developing a monitoring tool is to understand the application and purpose for monitoring. According to the aim and objectives of this research, the purpose of system identification based health monitoring discussed in Chapter 1 is to develop a capability that can detect anomalies or degradations in DC-DC power converters and the electronic components within. However, it is important to comprehend how system parameters can relate to detection of degradation of the electronic components. Section 3.2 defines the relationship between the system parameters and the degradations related to electronic components in the system.

The availability and resolution of the sensors that governs the quality of the measurements of the monitoring tool are discussed in Section 3.3 In addition; the section incorporates the selection of inter-sample behaviour, which influences the selection of a continuous-time or a discrete-time system model.

Subsequent to the above decisions, careful selection and design of perturbation signals defined in Section 3.4 define the procedure to acquire non-parametric FRF measurements with the required SNR or minimum uncertainty. These large sets of measurements captured at certain frequencies of interest extract non-parametric model identification and provide an initial estimate of the system behaviour discussed in Section 3.5.

Section 3.6 demonstrates parametric system identification by estimating best-fit system model using a WLS approach. The extraction of model parameters finally describes the extent of degradation or any anomalies in the system in Section 3.7.

3.1 Health-Monitoring Methodology

The flowchart in Figure 3-1 describes the stages in developing the health-monitoring methodology. The subsequent sections will discuss all the stages of the development tool.

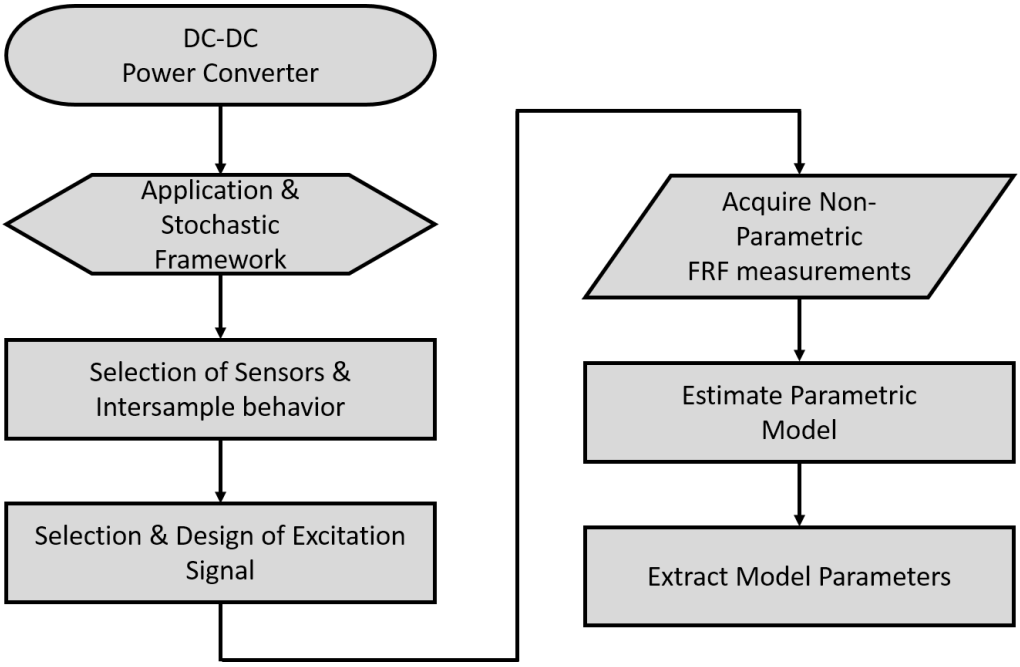

Figure 3-1 Flowchart of Health-Monitoring Tool

The proposed system identification based health-monitoring methodology or tool is executed on a basic DC-DC buck converter as shown in Figure 3-2.

3.1.1 DC-DC Power Converter

The block diagram of the monitoring tool includes the power stage network or the DC-DC power converter regulated by a digital controller in the feedback network. In digital control of power converters using either a DSP or a FPGA, the ADC discretises the output voltage signal $v_o(t)$ into a sequence of n samples $v_o(n)$ and computes the error between the digital reference and the digital signal. The digital corrector, usually a Proportional-Integral-Derivative (PID) controller or 3p3z digital filter, compensates the error to provide a digital sequence $d(n)$. The Digital Pulse-Width Modulator (DPWM) then commands a PWM duty signal $d(t)$ to regulate the control loop. The perturbation signal, which is digitised in the digital controller $p(n)$, excites the control loop and provides a small-signal AC response

of the system at the injected frequency of the perturbation. It is worth mentioning that the control loop is not broken and the frequency response is measured in a closed-loop condition.

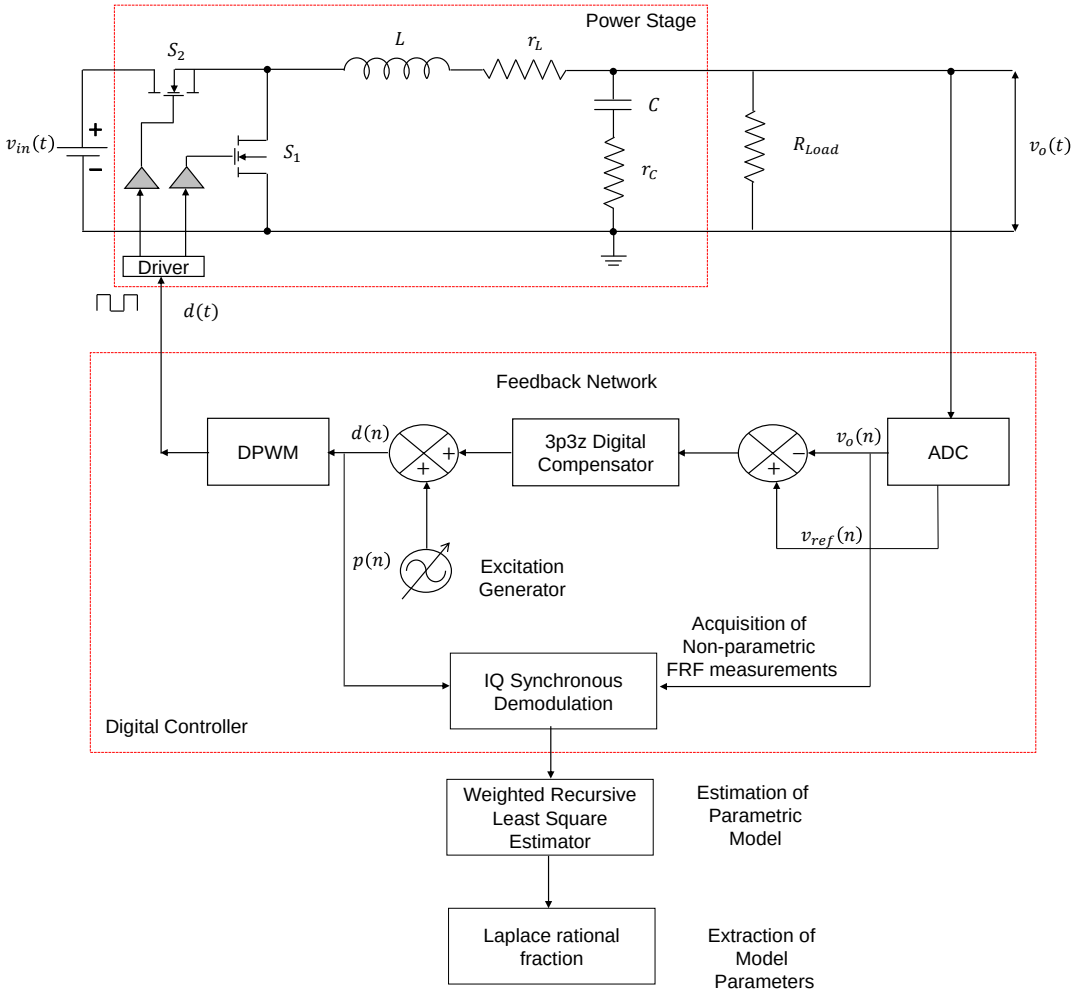

Figure 3-2 Block Diagram of System Identification Based Health-Monitoring Tool on Digitally-Controlled DC-DC Buck Converter

3.2 Application and Stochastic Framework

The majority of the power stage failures aggregate from degradations and failures in the capacitor C [28]. An electrolytic capacitor is a passive electronic component, which degrades and fails significantly, compared to other capacitors used in power converters. The ESR of the electrolytic capacitor is a prominent precursor to degradation that provides knowledge of anomalies in the capacitor

and the overall performance of the power converter. Therefore, the application or purpose is to detect these degradations from the global system parameters, such $v_o(t)$, $d(t)$, and $v_{in}(t)$.

Now, the question arises as to how these degradations in the capacitor and the overall system performance be detected through so-called global system parameters. In the frequency domain, the control-to-output transfer function of the power converter, defined as the ratio of $v_o(s)$ to $d(s)$, describes the dynamic behaviour of the power converter [17]. In the transfer function or system response of a basic DC-DC buck converter, the – 20 dB/decade asymptote provides knowledge of inductor and the output filter capacitor. Similarly, the – 40 dB/decade asymptote reveals information about the ESR of the output filter capacitor. This knowledge of the power stage network ensures that from the control-to-output transfer function response, the degradations and failures of power stage network elements (inductor and capacitors) can be detected, diagnosed, and prognosticated.

With respect to noise in the power converter, numerous factors contribute to noise in the system and lead to uncertainties and inaccurate estimation of degradation. Firstly, the inherent analog noise of the electronic components, including flicker noise, Johnson-Nyquist noise, etc., introduces uncertainty on the system parameters. Secondly, the use of digital techniques, such as quantisation, introduces digital noise. The signal processing and computational calculations of the measurements superimpose additional noise on the system parameters and propagate it on the model parameters.

All the above noise sources are part of the system and cannot be eliminated. However, careful use and choice of tools and techniques for data acquisition, signal processing, and model estimation can minimise the effect of these uncertainties and their propagation on model parameters. Sections 5.2 and 5.3 illustrate how the choice of sensors and the design of the perturbation signal are used to minimise these uncertainties in the development of the health-monitoring tool.

3.3 Sensor Selection

As discussed in the previous chapters, the majority of the identification techniques described use different digital control systems. Keeping in mind the strengths and challenges of digital control, the selection of digital controllers requires considering certain aspects. The number of bits of the ADC influences the choice of the digital controller. A 12-bit ADC provides resolution of 806 µV on a 3.3V signal. In practice, the noise of the input resistor, preamplifier and inherent noise of the ADC always cause the loss in 1 - 2 bits limiting the dynamic range of the ADC. Therefore, it is always beneficial to use a high-bit ADC. However, the 14-bit or 16-bit ADC might introduce additional non-linearity in the system and increase uncertainty.

The clock speed of the digital modulator is another criterion essential for a good resolution PWM signal. MacCleery et al. [94] acknowledge that a parallel hybrid FPGA running at 200 MHz outperforms a DSP and a microcontroller with regard to performance per chip and per watt. However, claims that designing FPGA based controllers require good knowledge of Register-Transfer-Level (RTL) programming, compared to high-level programming used by DSP or microcontrollers. The additional debugging, verification, and support for the RTL code adds an extra burden on the user.

A DSP/microcontroller-based digital controller allows fine-tuning the acquisition channels and the feedback loop from a single Integrated Development Environment (IDE), thereby minimising accompanying design and interfacing difficulties. In contrast, the external signal processing required in the use of a FPGA-based controller places further constraints on the user, whereas the in-built mathematical processor within the DSP or microcontroller allows the user to perform on-board complex signal processing. Based on the above review of FPGA and DSP-based digital controller, this research prefers to use a DSP-based microcontroller.

As discussed in the previous chapter, the band-limited assumption directs the presence of two anti-alias filters, system bandwidth less than half the sampling

frequency, and the presence of two measurement channels in the system. Herein, the switching power converter depicted in Figure 3-2 has an inherent anti-alias filter, i.e. a low-pass filter circuit. Therefore, the BL assumption satisfies the presence of anti-alias filters without the use of external filter circuits.

Generally, the closed loop bandwidth B_S of the power converter is $1/10^{th}$ or $1/20^{th}$ of the switching frequency F_S, let us say = 200 kHz. If the sampling frequency F_{SP} is greater than twice the signal bandwidth, according to the Nyquist-Shannon sampling theorem, the effect of aliasing is minimised. Conversely, there is negligible aliasing effect for PWM converters whose bandwidth is very small compared to the sampling frequency. Mathematically,

$$\mathrm{B}_S < \frac{F_{SP}}{2} \tag{3-1}$$

Therefore, the band-limited assumption of the sampled signals is best suited for this research application. The band-limited assumption promises the study of system characteristic features in continuous-time domain by limiting the bandwidth of the excitation signal to half the sampling frequency.

3.4 Excitation Signal

The use of excitation/perturbation signals is fundamental for non-parametric system identification. The amplitude and frequency of the perturbation signal decides the characteristic information the user wants to extract from the small-signal response of the converter.

As discussed before, high-frequency measurement is essential for health monitoring in this research because the zero introduced by the ESR of the output filter capacitor $F_{ESR} = 1/2\pi C r_C$ lies at high frequency region of the converter response between the cut-off frequency of the output filter $F_{OF} = 1/2\pi\sqrt{L\,C}$ and the switching frequency. Therefore, accurate measurement of attenuation and phase of the system requires the frequency sweep to excite the pass-band of the system between 10 Hz and 200 kHz.

Reflecting on the design objective to extract a small-signal response of the system at high frequencies, the amplitude spectrum of the PRBS, DIBS, and IRS excitations is not high enough to extract and quantify the high-frequency dynamics of the converter in the band-limited assumption. In addition, the above broadband excitation signals capture the entire frequency response using a single measurement in low computational time, but result in undesired loss of SNR at the higher frequencies.

As discussed in Chapter 2, the general class of perturbation signals, for instance, Dirac-Delta with a single pulse amplitude spectrum, is also not suitable to measure the response of this system. This is because the power of a single pulse at high frequencies close to the ESR frequency is not high enough to measure the output signal and will result in poor SNR.

Mathematically, the unity crest factor of PRBS sequence, which is identical to the crest factor of the delta function, is ideal for extracting the signal buried in the system noise. However, the amplitude spectrum of PRBS for the band-limited inter-sample assumption decreases inversely with the frequency, limiting the signal-extracting capability up to a certain frequency of the entire spectrum. Moreover, Pintelon and Schoukens [80] corroborate that the amplitude spectrum for increasing the length of the PRBS sequence decreases with frequency and hence, is undesirable for extracting signal information at high-frequency spectra of the power converter.

The use of single frequency sinusoid accurately measures the system response, but it consumes a significant amount of time to measure the system response. This is the reason why the majority of general excitation signals, such as pseudo-random white noise, impulse, and Dirac-Delta, are rejected because the amount of power available in the signal at high frequencies is not high enough to accurately measure the gain and phase of the system. Therefore, none of the above excitation signals is appropriate in this study.

The present research proposes a multi-tone sinusoid signal as an energy-rich excitation to extract a closed-loop frequency response of the power converter. A

multi-tone sinusoidal is a periodic, deterministic broadband excitation with full flexibility to define the amplitude spectrum and frequency resolution. The optimised multi-tone perturbation enables achieving the design objectives, i.e. signal extraction at high frequencies and reduced uncertainty on the FRF measurements. Furthermore, the multi-tone sinusoid signal enables optimising the amplitude spectrum for desired frequencies of interest before performing any measurements, saving significant post-processing and computational time.

From a signal-processing perspective, excitation of the system with inadequate energy in the perturbation signal will provide a low SNR or high uncertainty on the measurements. Therefore, based on the required SNR, the optimised multi-tone sinusoid perturbation excites the system at the required frequencies of interest. The system identification of such a system, wherein knowledge of both high and low-frequency dynamics is required, is not only complex but also challenging.

3.4.1 Frequency Sweep

Ideally, the frequency sweeps at every integer frequency up to half the switching frequency provides accurate frequency response measurement. This is similar to the operation of an FRA. However, the memory and computational power of the digital controller limits the feasibility of this approach.

Instead, the equally-spaced frequency sweep of ten or eleven integer frequencies provides maximum system information at the frequencies of interest without restricting the computational power consumption of the digital controller. This multi-tone frequency sweep excites the system at the user-defined frequencies and minimises power leakage in the adjacent harmonics. Therefore, frequency response measurements by perturbing and linearising the system with a user-defined frequency sweep provide better insight of anomalies and degradation of the system. More importantly, the selection of integer frequencies close to the ESR frequency and the cut-off frequency of the power converter enable extracting and understanding the degradation of the ESR and the capacitance of the output filter capacitor.

Prior to the selection of the perturbation frequencies, periodic perturbation is considered as it reduces measurement noise and enables the spectrum of the signal measured over an integer number of periods to be calculated precisely by the DFT.

Secondly, the perturbation frequency sweeps logarithmically by octaves from the start to the end frequency to generate a multi-tone signal. Mathematically, the frequency sweep F_P

$$\mathrm{F}_{P\,m} = \frac{\mathrm{F_S}}{l.2^{\mathrm{m}}}, \mathrm{m} = 2, 3, \ldots 12;\ l = 1 \tag{3-2}$$

where m and l are integers. l can be modified to values 3, 5, or 7 to generate different frequency sweeps.

The selection of l generates different logarithmic sweeps by octaves. Using Equation (3-2), F_S = 200 kHz and l = 1, the start and end frequency tones can be calculated. This equates to different frequency sweeps as shown in Table 3-1. For l = 7, eleven tones from 85.44922 Hz to 87500 Hz excite the pass band of the converter (zero until half the switching frequency). Similarly, for l = 5, eleven tones from 61.035 Hz to 62500 Hz can describe the entire response of the system, including the ESR frequency. For lower values of l, more frequency sweeps are available, for instance, twelve for l = 3 and thirteen for l = 1.

However, the intention is firstly to excite the system with the minimum number of sweeps to reduce measurement time and secondly to sweep only the frequencies that add knowledge to health monitoring. This infers to use the frequency sweeps either for l = 3, 5, 7. Nevertheless, the sweep frequencies are far apart for the above cases as shown in Figure 3-3.

F_P				
m	l =1	l =3	l = 5	l =7
2	50000	150000	250000	350000
3	25000	75000	125000	175000
4	12500	37500	62500	87500
5	6250	18750	31250	43750
6	3125	9375	15625	21875
7	1562.5	4687.5	7812.5	10937.5
8	781.25	2343.75	3906.25	5468.75
9	390.625	1171.875	1953.125	2734.375
10	195.3125	585.9375	976.5625	1367.188
11	97.65625	292.9688	488.2813	683.5938
12	48.82813	146.4844	244.1406	341.7969
13	24.41406	73.24219	122.0703	170.8984
14	12.20703	36.62109	61.03516	85.44922

Table 3-1 Selection of Frequency Sweep Based on the Value of l

For l = 1, on the contrary, 13 frequency sweeps can be reduced by eliminating the lower frequencies, such as 12.207 Hz, 24.414 Hz, and 48.828 Hz as they do not provide significant system information for this application. Therefore, for l = 1 and a power converter switching at 200 kHz, a maximum of ten equidistant discrete tones once every octave provides extensive information about the entire system response. This frequency scaling is essential because it enables proper representation of the power-train frequency response and it includes the power-train cut-off frequency and the zero introduced by r_C.

This comb spectrum injects the maximum energy at the specified frequency and eliminates spectral spurs that originate at frequencies other than the frequency associated with the discrete tones.

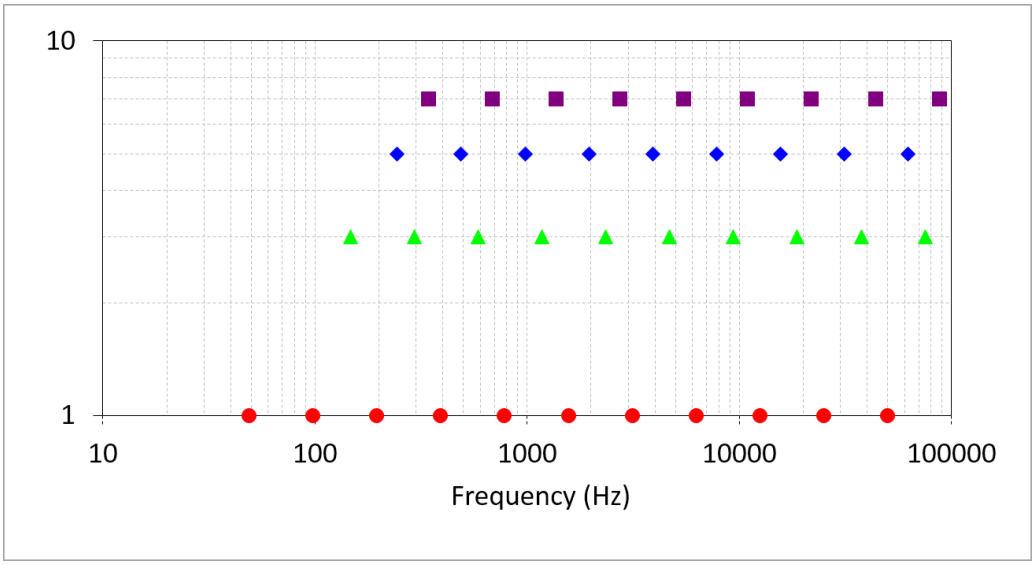

Figure 3-3 Comb Spectrum for l = 1, 3, 5, and 7

3.4.2 Perturbation Amplitude

The amplitude of the perturbation signal must be greater than ambient system noise to measure the system response precisely but small enough to keep the system linear and stable. Moreover, the amplitude of the perturbation signal governs the SNR of the non-parametric frequency response measurements and hence, the SNR of the system response.

The SNR can be defined as ratio of mean value to the standard deviation (noise) of the signal. A low standard deviation indicates high SNR. A fixed value of SNR cannot be defined; however, high SNR can be achieved by minimising variance of the signal. For instance, to achieve high SNR on magnitude of the buck converter transfer function, while injecting perturbation signal and using digital controller, the noise can be reduced by i) using high-bit ADC for low quantisation noise ii) periodic measurement of the signal, or, iii) averaging etc. Therefore, to achieve high SNR at all the frequencies of interest, it is necessary to optimise the amplitude of the perturbation with respect to the gain of the power converter. In order to achieve a given SNR and minimum uncertainty on the measured system response, different aspects of the digital controller and the power converter need to be analysed.

The control-to-output characteristics of the buck converter simulated in SIMetrix shown in Figure 3-4 depict the amplitude of the output voltage and the duty signal. The amplitude of the output voltage is high at lower frequencies compared to the duty signal. Correspondingly, the amplitude of the duty signal is high at higher frequencies, compared to the output voltage.

From the above analysis and assuming the presence of additive white Gaussian noise introduced by samplers, it is not feasible to maintain a constant SNR across the frequency spectrum by injecting a constant amplitude perturbation. This would mean injecting large signals at high frequencies leading to saturation of the duty signal. In addition, it follows that variations/ripple on the output voltage can be measured up to a certain frequency, typically crossover frequency $F_X = (1/20^{th}) \times F_S$ = 10 kHz and two more octaves. However, for the higher frequencies, typically 25 kHz and 50 kHz, the control loop has to be disturbed to measure a significant amount of variation of output voltage from the ambient noise while maintaining the SNR. For instance, assuming the entire loop noise is due to ADC quantisation noise, injecting more than 100 mV of perturbation amplitude would clamp the duty signal. This dictates that to achieve a given SNR

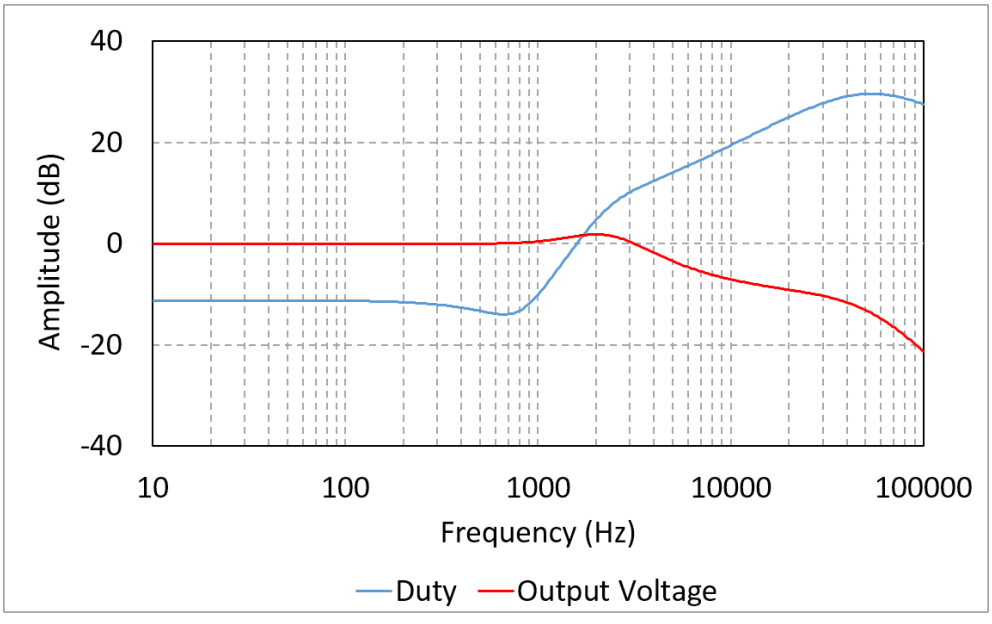

Figure 3-4 Output voltage and duty amplitude of Buck Converter

at higher frequencies, averaging a large number of measurements is essential. Consequently, if the SNR across the band of frequencies is not constant compared to the limited amplitude of the perturbation, which is certainly the case for frequencies greater than the crossover frequency, averaging over large measurements will yield a given SNR. This would certainly increase the measurement time at the expense of a constant SNR across the frequency spectrum.

Moreover, the quantisation noise introduced during analog to digital conversion diminishes the SNR on the transfer function. This can be resolved by using a high-bit ADC. However, if this not feasible (which is the case in the current study), it must be guaranteed that the amplitude of the perturbation signal is greater than the voltage resolution of the ADC at all frequencies of interest. In other words, the perturbation amplitude must be greater than single Least Significant Bit (LSB) of the ADC. Otherwise, the signal will be buried in the digital quantisation noise and will remain undetected during the frequency response measurements.

Therefore, at first, a constant amplitude perturbation signal is injected in the system to understand the characteristic behaviour of the system and estimate the standard deviation. The periodic and harmonically-related perturbation signal defined by the amplitude $\mathrm{A_p}$ and frequency $\mathrm{F}_p$describes

$$\mathrm{p(n)} = \sum_{\mathrm{k=1}}^{\mathrm{F}} \mathrm{A_{p_k}} \,.\sin\left(\frac{2\pi\, n}{N} 2^k + \,\theta_{\mathrm{p_k}}\right) \tag{3-3}$$

where F defines the total number of frequency sweeps providing harmonic sinusoids from 97 Hz to 50 kHz, *N* defines the length of the sequence as in power of two and θ_{p} is the phase between the different sinusoids. The phase is defined zero for initial measurements.

Consequently, perturbation amplitude is modified to achieve less than 2 % standard deviation on output voltage and between 3 %-5 % on duty signal. The

perturbation amplitude is then revised based on the following boundary conditions:

- For frequencies below the crossover frequency, low-perturbation amplitude satisfies a high SNR on the transfer function. However, high gain of the integrator necessitates superimposing a large AC perturbation of the order of 100 mV to measure the small-signal response of the output voltage.
- For frequencies above the crossover frequency, a high SNR on the duty signal, i.e. a large signal on the duty necessitates superimposing a small amplitude of the perturbation to achieve a given SNR on the transfer function.
- For intermediate frequencies, the perturbation amplitude must be relatively low to avoid clipping of the output signal.

The proposed multi-tone sinusoid reduces measurement time as the transients that appear at each frequency sweep will only be present at the first perturbation frequency.

3.5 Non-Parametric FRF Measurements

It is recognised from the principles that frequency-domain identification in continuous-time systems with the BL assumption associates the system model coefficients with the power stage components. Therefore, frequency domain identification of the power converter is best suited to realise the purpose of the health-monitoring tool.

The Fourier transform of a finite-length N of a sequence $x(n)$, i.e.

$$x(n) = \begin{cases} 0 \; for \; n < 0 \\ x(n) \; for \; n \geq N \end{cases} \tag{3-4}$$

is

$$X(\omega) = \sum_{n=0}^{N-1} x(n) e^{-j\omega n} \tag{3-5}$$

where $0 \leq \omega \leq 2\pi$ is the angular frequency and N is the total number of integer samples in a single period. The DFT of a real-valued sequence $x(n)$ sampled at equally-spaced frequencies $\omega = {2\pi k}/{N}$ where $k = 0, 1, 2 \ldots N-1$ has a complex spectrum defined by

$$X(k) = \sum_{n=0}^{N-1} x(n) e^{-j\frac{2\pi k}{N}n} \tag{3-6}$$

Generally, the length of the sequence N is fixed and an integer power of two. The rationale behind this selection is because memory address in the majority of digital controllers is byte-addressable rather than decimal-addressable, which minimises leakage errors in DFT computation. A sequence length $N \neq 2^9, 2^{10}, 2^{11}$, and so on, requires zero padding that introduces spectral spurs and inefficient detection of the signal at a frequency of interest.

The above complex-valued discrete-time sequence can also be represented as the sum of the in-phase and quadrature components, i.e. the

$$X(k) = X_I(k) + j\, X_Q(k) \tag{3-7}$$

where $X_I(k)$ and $X_Q(k)$ represent real-valued discrete quadrature sequences representing real and imaginary components. These quadrature components are calculated from sampled sequence multiplied with sine and cosine of the perturbation frequency $\omega_k = \frac{2\pi k}{N}$

$$X_I(k) = \frac{2}{N}\sum_{n=0}^{N-1} x(n)\sin\left(\frac{2\pi k}{N}\, n\right) \tag{3-8}$$

$$X_Q(k) = \frac{2}{N}\sum_{n=0}^{N-1} x(n)\cos\left(\frac{2\pi k}{N}\, n\right) \tag{3-9}$$

Similarly, the sampled output sequence yields

$$Y_I(k) = \frac{2}{N}\sum_{n=0}^{N-1} y(n)\sin\left(\frac{2\pi k}{N}\, n\right) \tag{3-10}$$

$$Y_Q(k) = \frac{2}{N}\sum_{n=0}^{N-1} y(n)\cos\left(\frac{2\pi k}{N}\, n\right) \tag{3-11}$$

The sampled complex in-phase and quadrature sequence at a specific perturbation frequency finally provides the magnitude and phase response of a sequence at that frequency.

$$|H(k)| = \sqrt{\frac{\left(Y_I(k)\right)^2 + \left(Y_Q(k)\right)^2}{\left(X_I(k)\right)^2 + \left(X_Q(k)\right)^2}} \tag{3-12}$$

$$\arg(H(k)) = \tan^{-1}\left(\frac{Y_I(k) + j\, Y_Q(k)}{X_I(k) + j\, X_Q(k)}\right) \tag{3-13}$$

This concept of quadrature demodulation to compute the non-parametric estimate of the system, instead of calculating the amplitude and phase response of the system directly, extracts even the smallest amplitude of the in-phase and

the quadrature phase sampled signal and provide a spectrally-efficient response of the demodulated signal.

The FRF algorithm based on the concept of in-phase and Quadrature (IQ) demodulation, initialise Sine and Cosine signals prior to injecting constant amplitude multi-tone perturbation as shown in Figure 3-5. The output voltage sampled by ADC, while duty signal captured by DPWM, is acquired and stored as variables Vout and Duty. These variables are then, i) summed to calculate steady state values, SumVout and SumDuty, and multiplied by sine and cosine signals to calculate in-phase and quadrature signals - $IV_{\mathrm{o}}(k)$, $QV_{\mathrm{o}}(k)$, $ID(k)$ and $QD(k)$.

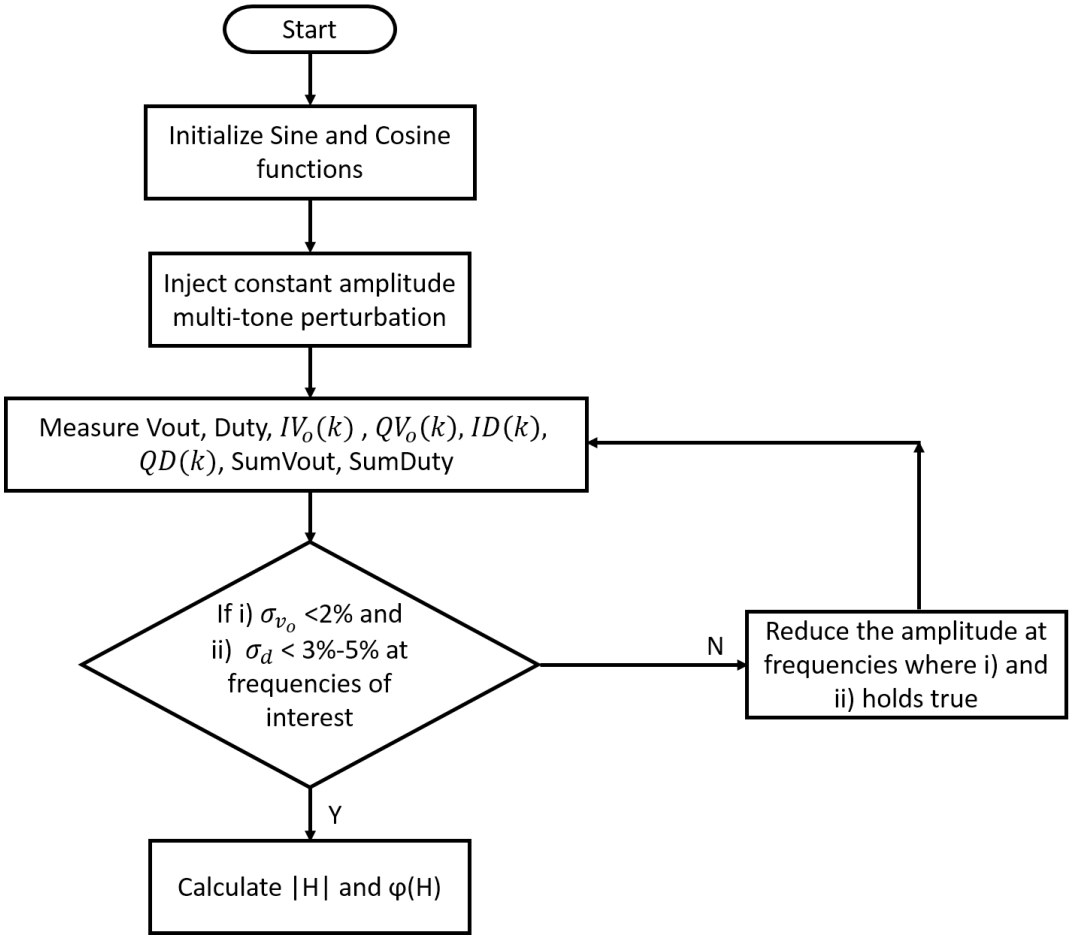

Figure 3-5 IQ demodulation algorithm

The algorithm stores steady state, quadrature output voltage and duty signals in six separate column vectors of size $Acq \times F$, where the first F rows of a column vector contain data of a single acquisition for all the perturbed frequencies and Acq as the number of acquisitions. For example, if the column vector length is 64×10, the first ten rows correspond to data for ten perturbation frequencies of a single acquisition. The six column vectors comprise $IV_{\mathrm{o}}(k)$ – the in-phase component of the output voltage, $QV_{\mathrm{o}}(k)$ – the quadrature phase component of the output voltage, $ID(k)$ – the in-phase component of the duty signal, $QD(k)$ – the quadrature phase component of the duty signal, SumVout – the steady state value of the output voltage and SumDuty – the steady state value of the duty signal. The four quadrature phase sequences are

$$IV_{\mathrm{o}}(k) = \frac{2}{N}\sum_{n=0}^{N-1} v_o(n)\sin\left(\frac{2\pi k}{N}\,n\right) \tag{3-14}$$

$$QV_{\mathrm{o}}(k) = \frac{2}{N}\sum_{n=0}^{N-1} v_o(n)\cos\left(\frac{2\pi k}{N}\,n\right) \tag{3-15}$$

$$ID(k) = \frac{2}{N}\sum_{n=0}^{N-1} d(n)\sin\left(\frac{2\pi k}{N}\,n\right) \tag{3-16}$$

$$QD(k) = \frac{2}{N}\sum_{n=0}^{N-1} d(n)\cos\left(\frac{2\pi k}{N}\,n\right) \tag{3-17}$$

where the complex sequence can be written as

$$V_o(k) = IV_{\mathrm{o}}(k) + j\,QV_{\mathrm{o}}(k) \tag{3-18}$$

$$D(k) = ID(k) + j\,QD(k) \tag{3-19}$$

The data from the four vectors ($IV_{\mathrm{o}}(k)$,$QV_{\mathrm{o}}(k)$,$ID(k)$, and $QD(k)$) is re-arranged to construct the output voltage matrix $V_{\mathrm{o}_{(Acq\times F)}}$ Equation (3-20) and duty signal $D_{(Acq\times F)}$ Equation (3-21) matrix of size $Acq \times F$, where Acq define the number of acquisitions = 64 and the F define the number of perturbation frequencies = 10. The first column represents the start frequency 97.65 Hz and last column represents the end frequency 50 kHz.

The start and stop frequency of 97.65625 Hz and 50 kHz for the perturbation signal define the pass-band for a second-order system. The signals below 100 Hz and above 50 kHz are important to understand overall system characteristics nevertheless, are insignificant for anomaly detection in discrete components. The start frequency is calculated based on the switching frequency of the converter and aforementioned frequency selection method. Therefore,

$$200\ kHz\ /\ (2\text{^}11)\ =\ 97.65625\ Hz\ and\ 200kHz\ /\ (2\text{^}2)\ =\ 50kHz.$$

$$V_{\mathrm{o}_{(Acq\times F)}} = \begin{bmatrix} IV_{\mathrm{o}_{(0\times F_{k0})}} + jQV_{\mathrm{o}_{(0\times F_{k0})}} & \cdots & IV_{\mathrm{o}_{(0\times F_{kF})}} + jQV_{\mathrm{o}_{(0\times F_{kF})}} \\ \vdots & \ddots & \vdots \\ IV_{\mathrm{o}_{(Acq\times F_{k0})}} + jQV_{\mathrm{o}_{(Acq\times F_{k0})}} & \cdots & IV_{\mathrm{o}_{(Acq\times F_{kF})}} + jQV_{\mathrm{o}_{(Acq\times F_{kF})}} \end{bmatrix} \tag{3-20}$$

$$D_{(Acq\times F)} = \begin{bmatrix} ID_{(0\times F_{k0})} + jQD_{(0\times F_{k0})} & \cdots & ID_{(0\times F_{kF})} + jQD_{(0\times F_{kF})} \\ \vdots & \ddots & \vdots \\ ID_{(Acq\times F_{k0})} + jQD_{(Acq\times F_{k0})} & \cdots & ID_{(Acq\times F_{kF})} + jQD_{(Acq\times F_{kF})} \end{bmatrix} \tag{3-21}$$

The complex division of $V_{\mathrm{o}_{(Acq\times F)}}$ and $D_{(Acq\times F)}$ matrix then constructs the complex transfer function matrix

$$H_{(Acq\times F)} = \begin{bmatrix} H_{(0\times F_{k0})} & \cdots & H_{(0\times F_{kF})} \\ \vdots & \ddots & \vdots \\ H_{(Acq\times F_{k0})} & \cdots & H_{(Acq\times F_{kF})} \end{bmatrix} \tag{3-22}$$

where

$$H_{(0\times F_{k0})} = \frac{IV_{\mathrm{o}(0\times F_{k0})} + jQV_{\mathrm{o}(0\times F_{k0})}}{ID_{(0\times F_{k0})} + jQD_{(0\times F_{k0})}} \tag{3-23}$$

From the above analysis, a non-parametric estimate of the continuous-time system model $H_{NP}(\mathrm{s_k})$ expressed as the ratio of output to input response calculates

$$H_{NP}(\mathrm{s_k}) = \frac{V_{\mathrm{o}}(\mathrm{s_k})}{D(\mathrm{s_k})} = H_{\mathrm{I}}(\mathrm{s_k}) + j\,\mathrm{H_Q}(\mathrm{s_k}). \tag{3-24}$$

The system response i.e. magnitude and phase matrices for all the perturbation frequencies is then defined by Equations (3-25) and (3-26).

$$|H(\mathrm{s_k})| = \sqrt{\left(H_{\mathrm{I}}(\mathrm{s_k})\right)^2 + \left(H_{\mathrm{Q}}(\mathrm{s_k})\right)^2} \tag{3-25}$$

$$\varphi\big(H(\mathrm{s_k})\big) = \tan^{-1}\left(\frac{H_{\mathrm{Q}}(\mathrm{s_k})}{H_{\mathrm{I}}(\mathrm{s_k})}\right) \tag{3-26}$$

$\mathrm{s_k}$ defines the set of injected perturbation frequencies.

From these FRF measurements at different perturbation frequencies, a non-parametric system model is estimated prior to parametric identification of the model. This identification enables understanding the source of different uncertainties and nonlinear distortions in the system and ultimately, extracting a non-parametric noise model. The graphical examination of the system model may

also require modification to the perturbation amplitude and the excited frequencies of interest for their intended applications.

3.6 Parametric Model Identification

The process of parametric model identification is dependent on the non-parametric FRF measurements. The uncertainties in the measured data, such as quantisation noise, switching noise, measurement errors, and errors including DFT noise, etc., influence accurate identification of the system model. These uncertainties further lead to inaccurate estimation of model parameters, extraction of component values, and erroneous interpretation of degradation. Therefore, it is emphasised throughout the development of the monitoring tool that uncertainties introduced by the digital control and the measurement process must be minimised. In this study, the majority of these uncertainties are eliminated by using a periodic excitation and synchronous demodulation of system dynamical characteristics. The combination of the above techniques ensures minimum uncertainty on the measured data set, as illustrated in the previous sections.

For parametric identification, the model estimator targets reducing the error between the measured transfer function $\mathrm{H_{NP}}(\mathrm{s_k})$ and the assumed system model $\mathrm{H_P}(\mathrm{s_k})$. The tool assumes the ratio of frequency-dependent complex polynomials $N(\mathrm{s_k})$and $D(\mathrm{s_k})$, i.e. Laplace rational fraction in continuous-time domain as the system model defined by Equation (2-6).

Mathematically, summing the magnitude of the residual sum of squares and equating the partial derivative of summation with respect to the coefficients equal to zero, the absolute error minimises to

$$|\varepsilon_k|^2 = \sum_{k=1}^{F} |\mathrm{H_{NP}}(\mathrm{s_k}) - \mathrm{H_P}(\mathrm{s_k})|^2 = \sum_{k=1}^{F} \left| \mathrm{H_{NP}}(\mathrm{s_k}) - \frac{\mathrm{N}(\mathrm{s_k})}{\mathrm{D}(\mathrm{s_k})} \right|^2 \qquad (3\text{-}27)$$

The above non-linear cost function can be minimised using non-linear optimisation techniques. However, such methods depend entirely on the initial values. The simple least squares estimator cannot identify the non-linear function expressed in the form of the rational fraction. Instead, a linear model is essential.

The linearisation of the cost function introduces a weighing function $D(s_k)$, which modifies the cost function to

$$|\varepsilon'_k \,.\, D(s_k)|^2 = \sum_{k=1}^{F} |H_{NP}(s_k) \,.\, D(s_k) - N(s_k)|^2 \tag{3-28}$$

This unknown weighing function, which is a frequency-dependent vector, results in an ill-conditioned normal equation for a transfer function measured over several decades of the frequency range. The cost function assumes relative maxima when the weighing function is in the local minima. Correspondingly, the local minima in the weighing function results in local minima of the measured transfer function. Concisely, the magnitude of the error is dependent on the weighing function. In addition, for noisy measurement data, the linearised cost function results in inaccurate fit of the model. Therefore, an iterative computation is required to achieve close approximation of the measured transfer function. The iterative algorithm minimises the cost function by constraining one of the coefficients to a constant and iteratively solves for the remaining coefficients.

$$|\varepsilon''_k|^2 = \left|\frac{\varepsilon_k \,.\, D(s_k)_i}{D(s_k)_{i-1}}\right|^2 = \sum_i \sum_{k=1}^{F} \left|\frac{H_{NP}(s_k) \,.\, D(s_k)_i}{D(s_k)_{i-1}} - \frac{N(s_k)_i}{D(s_k)_{i-1}}\right|^2 \tag{3-29}$$

where i denotes the iteration number. The subsequent iterations of the algorithm allow $D(s_k)_{i-1}$ to asymptotically approach $D(s_k)_i$ while updating the weighing function and the coefficients in every iteration. By assuming d_0 = 1 as the initial

starting value, the absolute error function/cost function is minimised at all the experimental points.

However, the absolute error function can still result in an erroneous estimate of the system model because the measured transfer function entails measurement errors and system uncertainties. In addition, there is still an unknown quantity in the cost function. To overcome this scenario, the relative error function/cost function is preferred. The relative error defines how large the error is in relation to the measured value rather than how large the error is. The modified cost function minimises the relative error between the measured transfer function and the estimate system model.

$$|\varepsilon'''_{\mathrm{k}}|^2 = \left|\frac{\varepsilon_{\mathrm{k}} \,.\, D(\mathrm{s_k})_{\mathrm{i}}}{\mathrm{D(s_k)_{i-1}} \,.\, \mathrm{H_{NP}(s_k)}}\right|^2 \tag{3-30}$$

$$|\varepsilon'''_{\mathrm{k}}|^2 = \sum_{\mathrm{i}} \sum_{\mathrm{k=1}}^{\mathrm{F}} \left|\frac{\mathrm{H_{NP}(s_k)} \,.\, \mathrm{D(s_k)_i}}{\mathrm{D(s_k)_{i-1}} \,.\, \mathrm{H_{NP}(s_k)}} - \frac{\mathrm{N(s_k)_i}}{\mathrm{D(s_k)_{i-1}} \,.\, \mathrm{H_{NP}(s_k)}}\right|^2 \tag{3-31}$$

In this method, at $\mathrm{i} = 0$, the unknown weighing function is defined based on previous analysis of the measured amplitude response. This algorithm is limited to only one iteration. However, the number of iterations can be increased for an optimum result. This relative error criterion combined with a weighing and iterative process yields best fit for the system model. The estimated best-fit model defined in the form of a Laplace rational fraction enables extracting the model coefficients and the component values thereafter. For example, if the best-fit model matches a second-order Laplace rational fraction of the system, comparison of the extracted and the actual circuit component values provides an estimate of degradation or anomalies in the system and the electronic components.

The parametric model identification algorithm based Weighted Recursive Least Square (WLS) is executed in MathCAD. The entire algorithm is explained in Appendix B.

3.7 Parameter Extraction

The majority of the research works described in the previous chapter identify the system model to inform its identification. However, they fail to estimate the model (numerator and denominator) coefficients and the subsequent power stage component values that give a clear indication of the deviation of the circuit components from their actual values. The identification of model parameters and subsequent circuit components is essential as it detects drift in the system and the components from its healthy state and enables accurate detection of degradation.

Reproducing the results from the previous section, the identified model defines the system as a second or third-order system depending on the power stage network. Using the equivalent Laplace model of a power stage network defined by

$$H(s_k) = \frac{n_0 + s_k\, n_1 + s_k^2\, n_2 + ..}{d_0 + s_k d_1 + s_k^2 d_2 + ..} \tag{3-32}$$

the model coefficients n_0, n_1, d_0,d_1 and d_2 represent the power stage network elements.

As an illustration, for a basic DC-DC buck converter in Figure 3-2, the power stage network forms a second-order system as it contains two energy storing passive components. Therefore, the equivalent Laplace model of a second-order is defined by

$$H(s_k) = \frac{n_0 + s_k\, n_1}{d_0 + s_k d_1 + s_k^2 d_2} \tag{3-33}$$

where the model coefficients represent

$$n_0 = K\frac{R_{Load}}{(R_{Load} + r_{L+S})} \tag{3-34}$$

$$n_1 = K\frac{R_{Load}}{(R_{Load} + r_{L+S})} C r_c \tag{3-35}$$

$$d_1 = \frac{r_{L+S} C (R_{Load} + r_C + R_{Load} r_C) + L}{(R_{Load} + r_{L+S})}. \tag{3-36}$$

$$d_2 = L C\frac{(R_{Load} + r_C)}{(R_{Load} + r_{L+S})} \tag{3-37}$$

K defines the sum of input voltage and S_2 knee voltage drop.

3.8 Chapter Summary

This chapter answers the second research question of analysing the specific algorithms that are robust and rugged in terms of system change and other dependencies. The approach for system identification based health monitoring tools and techniques reveal that the choice of the identification scheme is highly dependent on the application and the underlying noise characteristics. A clear understanding of the application provides a direct answer to some of the methods the user should take into consideration.

Reflecting the design objective of this research to detect degradations and anomalies in passive power supply components, the research proposes a dual-system identification that combines both non-parametric and parametric methods. The main developments of this chapter can be outlined as follows:

- A band-limited inter-sample interpolation of the sampled signals rather a conventional Zero-Order-Hold assures that the observed signals contain no energy above a certain frequency.

- The use of multi-tone perturbation with an optimised amplitude spectrum and user-defined frequency resolution to address the design objective, i.e. to understand the characteristics of the system at the ESR frequency of interest.
- The selection of a continuous-time model to describe the physical aspects of the system.
- A coherent/synchronous demodulation algorithm to extract the frequency response of the system.
- A parametric frequency-domain identification of the continuous-time model using a Weighted Recursive Least Square estimator that minimises the relative error instead of the absolute error.
- The parametric extraction of the model coefficients and circuit component values from the identified model.

4 Experimental Results

The intention of this chapter is to implement and substantiate the proposed methodology as a potential technique for detection of degradation or anomalies in the system.

The third chapter demonstrated the proof of concept on a simple ‘buck’ topology of DC-DC power converters. A COTS digital controller regulates the DC-DC converter through feedback compensation while performing online health monitoring. The study uses an Integrated Development Environment (IDE) development tool to demodulate the frequency response measurements synchronously and MathCAD to estimate and identify the parametric system model. The IDE injects a digital perturbation signal in the closed control loop and executes the measurement algorithm. MathCAD uses the measured non-parametric system response to identify the parametric model and extract the model coefficients and the circuit component values.

4.1 Experimental Setup

A practical electronic system is required to demonstrate and verify the proposed technique. The search for an electronic system, in particular, a digitally-controlled DC-DC low-voltage power converter started by finding a COTS application kit. Texas Instruments provides a range of experimental kits for power supply applications. However, these are limited to a high voltage range. Therefore, this research adopts integrating a COTS synchronous low-voltage forward converter and a COTS digital controller. The rationale for using a low-voltage converter is to emulate the power supply rail of the digital load, such as FPGA constrained by the tight voltage tolerance. The typical tolerance requirement of the low-voltage power rail is 2 – 3 %, compared to 5 – 6 % on a high-voltage power rail (for instance, 15 V). This restriction on the selection of the low-voltage power converter enables recognising the implementation of the method on the low-voltage industrial applications.

Given the pros and cons of the FPGA and DSP-based digital controller, a DSP-based microcontroller is preferred. Highlighting the use of digital controllers for health monitoring, this research selects a 32-bit floating-point arithmetic with an integrated ADC, PWM, and an embedded RAM. A large embedded memory allows the user to debug and execute a health-monitoring algorithm on-board the digital controller. The real-time C28x Delfino and Piccolo series MCUs from Texas Instruments (TI) provide sufficient embedded memory to implement the proposed methodology. Therefore, the research selects the 32-bit floating point Piccolo series F28069 control STICK [95] as the digital controller and a low-voltage buck converter as depicted in Figure 4-1.

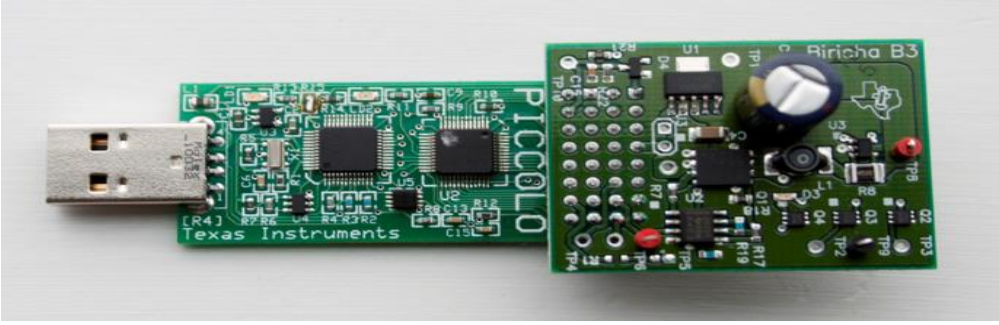

Figure 4-1 Experimental Test Module

The digital controller interfaces to the PC via an on-board USB and the Code Composer Studio (CCS) development tool from Texas Instruments provides on-board JTAG emulation, access to peripherals such as ADC and PWM, and real-time debug to the control algorithm [96]. The CCS IDE controls and monitors the power converter wholly via software re-programmability and flexibility.

Figure 4-2 illustrates the synchronous POL converter powered from input $v_{in}(t)$ =3.3 V to provide a regulated low-voltage output $v_o(t)$ = 1.2 V. The power-train circuit component inductor L, output filter capacitor C and its ESR r_C, resistance of the switching devices, and the output load R_{Load} are defined as L = 150 µH, C = 220 µF, r_C = 90 mΩ, r_{L+S} = 840 mΩ and R_{Load} = 10 Ω. S_1 and S_2 define synchronous switching devices, typically MOSFET or FETKY.

The resistance r_{L+S} signifies the combined resistance of r_L, r_{S1}, r_{S2} and the shunt resistance r_{Shunt}.

$$r_{L+S} = r_L + D\, r_{S1} + (1 - D) r_{S2} + r_{Shunt} \tag{4-1}$$

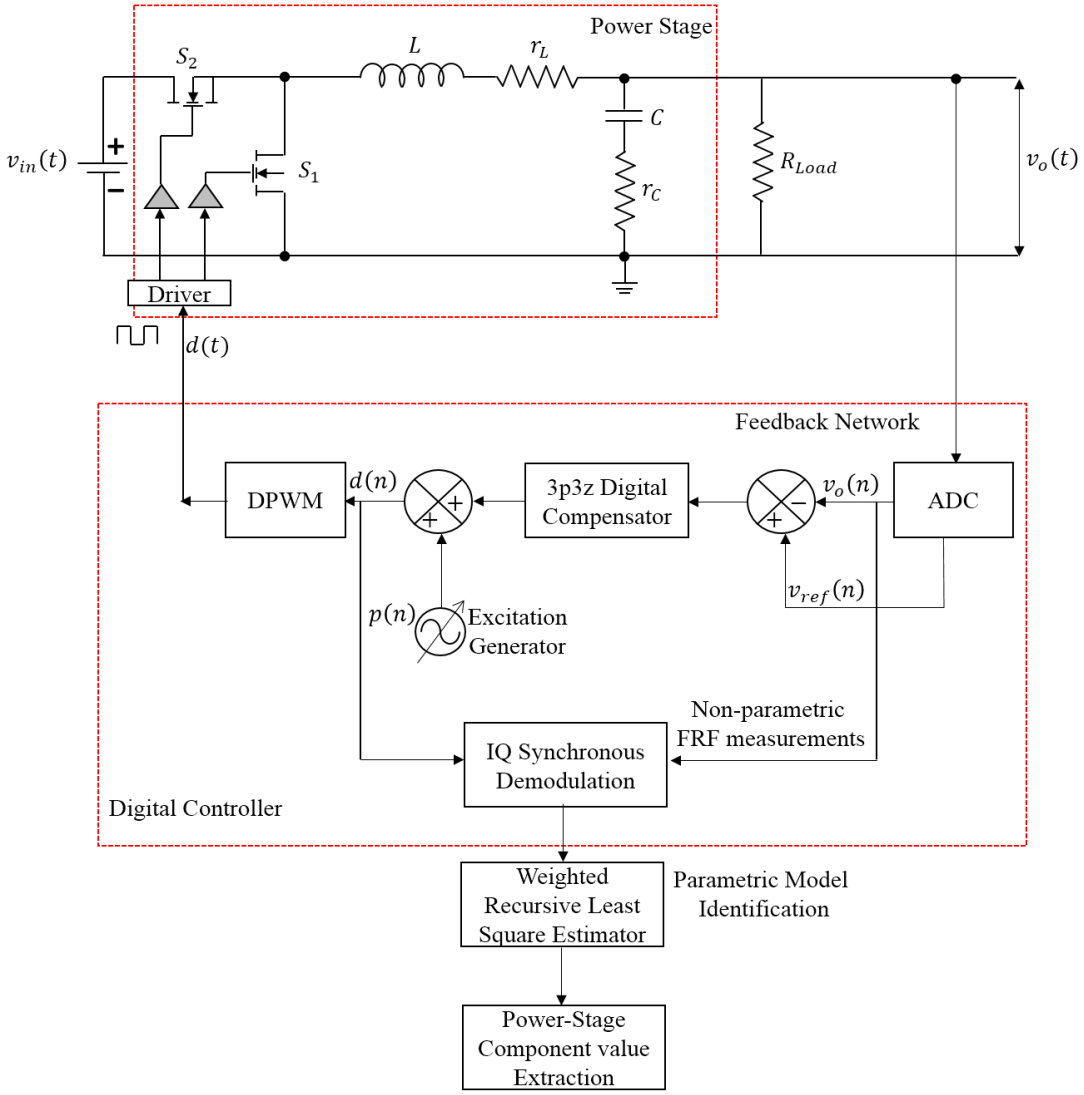

Figure 4-2 Block Diagram of Experimental Test Module

The 12-bit Successive Approximation Register (SAR) ADC with an integrated Sample and Hold (S/H) circuit samples the output voltage $v_o(t)$ at a sampling frequency F_{SP}. The timer-based PWM module generates a pulse width modulated duty signal $d(t)$ after the addition of an excitation signal to the compensated control voltage. The voltage resolution of the timer module, defined as the ratio

of the system clock period and the user-defined switching period F_S, governs the resolution of the duty signal. The Piccolo PWM timer module provides a duty signal resolution of 2.5 mV, given the system period is 12.5 ns and a switching period is 5 µs [97]. To avoid limit cycling [98], Micro Edge Positioning (MEP) integrated in the controller provides a much finer PWM resolution of the order of 36 µV. The CCS IDE provides the selection of the reference signal for the integrated ADC, the design of discrete 3pole-3zero digital Infinite Impulse Response (IIR) filter, and the configuration of the digital pulse-width modulator. The anti-alias filters are designed on the Buck converter PCB.

It is necessary to acknowledge that the input filter modifies the control-to-output system response. However, for initial assessment of the proposed methodology, the study does not consider its design and implications.

In this study, the design of the low-voltage AC perturbation is such that the maximum variation on the output voltage is within ±2.0% of the nominal value and the maximum variation on duty is ±3.0% - ±5.0% of the nominal to achieve a constant SNR across the desired frequency spectrum. Figure 4-3 a) illustrates the outline of the digital perturbation written in C++ and programmed in the digital controller.

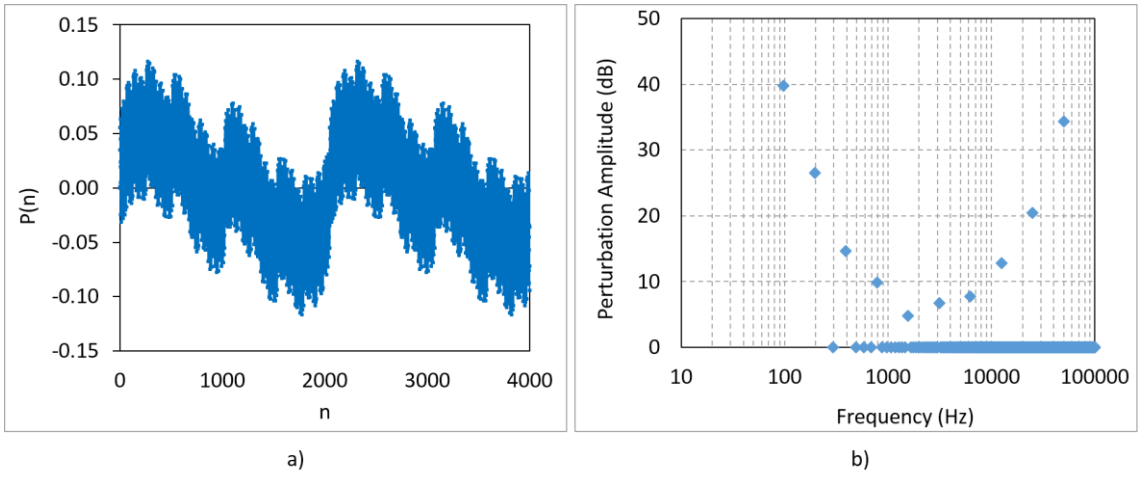

Figure 4-3 Perturbation Signal

a) Discrete domain b) Amplitude spectrum

The amplitude of the perturbation is greater than the voltage resolution of the ADC, ensuring the signal will not be buried in the quantisation noise and the analog noise of the system.

Since the perturbation signal is the sum of harmonically-related sinusoids, the frequency spectrum of the signal represents a comb spectrum as shown in Figure 4-3 b). The discrete tones are synchronised with the switching frequency of the digital controller to minimise leakage errors and the effect of harmonics. Moreover, the factor of two between each frequency gives a programming advantage where the variable ‘frequency’ is right shifted every time to obtain the next frequency thereby saving a lot of computational time. The comb spectrum only injects ten frequency sweeps to obtain the frequency response of the entire system.

4.2 Non-parametric Frequency Response Function (FRF) Measurements

The steady state response of the output voltage and the duty signal in Figure 4-4 depicts that superimposing an optimised multi-tone signal at frequencies of interest does not disturb the steady state response of the converter. The difference between the dashed and the solid lines on the duty signal clearly signifies the low magnitude of perturbation injected in the control loop. Subsequent to this phenomenon, the solid and dashed lines of the output voltage indicate that the superimposed perturbation signal limits the output voltage swing between ±2 %. i.e. 24 mV for a 1.2 V signal.

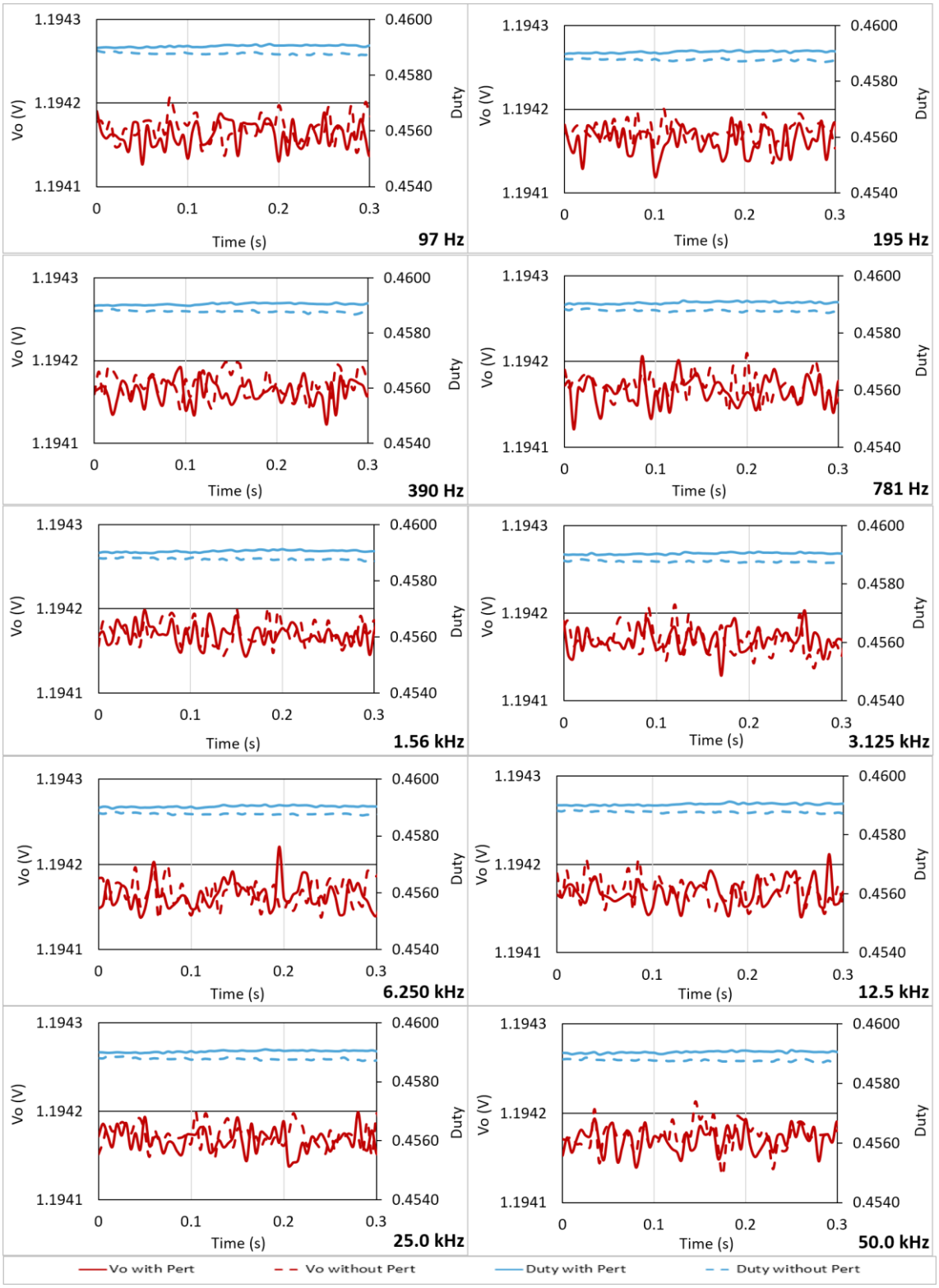

Figure 4-4 Steady State Response of
Output Voltage and Duty with and without Perturbation

The extracted low relative standard deviation on the output voltage σ_{v_o} and the duty σ_d quadrature signals in Figure 4-5 demonstrate that the injected multi-tone perturbation limits the duty within 3 % of its nominal value and the output voltage within 2% for all the frequencies of interest. There is low noise on the output voltage and the duty signal, considering there are other uncertainties in the system, such as quantisation noise of the samplers, measurement noise, and the inherent analog noise of the system. Consequently, this low percentage of the relative standard deviation on the input (output voltage) and the output (duty) indicates low variability on the data set and hence a high SNR on the transfer function.

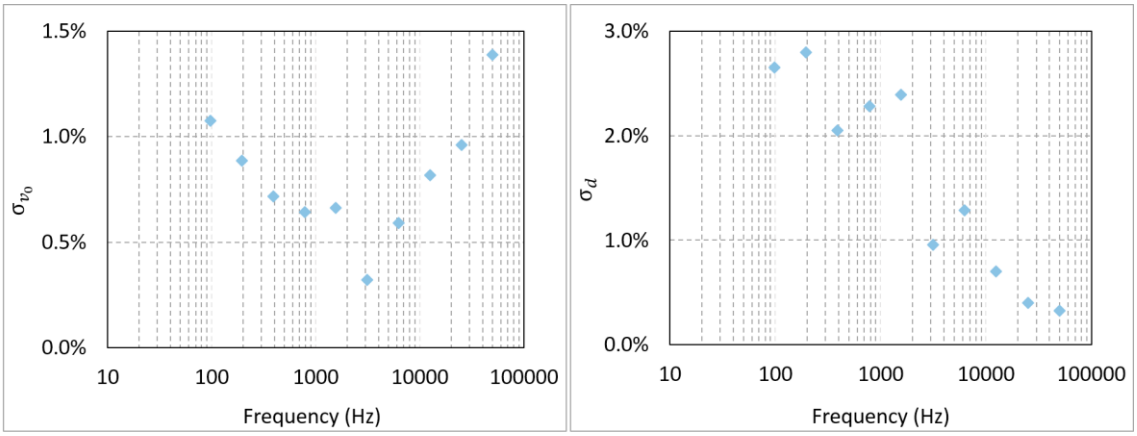

Figure 4-5 Relative Standard Deviation on
a) Output Voltage Signal and b) duty signal

Figure 4-6 shows the measured system response matches the dynamic behaviour of a second-order system. The measured system response matches the dynamic behaviour of a second-order system. However, the uncertainty on the magnitude and phase response describes how the SNR is preserved across the defined frequencies of interest as depicted in Figure 4-7.

The high variability at low frequencies, compared to higher frequencies on both magnitude and phase indicate more noise at the lower frequencies. This noise can be the quantisation noise of the ADC, DPWM or the analog noise of the

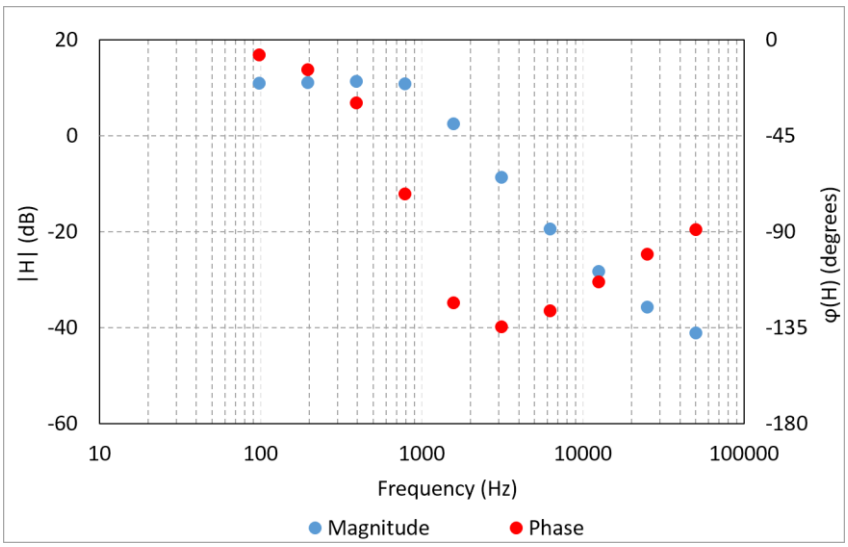

Figure 4-6 Measured System Response

system. The analysis of this noise source is analysed in the following chapters. The high variability at low frequencies, compared to higher frequencies on both magnitude and phase, indicates more noise at the lower frequencies. This noise can be the quantisation noise of the ADC, DPWM or the analog noise of the system. This noise source is analysed in Chapter 6.

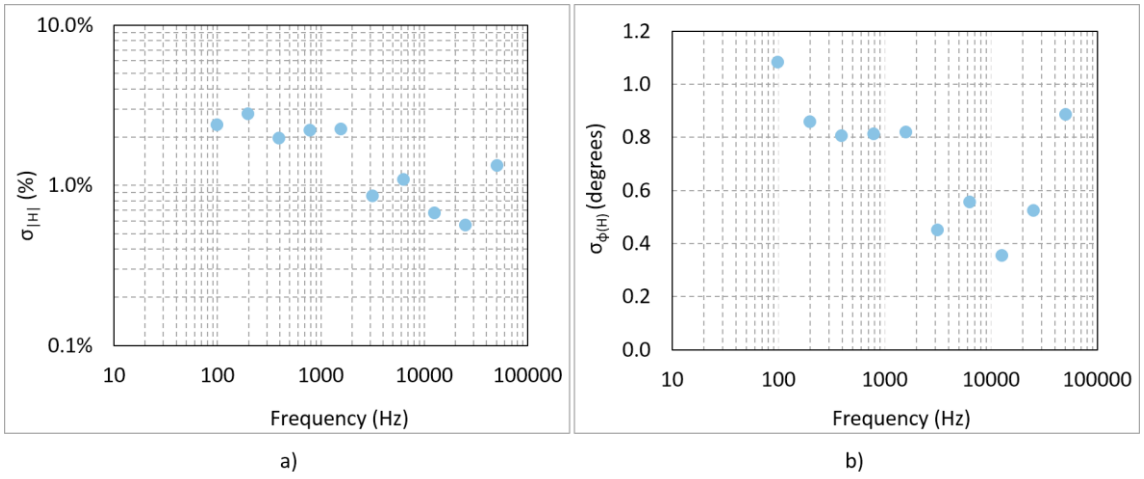

Figure 4-7 Relative Standard Deviation on a) |H(s)| b) φ(H(s))

4.3 Parametric Model Identification

With reference to the results in Figure 4-6, where the amplitude response asymptotically decays by -20 dB/decade at frequency 1 kHz and further rolls off by -20 dB/decade at 5 kHz, the assumption of a second-order system with n = 2 and d = 3 represents a good estimate of the system as illustrated in Figure 4-8. However, the model is verified against a third-order system with n = 2 and d = 4.

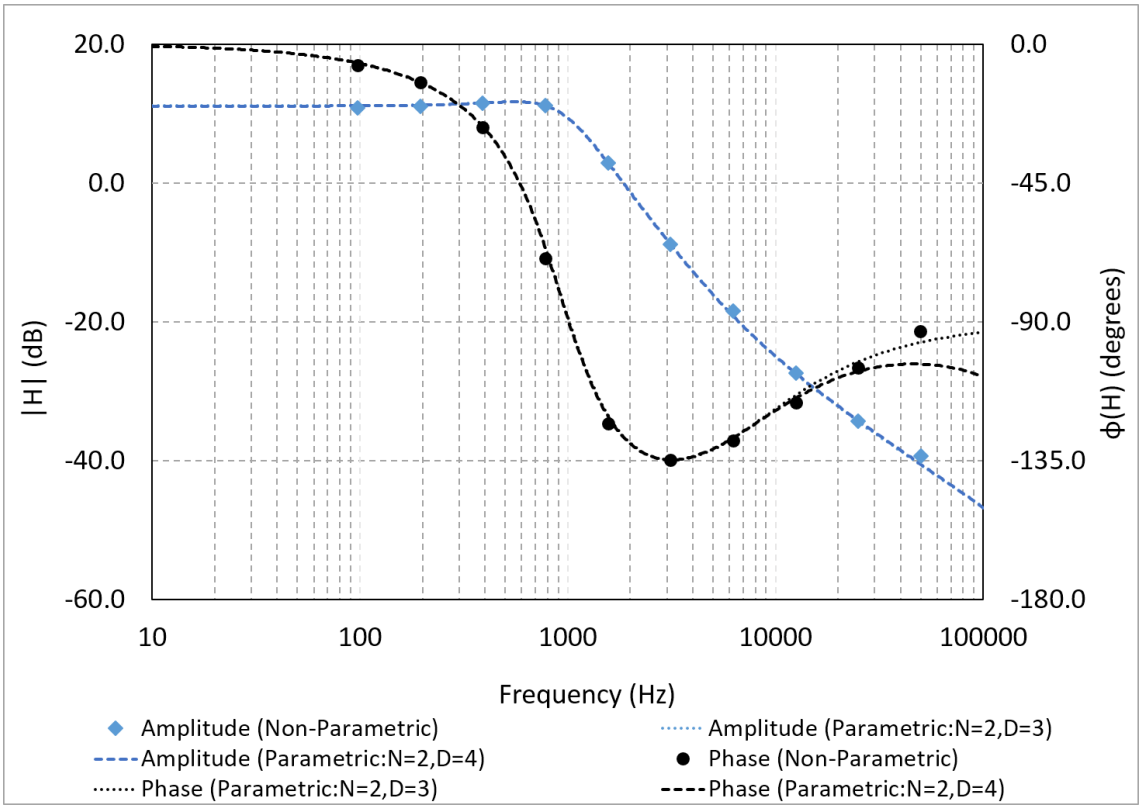

Figure 4-8 Measured System Response and Estimated System Model Order

The response evidently signifies the difference in phase response with a second and a third-order system at the higher frequencies. The close match between the non-parametric measurements and the estimated parametric second-order model of the system indicates that minimising relative error using a Weighted Least Square (WLS) estimator provides a good fit. In addition, the estimator provides a good fit over a wide frequency range from 10 Hz to 10 kHz. In addition, the proposed model identification algorithm does not introduce large errors in the presence of system uncertainties and noisy measurements.

Assuming the inductance and the output load does not change, an estimate of the output capacitance, the ESR of the output filter capacitor, and the resistance of the inductor including the switches can be calculated. Table 4-1 illustrates the comparison between the extracted and actual component values on the buck converter. The estimated capacitance value is within the 20% tolerance of the actual value. Similarly, the extracted ESR shows a consistent result with the actual ESR on the board. It is important to mention that the equivalent Laplace model considers a simple model of the capacitor against a realistic RC ladder model of the electrolytic capacitor.

Component	Actual Value	Estimate Value
C (µF)	220.0	217.8
r_C (mΩ)	90.0	108.0
r_{L+S} (mΩ)	840.0	812.0

Table 4-1 Comparison of Actual and Estimate Component Values

This assures that the proposed parametric identification can be used to detect degradations in switch-mode power supply topologies whilst proper care is taken for the design of perturbation selection, non-parametric FRF measurements, and extraction of model coefficients to minimise the variance on the transfer function.

An important result of the model coefficients in Figure 4-9 demonstrates that all model coefficients converge within one or a maximum of two iterations with an accuracy of ±1%. This reduces the complexity of the model and provides fast identification of the system.

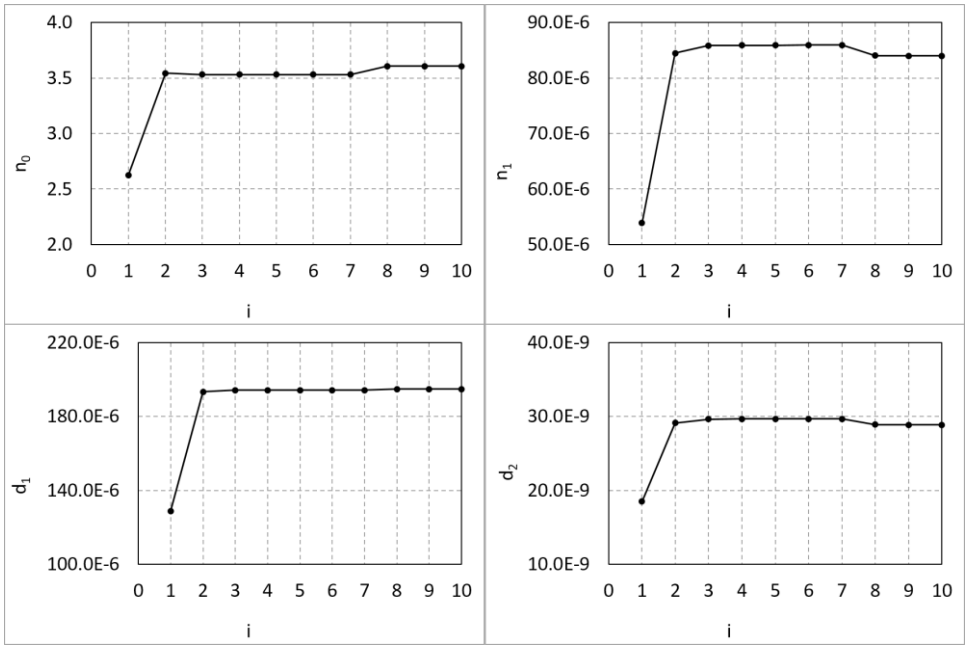

Figure 4-9 Model Coefficient Convergence

4.4 Chapter Summary

This chapter implements the proposed system identification based-health monitoring method on a basic power supply topology. A multi-tone sinusoid perturbation signal with optimised amplitude excites the dynamic non-linear power supply system at specified frequencies of interest. The researcher selects the perturbation frequency based on the characteristic behaviour of the system and the design objectives. The FRF measurement by synchronous demodulation of quadrature signals provides system parameters that govern the inputs to the model identification algorithm. Finally, the WLS estimator reduces the relative error to approximate the Laplace rational fraction of the power supply topology and extract the model coefficients. The extracted component values, in comparison to the actual component values on the experimental test module, proves that the proposed health-monitoring method is accurate and can be used to detect ageing degradations in passive electronic components. The main developments of this chapter can be described as:

- The experimental illustration of the research methodology for a low-voltage power converter evidently assures the method is rugged and robust for high-voltage power converters.
- The observed deviation on the steady-state output voltage and the duty signals proves that the injected multi-tone perturbation limits the output voltage and the duty signals within the required tolerance at all frequencies of interest.
- The synchronous/coherent demodulation of characteristic system parameters provides accurate non-parametric FRF measurement using only ten perturbation frequencies, saving a lot of computational time and reduced complexity. The said development reveals low uncertainty on the system parameters and the measurements, despite the presence of quantisation noise of the samplers, discretisation noise, DFT noise, and analog noise present in the system.
- The parametric identification of the system model with relative minimisation of the cost function across the logarithmic frequency range provides accurate extraction of the power-train component values of the power converter and extracts accurate component values, compared to the actual component values on the buck converter.

  .

5 Anomaly Detection Using System Change

Chapter 5 formulated the modus operandi of the proposed system identification methodology and Chapter 6 described the implementation on a DC-DC digitally-controlled power converter. This chapter intends to corroborate the discussed research methodology for detection of anomalies in the passive electronic components using system change.

5.1 Introduction

The hypothesis that a method can detect ageing degradation or anomalies in passive electronic components is challenging because uncertainty in component tolerances and changes in ambient conditions propagate uncertainty on power-train components. These uncertainties influence the interpretation of degradations stimulating in passive components. Therefore, there will always be a percentage of uncertainty probability associated with the amount of degradation.

The majority of the prognostic and health-monitoring research community proves the hypothesis by performing different acceleration tests. For instance, the acceleration tests, typically HAST or thermal stress, etc., stress the system environmentally or operationally to predict the end of life of the system and/or its components. Subsequently, the continuous monitoring and measurement of certain system parameters along with their theoretical models provide knowledge of anomalies in the system and the components. These predictions are formulated when the system is functioning outside its normal operating conditions. The knowledge of degradation of a system and its components functioning within its operating conditions is not available. In contrast, this study proposes detecting anomalies in passive components by operating the system under normal working conditions.

One method could be to increase the circuit component value and recognise that the health-monitoring methodology detects the system change. For example, an external capacitor connected in parallel with the output capacitor would increase

the overall capacitance of the output filter. It follows from here that if the health-monitoring technique detects the increased external capacitance, it can be argued that the methodology can be used to detect anomalies or ageing degradations in passive electronic components.

5.2 Theoretical Analysis

The analysis of the above hypothesis is first carried out by modelling the system. The system can be modelled in a circuit simulation tool, such as SIMPLIS or a programming tool, such as Simulink. SIMPLIS, a circuit simulation tool, which models the behaviour of non-linear devices effectively is used to model and simulate the second-order buck converter.

A second-order model depicted in Figure 5-1 is a non-synchronous analog voltage-mode buck converter. The analog model includes the parametrised operational amplifier X1 modelled to act as an error amplifier and a parametrised comparator U1 used to compare the error signal and the PWM ramp. The output of this comparator generates a duty signal to switch ON and OFF the power MOSFET. The power MOSFET is modelled as a combination a parametrised switch S2 and a Piecewise Linear Voltage Source (VPWL) R2. Similarly, the Schottky rectifier is modelled as a VPWLS1. The use of parameterised circuit components in the model gives the opportunity to define the behaviour of devices very close to the experimental buck converter. The model also includes ten sinusoidal perturbations (modelled as a sinusoidal waveform generator V4-V13) to represent the AC excitation on the output voltage and the duty.

The power-train components L = 150 µH, C = 220 µF, r_C = 90 mΩ, r_{L+S} = 840 mΩ and R_{Load} = 10 Ω represents the power stage of the buck converter. The model is powered from a 3.3 V input to provide a 1.2 V regulated output voltage.

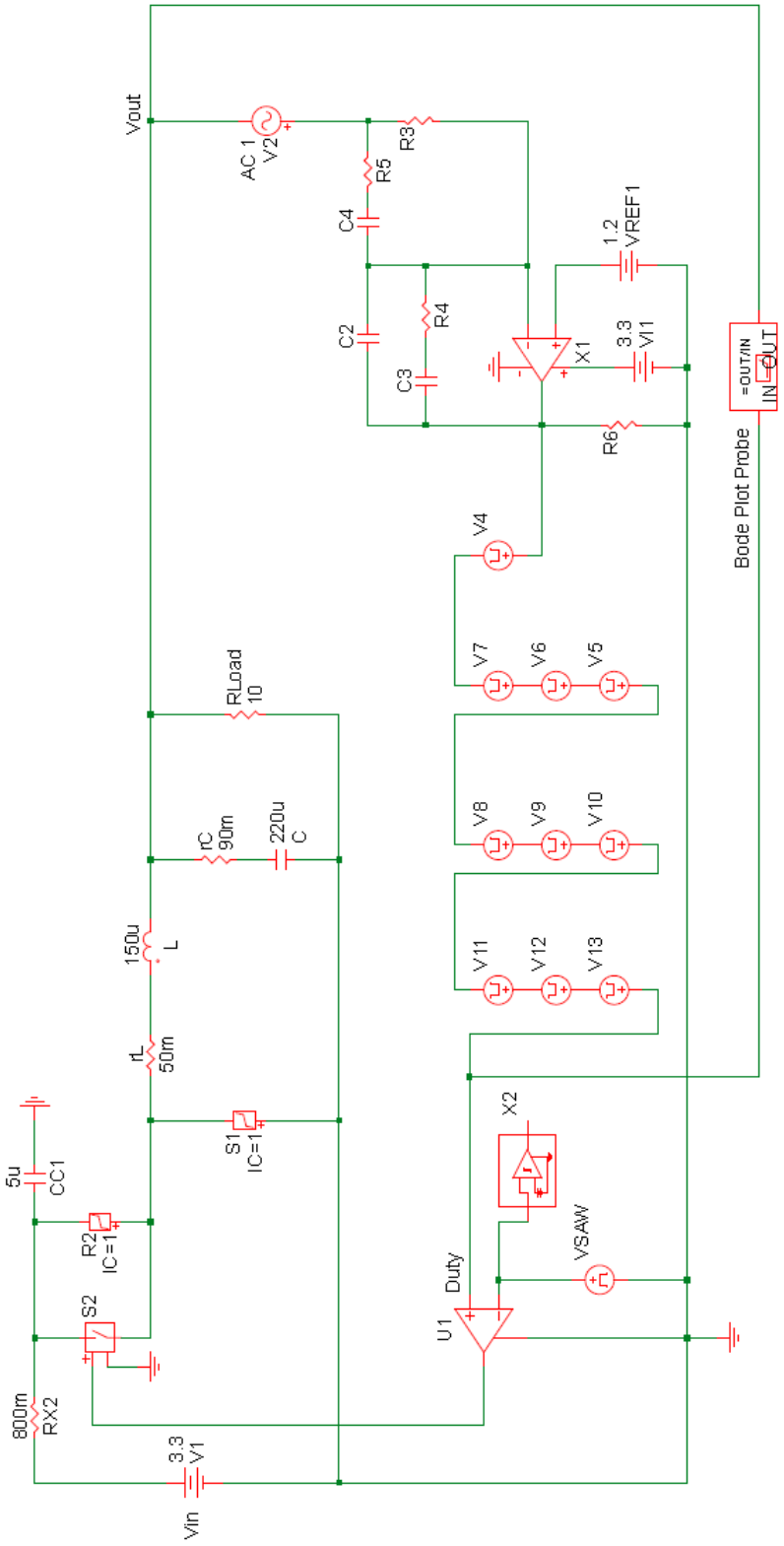

Figure 5-1 Theoretical Model

The transient analysis of the above model shown in Figure 5-2 illustrates the presence of AC excitation on the output voltage and the duty as expected on the experimental buck converter.

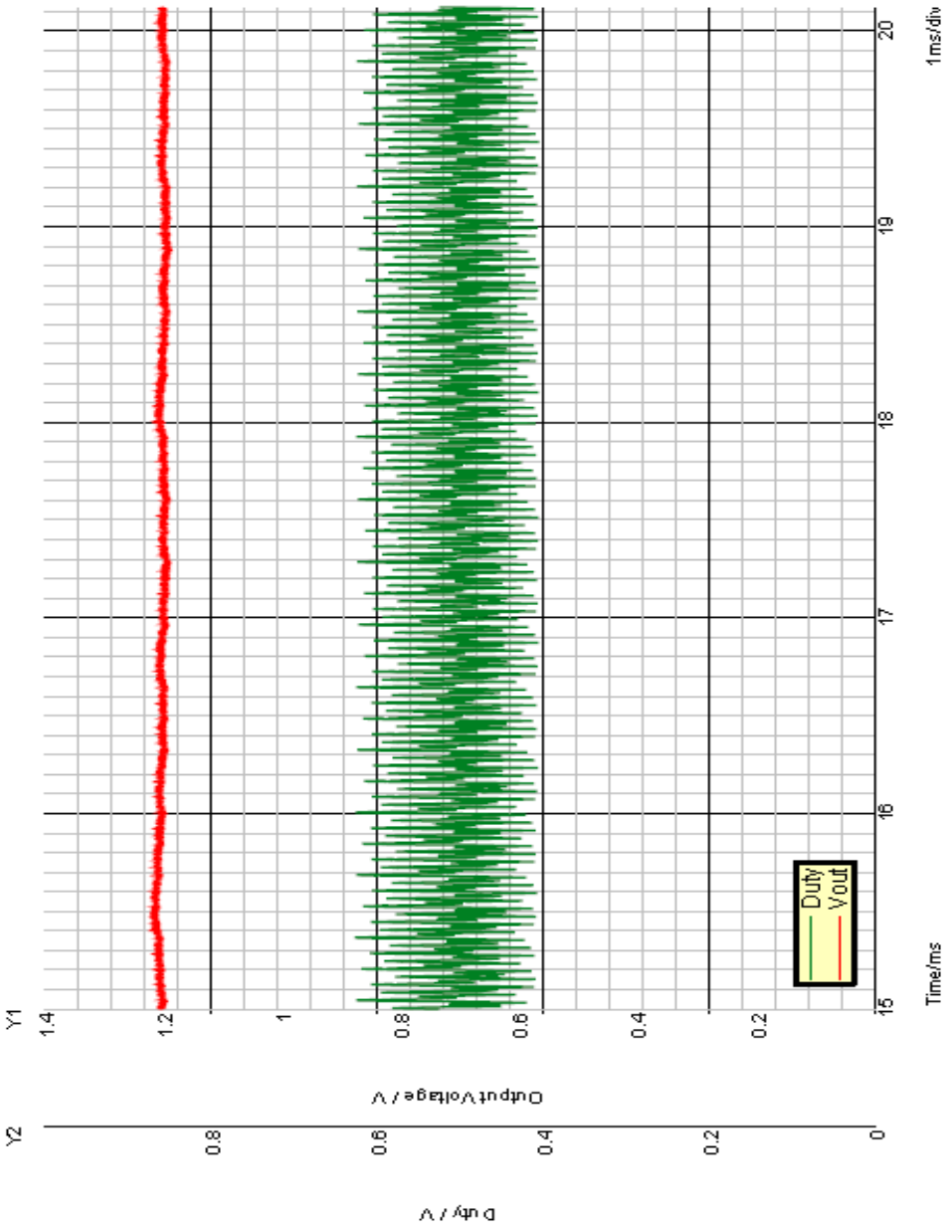

Figure 5-2 Transient Analysis of the Theoretical Model

The fixed Bode plot probe is placed on the duty and the output voltage signal. The Periodic Operating Point (POP) X2 trigger the AC analysis and provides control-to-output transfer function response $H(s)$. Figure 5-3 compares the

theoretical system response obtained from SIMPLIS and the measured transfer-function from the experimental setup.

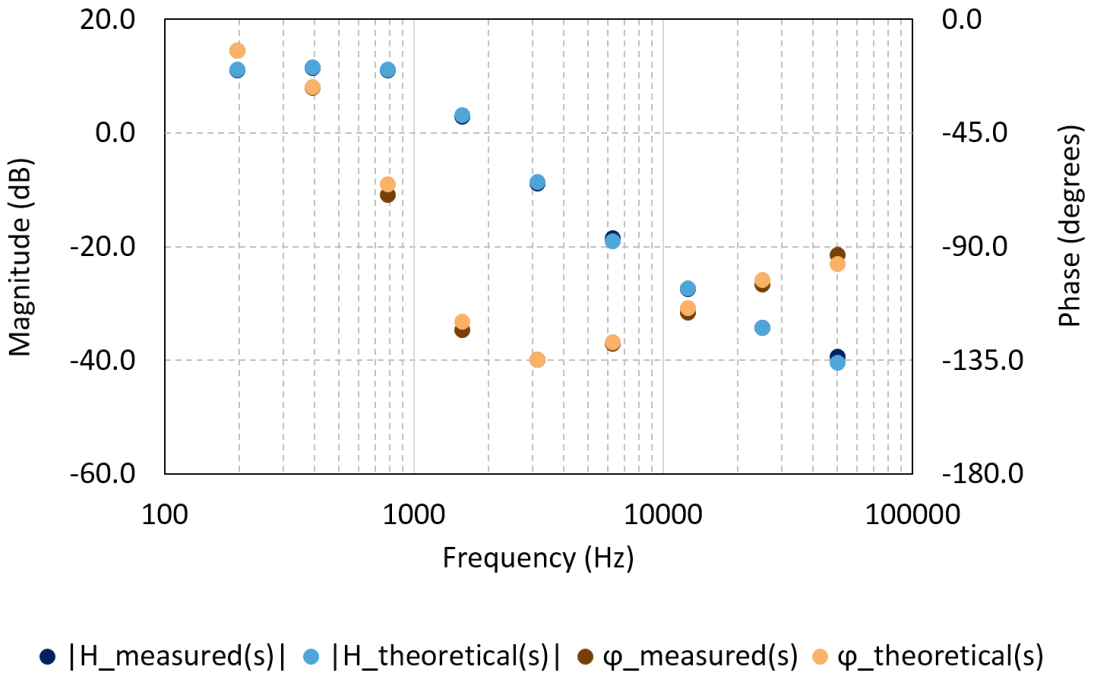

Figure 5-3 AC Analysis of the Theoretical Model Compared with the Measured Transfer Function from the Experimental Test Setup

The equivalence of the magnitude and phase response between the theoretical and the measured transfer function indicate that the theoretical model can be used to represent the experimental test setup. As discussed before, for anomaly detection, an external capacitance C_{EXT} of values 2 µF, 4 µF and so on, is added across the output capacitor, as shown in Figure 5-4. Twelve capacitors with values ranging from 2 µF to 30 µF are placed sequentially as external capacitance in the circuit.

According to the above hypothesis, if the WLS identification algorithm is able to detect this change from the measured theoretical transfer function, it infers that the algorithm is robust and rugged enough for use in system identification applications.

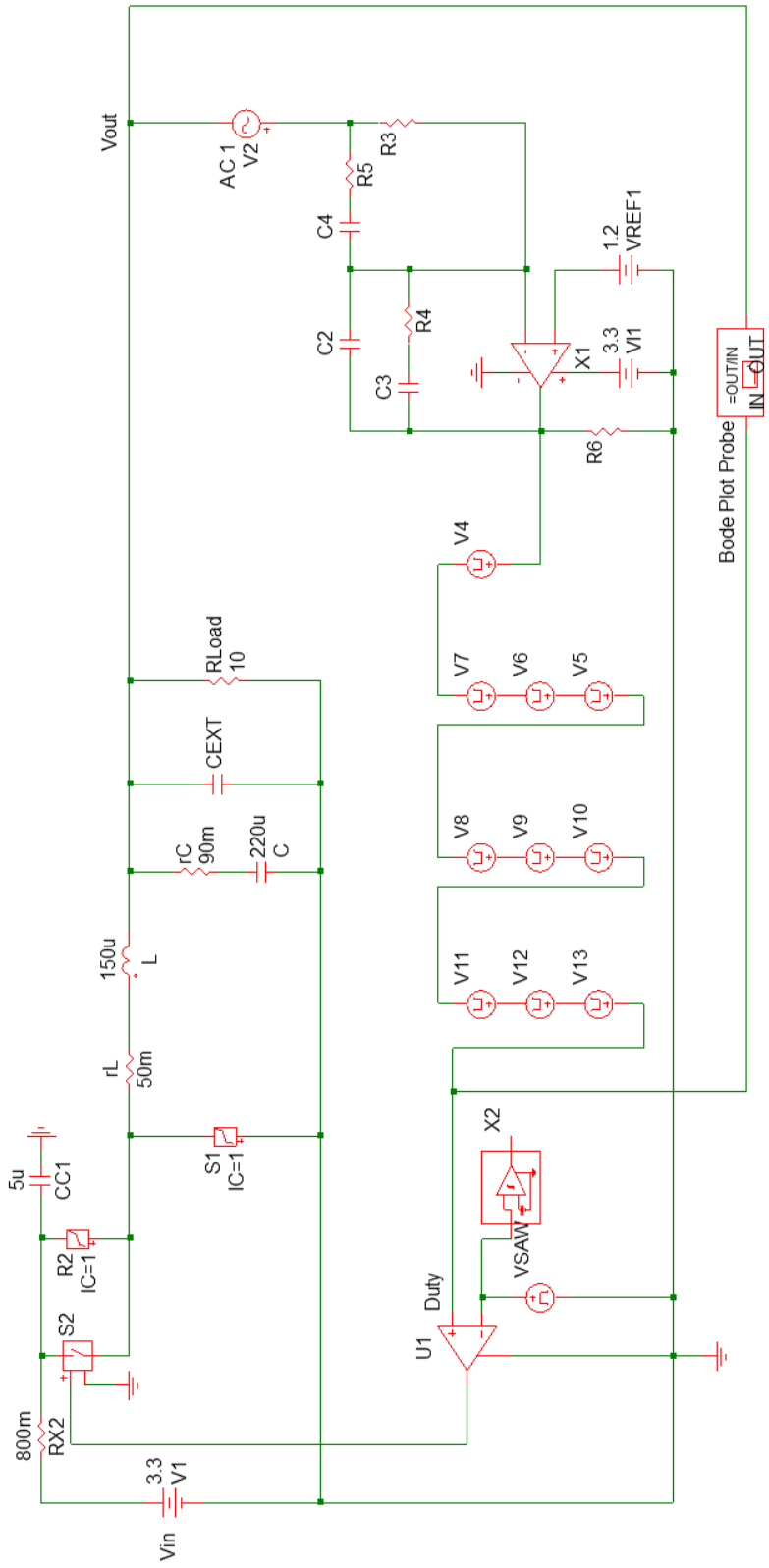

Figure 5-4 Theoretical Model with External Capacitor for Anomaly Detection

The WLS identification of the total capacitance from the theoretical transfer function response with different external capacitors depicted in Figure 5-5 indicates that the identification algorithm followed by parameter extraction closely estimates the external capacitance added in the circuit. The rational fraction coefficients and the value of the total capacitance (with C_{EXT}) is extracted using (3-34), (3-35), (3-36), and (3-37). This analysis outlines that the identification model can detect changes in the system and/or its components.

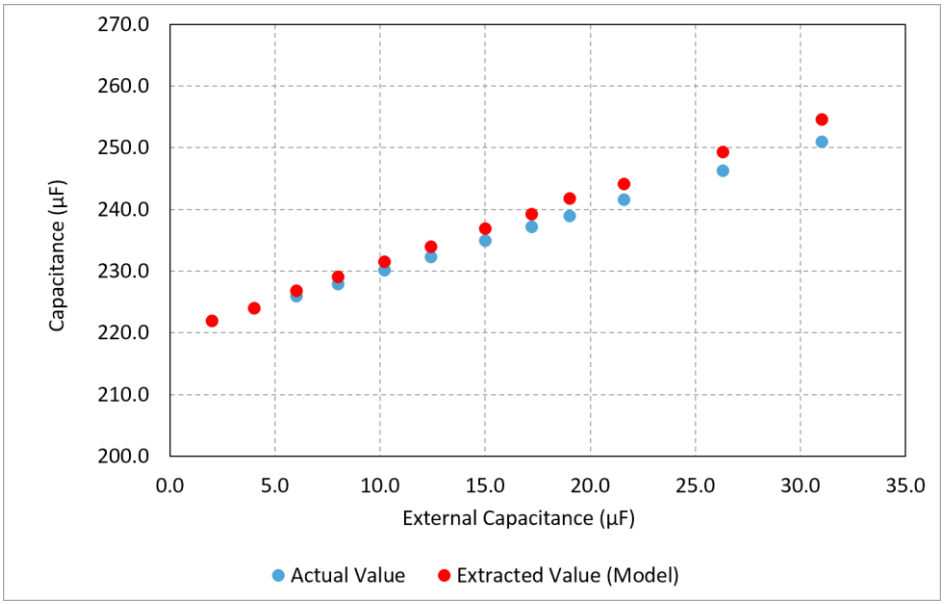

Figure 5-5 Comparison between Actual Capacitance Value Used on the SIMetrix Model and Extracted Value from the System Identification Algorithm

Furthermore, typical degradation of the capacitor ESR is used to test the ruggedness of the identification algorithm. An external resistor rC_{EXT}, which represents the degradation in ESR of the capacitor, is modelled in the circuit as an anomaly as shown in Figure 5-6. Subsequently, the identification algorithm is used to detect this change in the circuit.

The observed results in Figure 5-7 depict that from the transfer function response and using the WLS identification model, the increase in the ESR of the capacitor can be estimated accurately enough to reveal degradation in the series resistance of the capacitor.

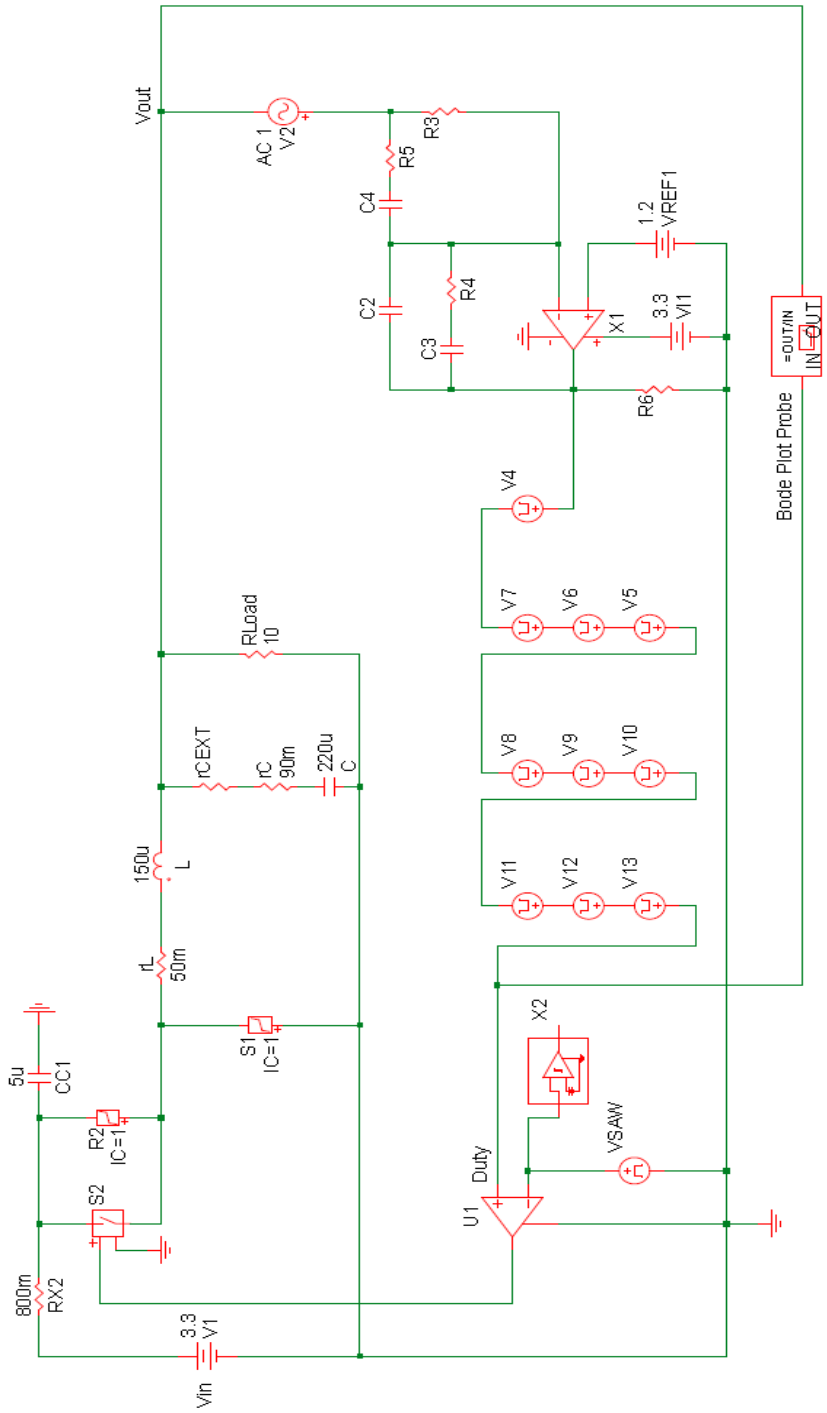

Figure 5-6 Theoretical Model with Additional ESR of the Capacitor for ESR Anomaly Detection

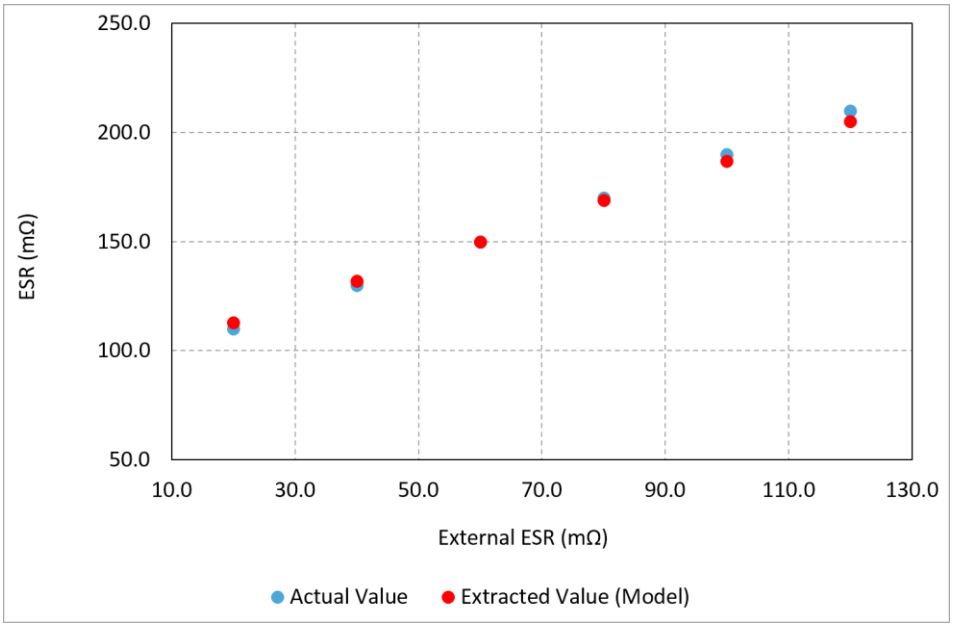

Figure 5-7 Comparison between Actual ESR Value Used on the SIMetrix Model and Extracted Value from the System Identification Algorithm

5.3 Experimental Analysis

The above hypothesis can be experimentally validated by implementing the same methodology on the modified circuit illustrated in Figure 5-8 without changing the design and implementation of the ADC, digital compensator, and the DPWM. The measurement algorithm is encoded in the Piccolo™ F2806x while system identification and parameter extraction algorithm is implemented in MathCAD.

The modified power stage depicts the addition of external capacitance C_{EXT} in parallel to the output capacitor. Twelve ceramic capacitors with values ranging from 2 µF to 30 µF are placed sequentially as external capacitance in the circuit. The tolerance of selected ceramic capacitors is low, 1%, compared to tolerance of the output capacitor, 20%. In addition, the ESR of ceramic capacitors is trivial in comparison to the ESR of the electrolytic output capacitor. The selection of the external capacitor assures that the transfer function will be stable and within its operating conditions.

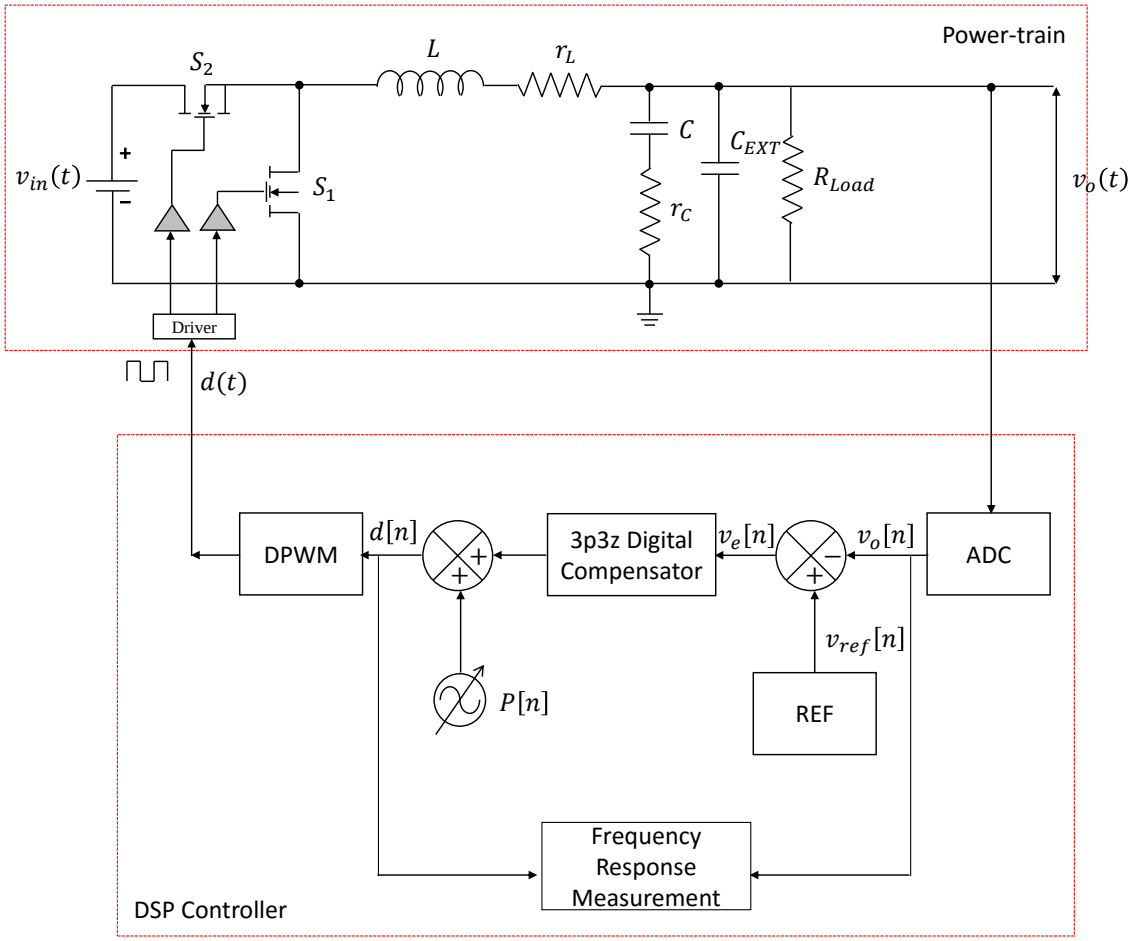

Figure 5-8 Block Diagram of Experimental Test Module with External Capacitance

The transfer function measurement by perturbing the modified system followed by system identification and parameter extraction using WLS extracts Laplace rational fraction coefficients and the associated power-train component values. The rational fraction coefficients and the value of total capacitance (with C_{EXT}) is extracted using Equations (3-34), (3-35), (3-36), and (3-37).

Initially, the power-train component values are extracted with no external capacitance in the circuit using the detection algorithm. Subsequently, a 2μF-capacitor is inserted in the circuit and the overall capacitance is measured and finally, the same procedure is performed using different values of the capacitor.

The results describe that the overall capacitance follows a rising trend indicating an increase in overall capacitance of the circuit as shown in Figure 5-9. Evidently, the extraction algorithm accurately estimates the overall capacitance across the

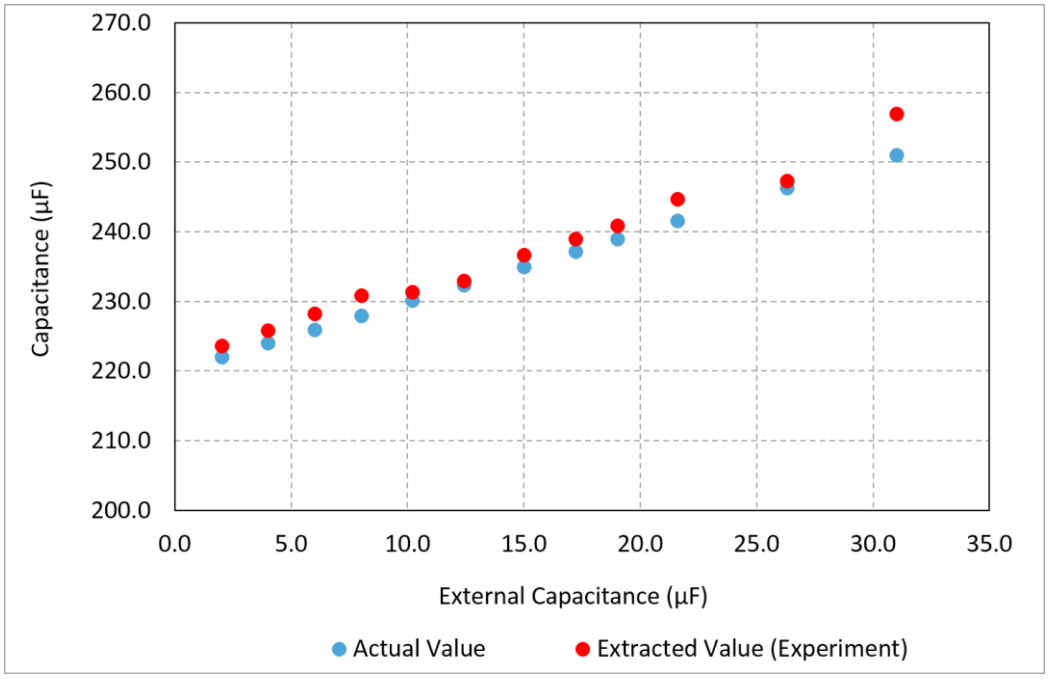

Figure 5-9 Comparison between Actual Capacitance on the Circuit and Extracted Value from the System Identification Algorithm

output of a buck converter, taking into consideration the tolerance of the components and the uncertainty associated with the measurements, modelling, and component extraction.

While the approximate value of C_{EXT} is detected, the trend in the data values satisfies the susceptibility of the algorithm to detect anomaly change in the power stage circuit. The above results signify that the proposed methodology can be used to identify and predict ageing-related degradations in the power-train component values. Moreover, the stated methodology including transfer function measurement, system identification, and parameter extraction extracts the change in the power-supply components with no additional electronic instrumentation/sensors and complex physics-of-failure based modelling.

5.4 Chapter Summary

This chapter corroborates the use of the proposed system identification based health-monitoring method for anomaly detection using system change. This chapter put forward the hypothesis that the system identification health-

monitoring method can detect changes in the passive power-train component values.

Theoretical verification of the above hypothesis carried out by modelling the system in SIMPLIS incorporates an external capacitor connected in parallel to the output filter capacitor, wherein the external capacitor signifies an anomaly in the system. It is observed that the gain and phase response obtained from AC analysis approximates to the extracted magnitude and phase response (obtained from the WLS identification algorithm). The parameter extraction algorithm finally estimates the power-train component values very close to the component values used in the theoretical model.

This theoretical analysis is further corroborated by experimental investigation. The experimental setup incorporates the system identification methodology by incorporating an external capacitor in parallel to the output filter capacitor. The health-monitoring method echoes power-train component values close to the actual component values on the experimental setup with a small percentage error. This concludes that besides the uncertainty in the system including the digital controller and the analog noise, the health-monitoring method is able to detect anomalies in the system.

The main accomplishment of this chapter can be summarised that the health-monitoring capability is robust and rugged enough to detect anomalies in the passive power stage component values while the system is functioning under normal operating conditions.

6 Uncertainty Analysis

Uncertainty analysis is the mathematical analysis of a system that investigates variability on its variables. This variability can instigate from different sources that are inherent to the system or from various external factors. The variability on system variables due to ambient noise of the system, discretisation of the variables, etc., signifies internal noise in the system. Correspondingly, environmental factors, such as change in temperature, humidity, and vibration, contribute external uncertainties on the system variables. In particular, the system excitation introduces external variability on the variables.

This chapter aims to analyse uncertainty on the measured transfer function and the estimated model coefficients. The knowledge of uncertainty on the measurands and the estimated model coefficients illustrates non-linear characteristics and thus assists in predicting the uncertainties in the system.

The first section of this chapter quantifies the uncertainty on the measured transfer function and the model coefficients through numerical analysis. The subsequent section acknowledges the source of this uncertainty/variability by comparing the results with the theoretical model of the system.

This chapter meets the fourth objective of the research.

6.1 Introduction

Recent advancements in sensing and signal processing provide the capability to sense, measure and identify characteristics of a system under various normal and adverse environmental conditions. Nevertheless, the reliability of the measurements and the identification algorithms is highly influenced by inevitable uncertainties introduced by non-stationary and nonlinear characteristics of the system. Specifically, the quantisation noise from discretisation of an analog signal, electronic noise of the components, noise introduced during FFT, etc. propagate a random and unavoidable source of noise in the system and hence, on the measurements.

Several researchers acknowledge uncertainties that originate as the result of variability in physical characteristics and the random nature of the system as physical uncertainty. For example, the inherent electronic noise of the electronic components, typically thermal noise, flicker noise, etc., constitute random/physical uncertainty in the system.

From an experimentation perspective, the uncertainty/variability in experimental measurements due to discretisation errors, including rounding and truncation errors, contribute to data uncertainty in the system. Besides this, numerical uncertainty associated with the methods and technique used to measure and characterise the system response apportion statistical uncertainty. For instance, numerical errors in performing FFT on a set of discrete measurements introduce mathematical variability on the transfer function. Importantly, the statistical uncertainty is highly influenced by the availability of the measurands. This is because if the measured data is sparse, it is impossible to identify the source and quantify the uncertainty in the system.

From a theoretical model perspective, the uncertainty associated with the model and model identification is categorised as modelling uncertainty. The modelling uncertainty may also include numerical uncertainty caused by mathematical approximations of the model.

Herein, the uncertainties on the measured transfer function response originate from the dynamical properties of the system, the measurement technique and the model identification. For instance, the uncertainty in the input/output and uncertainty in the process all contribute towards parametric uncertainty on the transfer function. Specifically, the discretisation of analog input/output and the associated analog circuitry, such as conditioning circuits and anti-alias filter, constitute data uncertainty in the input and output. From a system identification perspective, the periodic and aperiodic fluctuations in the perturbation signal, measurement uncertainty from DFT and numerical uncertainty from model identification add to the experimental and modelling uncertainty on the transfer function.

In system identification applications, accurate model identification relies on accurate measurement of the data. However, the measurement data nor the system model is free of uncertainties. Additionally, since the measured data contributes to identifying the system model, any uncertainty associated with the data will definitely hamper the effectiveness of model identification and the estimation of system parameters.

Eventually, the quantification of the above uncertainties in the system is the overall goal of uncertainty analysis. The entire quantification process requires identification of the source of these uncertainties, their combined mathematical influence on the transfer function and on the performance of the system. In the literature, uncertainty quantification is dealt with two types of principles. The quantification of uncertainty on the output that propagate from the parametric uncertainty on the input is explicitly known as forward uncertainty propagation.

As an illustration, the study of uncertainty on the output, y, because of uncertainty on the input, x, and process noise, etc. is a forward problem. On the other hand, the uncertainty quantification of input x and the model parameters, α, based on a set of measurements of y symbolise an inverse uncertainty quantification. Model calibration and bias reduction are some of the problems that are quantified using inverse uncertainty principles. Conversely, model estimation and correction is also considered as an inverse problem in system identification based methodologies.

In the literature, several probabilistic and non-probabilistic methods enable quantifying forward uncertainty in a system. Monte Carlo simulations and numerical integration based methods are methods to evaluate the dependency of uncertain input on the output.

In this study, forward uncertainty on system outputs in relation to prospective inputs, such as output voltage and duty signal, is estimated from the measured data. This includes the estimation of relative uncertainty on magnitude and uncertainty on phase of the transfer function. Subsequently, relative uncertainty on model coefficients is predicted with respect to the amplitude of multi-tone

perturbation. Finally, relative uncertainty on model coefficients anticipates relative variability on the power-train components extracted from the Laplace rational fraction.

Additionally, relative uncertainty on model coefficients based on the uncertainty on the transfer function is analysed theoretically and then compared to the measured results.

6.2 Uncertainty on Measured Output Voltage and Duty Signal

Initially, the uncertainty on measured data is analysed by acknowledging its statistical properties. As discussed earlier, uncertainty in the experimental data initiates primarily from limited accuracy of the quantisers, typically ADC and DPWM, physical analog noise in the system, numerical uncertainty through IQ demodulation and data processing, etc.

If a discrete sequence $X(k)$ is corrupted with noise, it can be described as a random sequence. In a similar context, the discrete output voltage and duty contaminated with noise/uncertainty from different sources, as discussed above, can be considered as random sequences.

The probability distributions provide preliminary insight of characteristic behaviour of random variables of a random sequence. In general, a histogram or Empirical Cumulative Distribution Function (ECDF) graphically depicts distribution of the data. However, commonly-used histograms introduce bias due to binning of the data samples. Binning deludes the characteristic features of the data set, thereby, giving an inaccurate estimate of order statistics, such as skewness and granularity. Moreover, the choice of bin origin and its width can affect the appearance of the histogram and provide a false indication of the probability distribution.

Instead, a Q-Q (Quantile-Quantile) similar to p-p (Probability-Probability) plot provides graphical “goodness of fit” of the distribution of the data. By definition, a quantile is a class of variate that divides all the samples of a distribution into equal proportions. Generally, a normal Q-Q plot is widely used to estimate normality of

the data. However, various other theoretical distributions can also be used to predict the distribution of the data set. In this case, the Q-Q plot compares data quantiles of the measured data set to quantiles of a known standard theoretical distribution.

A quantile is uniquely defined for each data sample and is defined either by the expected value of the order statistic as formulated by the Shapiro-Wilk test or using a heuristic approach. Using a heuristic approach, literature defines different formulae to calculate a quantile. The typical formulae used in the majority of the studies define quantile q as

$$q = \frac{i}{n+1}; q \in (0,1) \tag{6-1}$$

where i represents the rank of the sample and n represents the total population. The selection of a theoretical quantile is based on the criterion that it has an equivalent mean and standard deviation as the data set. Therefore, the present study calculates the quantile using

$$q = \frac{k-0.375}{n+0.25};\ q \in (0,1) \tag{6-2}$$

Subsequently, the quantile function $\Phi(X)$ of a random variable X defined by the inverse of its Cumulative Distribution Function (CDF) is estimated. Mathematically,

$$\Phi(X) = F^{-1}(X);\ F(X) = P(X \leq x) \tag{6-3}$$

This theoretical quantile function (Refer to Appendix D for quantile function of symmetrical triangular, uniform and normal distribution) is plotted against the quantile of the measured data set to depict the probable distribution of the measured data. The predictive Q-Q plot of the measured output voltage and duty at each perturbation frequency data resembles a normal or triangular distribution as illustrated in Figure 6-1 and Figure 6-2. This is an expected behaviour for the sum of two or more independent and identically-distributed random noise variables. The quantisation noise of the quantisers in addition to analog noise

superimposes this random noise on the output voltage and the duty signal. It is difficult to differentiate the distribution of data set at each perturbation frequency because the triangular distribution matches the entire data set with departure at the tails. However, the analysis clearly reveals that the measured data does not follow a uniform distribution.

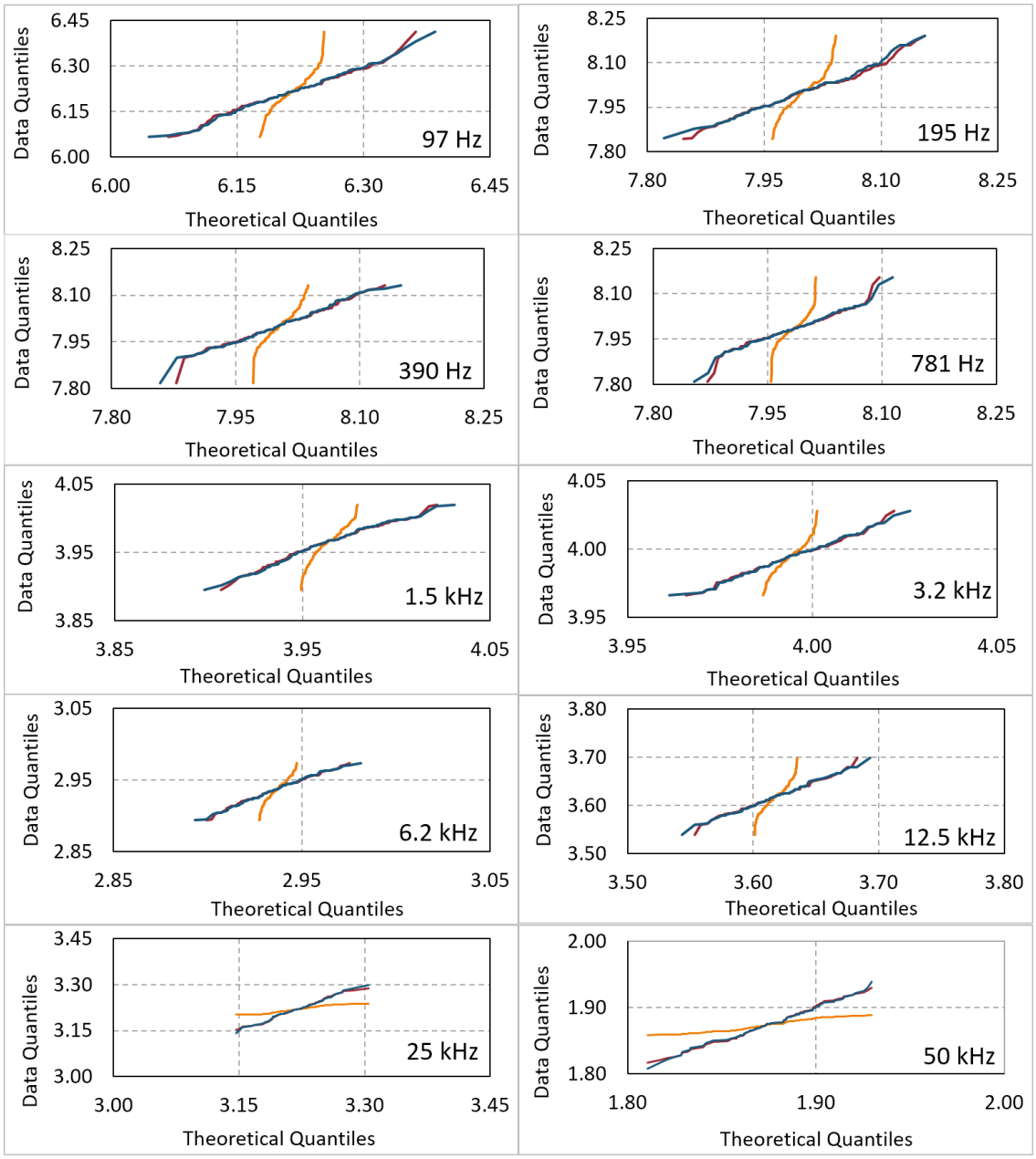

Figure 6-1 Q-Q Plots of Measured Output Voltage (Orange represents Uniform, Dark Blue represents Normal and Red represents Triangular distribution)

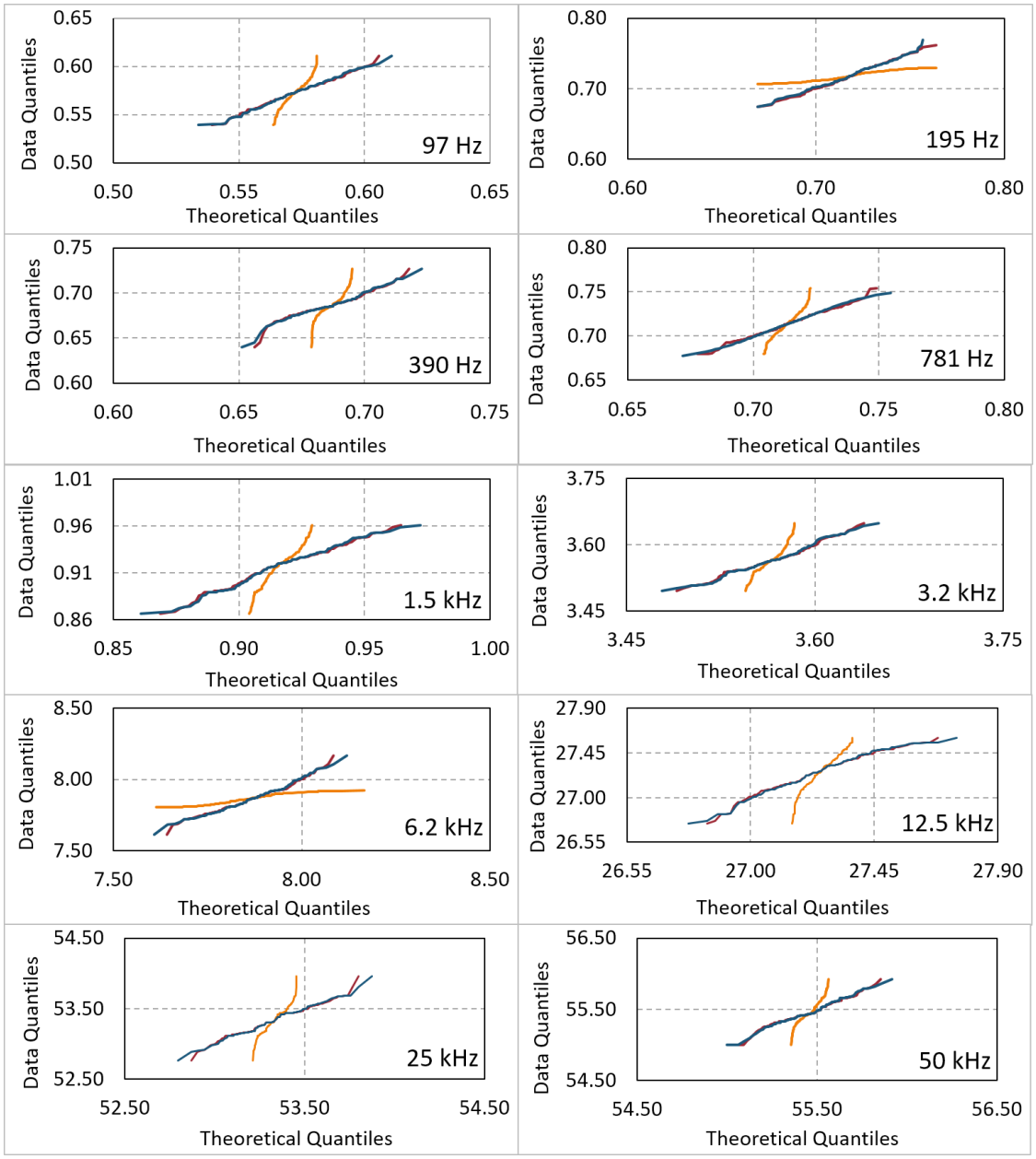

Figure 6-2 Q-Q Plots of Measured Duty Signal (Orange represents Uniform, Dark Blue represents Normal and Red represents Triangular distribution

The graphical interpretation predicts the nature of the measured data set. However, it fails to provide a quantitative measure of uncertainty in the data. Hence, uncertainty on the control-to-output transfer function is analysed with respect to the amplitude of the input (output voltage) and the output signal (duty signal).

6.3 Uncertainty on the Transfer function

6.3.1 Experimental Analysis

Uncertainty/Variability/Noise on the measured transfer function is quantified with respect to its input and output signal, i.e. the output voltage and the duty.

Five sets of experiments were designed where the system was perturbed with different perturbation amplitudes. In each of the experiments, the output voltage and the duty signal is measured by injecting a multi-tone sinusoid of frequency F_P while the amplitude A'_P (expressed in LSB) is varied according to

$$A'_P = t.A_p \; ; t = \; 2^o \; ; \; o = \; -2, -1, 0, +1, +2 \tag{6-4}$$

where A_p defines the amplitude defined in Equation (3-3). In other words, the perturbation amplitude is varied from a quarter of an LSB, to half of an LSB to a quad of an LSB in every consecutive experiment. Successively, five sets of the transfer function are accessible based on five sets of experiments.

Prior to uncertainty analysis, each transfer function measurement is averaged to obtain a high SNR. The uncertainty on the transfer function magnitude $|\mathrm{H}|$ illustrated in Figure 6-3 a) and phase $\varphi(H)$ in Figure 6-3 b) is plotted with respect to the peak amplitude of the output voltage. The uncertainty on the magnitude response is expressed as relative uncertainty (Standard Deviation Ratio) in percentage and as uncertainty (Standard Deviation) in degrees on the phase response.

Careful examination shows low uncertainty/noise on the magnitude and phase response as the amplitude on the output voltage is increased. This is an expected result while extracting a signal buried in the Additive White Gaussian Noise (AWGN). Conversely, it is the characteristic behaviour of a signal suppressed in AWGN of the quantisers and random analog noise of the system.

Similarly, the relative uncertainty on the magnitude (Figure 6-4 a)) and phase (Figure 6-4 b)) response is quantified with respect to the peak amplitude of the duty signal. The relative standard deviation on the magnitude plot varies inversely

to the amplitude of the duty signal. This analysis evidently depicts the source of AWGN in the system and its influence on the transfer function magnitude and phase response.

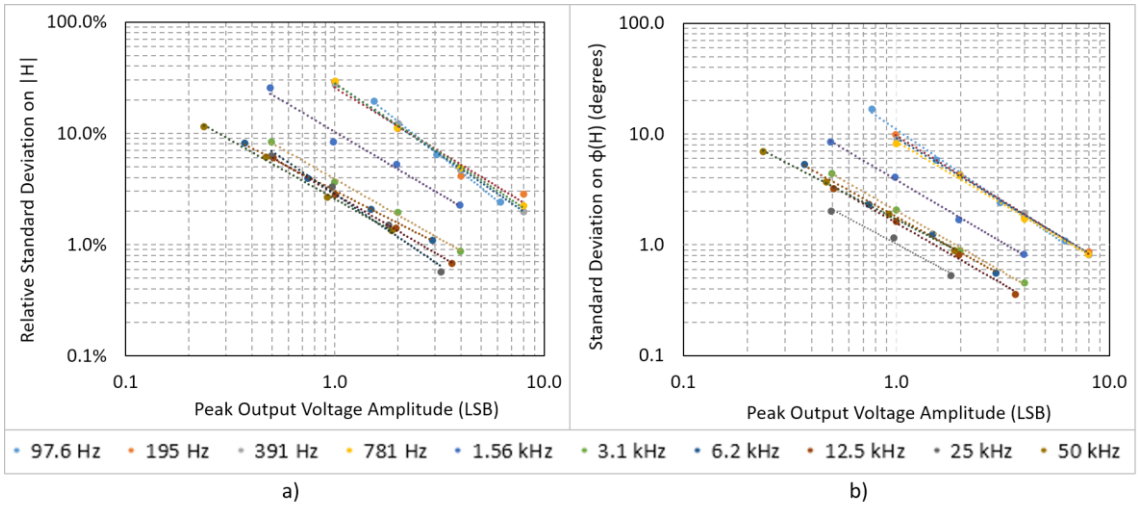

Figure 6-3 Relative Standard Deviation

a) |H| with respect to Peak Output Voltage Amplitude

b) φ(H) with respect to Peak Output Voltage Amplitude

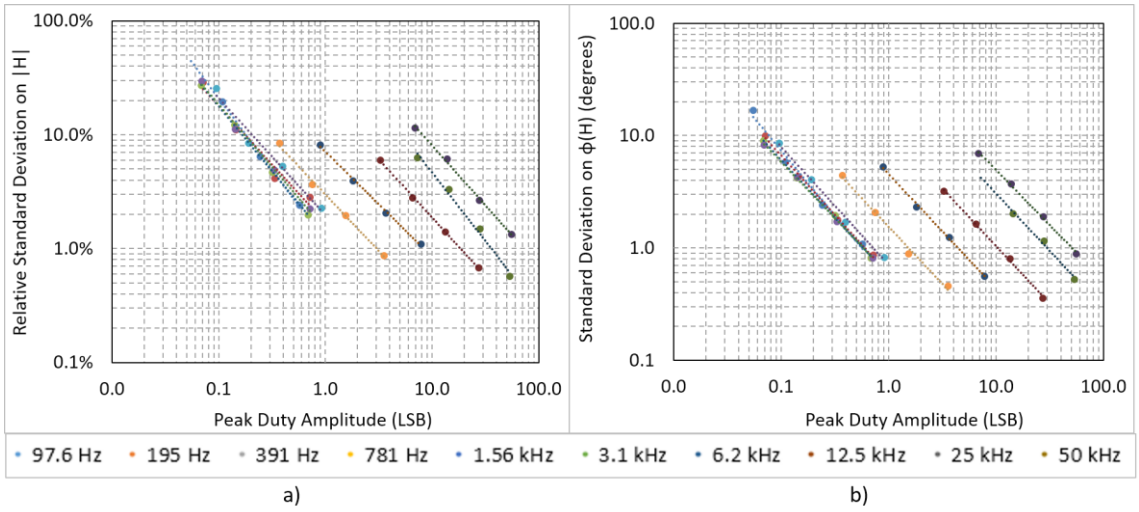

Figure 6-4 Relative Standard Deviation

a) |H| with respect to Peak Duty Amplitude

b) φ(H) with respect to Peak Duty Amplitude

From the above analysis, it can be expressed that the relative uncertainty (standard deviation) on the $|H|$ and the uncertainty on $\varphi(H)$ response with respect to the peak output voltage amplitude or the duty shadows a power law of the form

$$\sigma_{|H|} = a.(v_o)^b \tag{6-5}$$

$$\sigma_{\varphi(H)} = c.(v_o)^d \tag{6-6}$$

$$\sigma_{|H|} = e.(duty)^f \tag{6-7}$$

$$\sigma_{\varphi(H)} = g.(duty)^h \tag{6-8}$$

whereby the regression coefficients a, c, e, g are the scaling factors and b, d, f, h in Table 6-1 define the dependency of uncertainty on the transfer function in relation to the peak amplitude of the output voltage/duty.

Frequency (Hz)	$\|\bar{H}\|$	$\varphi(H)$	a	b	c	d	e	f	g	h
97	3.502	-7.0	0.360	-1.5	10.997	-1.3	0.012	-1.3	0.514	-1.2
195	3.594	-12.8	0.256	-1.1	9.666	-1.2	0.017	-1.0	0.580	-1.1
391	3.757	-28.0	0.280	-1.3	9.205	-1.2	0.013	-1.1	0.566	-1.0
781	3.609	-71.4	0.280	-1.2	8.533	-1.1	0.015	-1.1	0.579	-1.0
1560	1.395	-127.0	0.103	-1.1	3.843	-1.1	0.020	-1.0	0.708	-1.0
3100	0.361	-143.1	0.039	-1.1	2.025	-1.1	0.030	-1.0	1.543	-1.0
6250	0.120	-145.2	0.030	-1.0	1.788	-1.1	0.078	-0.9	4.550	-1.0
12500	0.043	-149.9	0.028	-1.1	1.575	-1.1	0.197	-1.0	11.050	-1.0
25000	0.019	-172.3	0.028	-1.3	2.033	-1.1	0.743	-1.2	29.850	-1.0
50000	0.011	131.9	0.026	-1.1	1.699	-1.0	0.899	-1.0	47.237	-1.0

Table 6-1 Regression Coefficients of Relative Standard Deviation on |H| and φ(H) at Frequencies of Interest

In other words, the exponent b, d, f and, h signifies that the uncertainty on transfer function is inversely proportional to the amplitude of the output voltage/duty. This result satisfies the inverse interdependence between the input amplitude and the variability on the transfer function.

Pictorially, the shape of the regression coefficients with respect to the plurality of frequencies of interest depicts that the SNR on the transfer function is not consistent across the bandwidth under consideration. In other words, there is large uncertainty on both the magnitude and phase response at lower frequencies from 97 Hz to 781 Hz, compared to relatively low noise variance at higher frequencies, typically 3.1 kHz to 50 kHz. The possible source of uncertainty can result from the quantisation noise of the ADC/DPWM, analog noise, etc. However, it is difficult to describe the origin of this uncertainty. Nevertheless, it is important to quantify this noise source because the SNR on the transfer function influences the estimate of uncertainty on the model coefficients.

To recognise the source of this uneven SNR on the transfer function magnitude and phase, firstly, open-loop characteristics of the system are determined. By superimposing a sinusoidal noise source of amplitude equivalent to 1 % variation of the output voltage (12 mV), the noise spectral density of the quantiser (ADC) is analysed at a frequency band of interest.

The noise spectral density is extracted by performing FFT on single acquisition of the measured output voltage. Since noise is not constant/flat, this method yields biased results especially for lower frequencies. Therefore, for accurate estimation, the square root of the sum of squares of the individual noise spectral densities over several acquisitions of the output voltage is calculated. Mathematically, the total noise spectral density over N acquisitions expressed in $V/\sqrt{Hz}$ is

$$\sigma_{v_o} = \sqrt{\frac{1}{n}\sum_{n=1}^{N}\left(\sigma_{v_o n}\right)^2} \tag{6-9}$$

Similarly, the noise spectral density of the quantisers is computed for each perturbation frequency. Figure 6-5 a) depicts the amplitude noise spectral density of the output voltage of an ADC including the DC components and the harmonics.

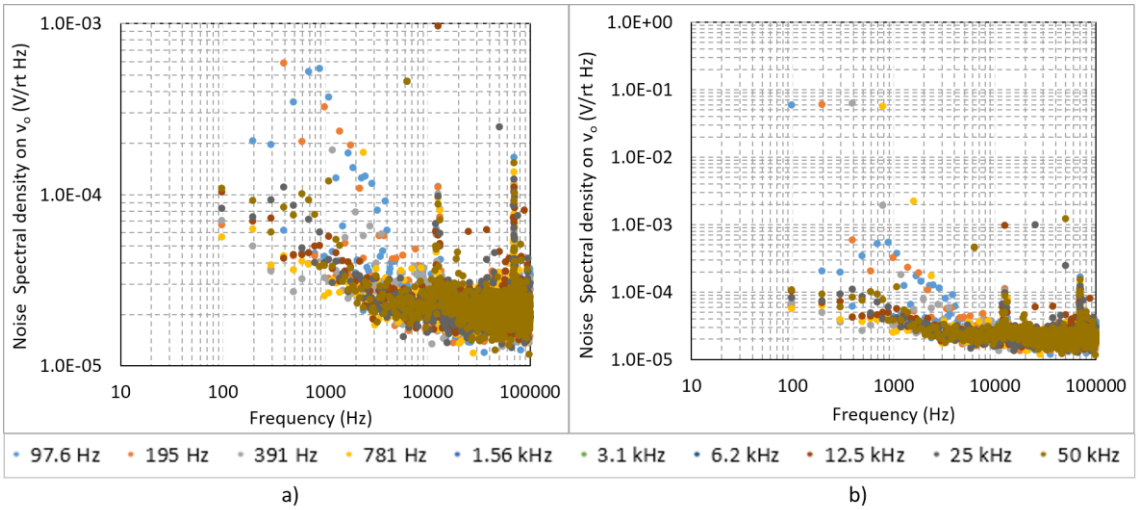

Figure 6-5 Amplitude Noise Spectral Density on
a) Output Voltage Including DC and Harmonic Components
b) Output Voltage Excluding DC and Harmonic Components

Neglecting DC components associated with each perturbation frequency as shown in Figure 6-5 b), two inferences can be formulated.

First, the amplitude noise spectral density over the measured Nyquist bandwidth represents a flat-band noise with average noise spectral density three times the variance of the quantisation noise. Secondly, the noise spectral density decreases linearly with frequency from 10 Hz to approximately 3 kHz. The result advocates the existence of flicker noise in the system with a corner frequency of 3 kHz and flat in-band quantisation white noise with noise spectral density equivalent to three times the variance of the ADC quantiser. Now both these noise sources may reduce the SNR on the transfer function. However, theoretical justification is required. Therefore, a simulation model is created in SIMetrix to validate the above results.

6.3.2 Theoretical Analysis of Uncertainty on the Transfer Function

It is understood that an estimate of uncertainty on the output voltage and the duty provides an estimate of uncertainty on the transfer function response. The theoretical validation of uncertainty on the measured transfer function is

evaluated by modelling flicker noise source along with the quantisation noise source of the quantisers.

A second-order closed-loop buck converter, 3.3 V input and 1.2 V output, with power-train component values equivalent to L = 150 µH, C = 220 µF, r_C = 90 mΩ, r_{L+S} = 840 mΩ and R_{Load} = 10 Ω is modelled in SIMetrix. Additionally, the quantisation noise variance of the ADC and DPWM is modelled to understand their influence on the output voltage and the duty.

6.3.2.1 Quantisation Noise Model

An ideal N-bit quantiser causes a maximum error of $\pm\frac{1}{2}LSB$ when digitising an analog signal where 1 LSB or quantisation level Δ is defined as

$$\Delta = \frac{V_{max} - V_{min}}{2^{N-1}} \tag{6-10}$$

where $V_{max} - V_{min}$ represents full-scale amplitude of the analog signal.

The non-linear quantisation noise due to rounding has a zero mean with average noise power

$$\mu_{QR} = 0\,;\ \sigma_{QR}^2 = \frac{\Delta^2}{12} \tag{6-11}$$

Consequently, the truncation error has a non-zero mean with average noise power described by

$$\mu_{QT} = \frac{\Delta}{2}\,;\quad \sigma_{QT}^2 = \frac{\Delta^2}{3} \tag{6-12}$$

Assuming the total quantisation noise is only due to rounding, the quantisation noise can be modelled as an additive, signal-independent, white noise uniformly distributed over the interval $[-\frac{\Delta}{2}, +\frac{\Delta}{2}]$ with variance defined by

$$\sigma_T^2 = \frac{\Delta^2}{12} \tag{6-13}$$

where σ_T^2 is the variance of the quantisation noise. Subsequently, the flat and uniformly-distributed power spectral density of quantisation noise measured over

the full Nyquist bandwidth from DC up to half the switching frequency $\frac{F_S}{2}$ can be defined as

$$PSD_T = \frac{\sigma_T^2}{\left({F_s}/{2}\right)} = \frac{\Delta^2}{6\,F_s} \tag{6-14}$$

From the above known quantisation noise characteristics, the quantisation noise of the ADC and DPWM are modelled in SIMetrix. The quantisation noise is generally modelled as a white noise source. A white noise is random in nature and exhibits uniform distribution over the frequency of interest. However, some researchers disagree on the whiteness of the quantisation noise. However, in most cases, white noise source can be effectively modelled as a quantisation noise source.

Moreover, when the voltage resolution of the quantisers is small, compared to the magnitude of the signal, it is reasonable to assume that the quantisation error is stationary white noise and uniformly distributed over the interval $\pm\frac{\Delta}{2}$.

The simplest method to implement a white noise source is to use a resistive noise model. The noise of an ideal resistor commonly known as thermal noise or Johnson-Nyquist noise is flat with a power spectral density PSD_{TH} per hertz of bandwidth expressed as

$$PSD_{TH} = 4\,k_B T\,R \tag{6-15}$$

where k_B defines the Boltzmann constant in Joules/Kelvin, T is the operating temperature measured in Kelvin, and R is the resistance expressed in ohms. Using (6-14) and (6-15), an equivalent resistance that exhibits quantisation noise can be calculated

$$R = \frac{\Delta^2}{24\,k_B\,T\,F_s} \tag{6-16}$$

Now, by simulating noise analysis over the Nyquist bandwidth from DC to half the Nyquist frequency with the above noise sources, the noise spectral density on

output voltage and duty can be estimated. The effect of quantisation noise of the ADC and DPWM is estimated individually on the output voltage and the duty.

Firstly, the noise spectral density on output voltage is predicted by assuming that the noise in the system is only due to the quantisation noise of the ADC, i.e.

$$\sigma_{v_o(ADC)} = \sigma_{ADC} \; ; \sigma_{DPWM} \sim 0 \tag{6-17}$$

Subsequently, the influence of DPWM quantisation noise is predicted by assuming there is no quantisation noise introduced by the ADC, i.e.

$$\sigma_{v_o(DPWM)} = \sigma_{DPWM} \; ; \sigma_{ADC} \sim 0 \tag{6-18}$$

Hence, the total noise spectral density on the output voltage is computed as the square root of the sum of squares of the quantisation noise of the ADC and the DPWM measured individually at the output of the ADC.

$$\sigma_{v_o} = \sqrt{\sigma^2_{v_o(\mathrm{ADC})} + \sigma^2_{v_o(\mathrm{DPWM})}} \tag{6-19}$$

Similarly, the noise spectral density on duty (6-22), square root of the sum of squares of the quantisation noise of the ADC and the DPWM, is measured individually at the output of the DPWM using (6-20) and (6-21)

$$\sigma_{d(ADC)} = \sigma_{ADC} \; ; \sigma_{DPWM} \sim 0 \tag{6-20}$$

$$\sigma_{d(DPWM)} = \sigma_{DPWM} \; ; \sigma_{ADC} \sim 0 \tag{6-21}$$

$$\sigma_d = \sqrt{\sigma^2_{\mathrm{d(ADC)}} + \sigma^2_{\mathrm{d(DPWM)}}} \tag{6-22}$$

The simulated results illustrated in Figure 6-6 a) and b) reveal that quantisation noise of the ADC largely influences the noise spectral density on the output voltage and the duty, compared to the quantisation noise of the DPWM. Note that orange curve is below the grey curve. However, the above model does not include the characteristics of flicker noise.

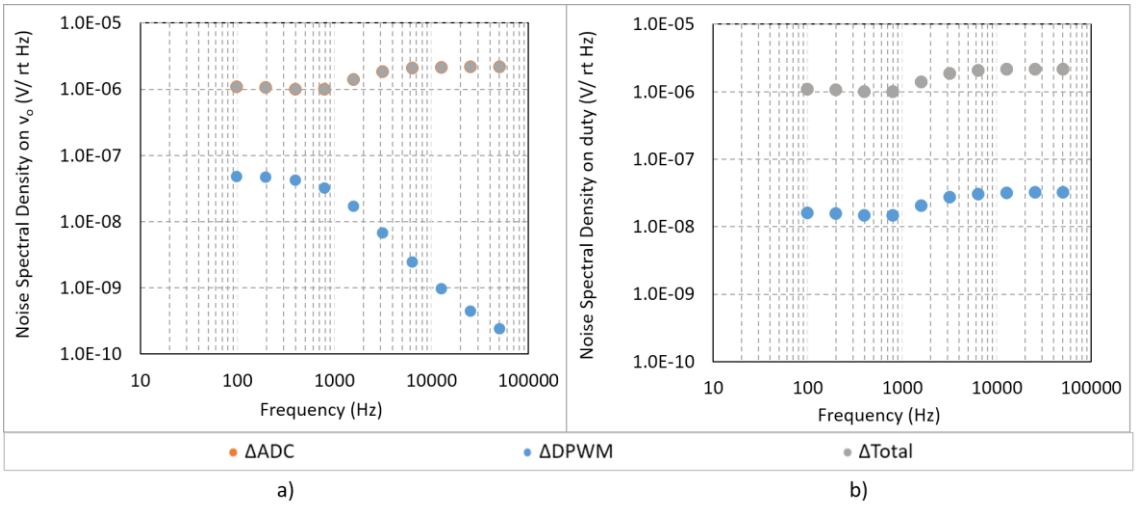

Figure 6-6 Noise Spectral Density due to ADC and DPWM Quantisation Noise a) Output voltage b) duty

6.3.2.2 Flicker Noise Model

The flicker noise, also known as $1/f$ noise, is an electronic noise governed by low-frequency noise and a high-frequency flat band white noise. It is often characterised by a corner frequency f_c. The corner frequency governs the power spectral density of the flicker noise. In particular, the power spectral density is inversely proportional to the frequency of the signal below the corner frequency and a flat power spectrum above the corner frequency.

The measured noise spectral density in **Error! Reference source not found.** demonstrates flicker noise with a corner frequency of approximately 3 kHz and a flat white noise spectral density equivalent to three times the variance of the ADC quantisation. Based on the above characteristics of the flicker noise, a resistive flicker noise source is modelled to understand the residual inconsistency in the SNR on the transfer function.

The resistive flicker noise parameters in the SIMetrix Simulator Reference Manual define the power spectral density of the flicker noise as

$$\mathrm{PSD}_{FL} \propto \frac{\mathrm{KF}}{f^{EF}} \tag{6-23}$$

where EF defines the flicker noise exponent and KF is the flicker noise coefficient.

The modelled noise spectral density including the above noise characteristics demonstrates that majority of the uncertainty on the measured output voltage is due to resistive flicker noise source as illustrated in Figure 6-7 a).

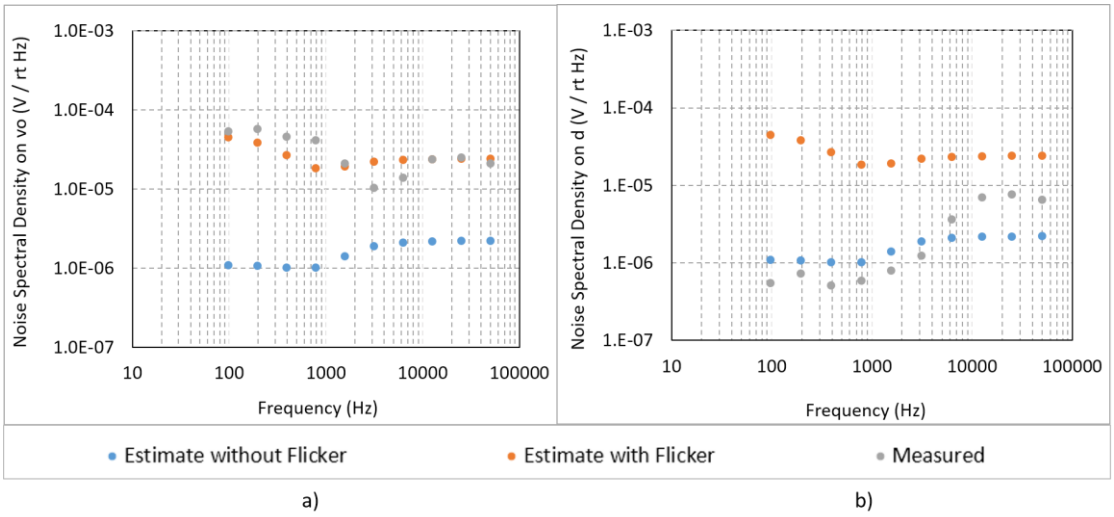

Figure 6-7 Noise Spectral Density on
a) Output Voltage b) Duty

In contrast, the flicker noise modulates the same effect on the duty as shown in Figure 6-7 b). The theoretical quantification of noise spectral density on output voltage and duty due to quantisation effect of quantisers and the flicker noise justify the presence of high relative standard deviation on the transfer function. Conversely, it is evident that flicker noise significantly increases the level of uncertainty on the output voltage and hence on the transfer function.

This uncertainty significantly affects the overall performance of the health-monitoring methodology. It can be summarised that based on the careful selection of perturbation amplitude, the uncertainty on the measurements is influenced by different noise sources in the system except the digital quantisation noise.

Therefore, the above analysis concludes that it is imperative to understand and acknowledge system-inherent noise sources prior to measurements. This is

because the presence of such noise sources significantly degrades the SNR of the measurements which consecutively propagate uncertainty on the measurements, the system identification algorithm and finally, on the estimation of power-train component values.

6.4 Uncertainty on Model Coefficients

According to the definition of forward uncertainty, the uncertainty on the output voltage and the transfer function directly propagates uncertainty on the model coefficients. Successively, this uncertainty drifts on power-train components and deceives the estimation of degradation or anomaly detection. Therefore, it is necessary to understand the characteristics and quantify the uncertainties on the model coefficients.

The first sub-section evaluates forward uncertainty on model coefficients with respect to the change in perturbation amplitude or in other words, output voltage amplitude. The second sub-section estimates relative uncertainty on model coefficients based on relative uncertainty on the transfer function. The theoretical results are finally compared to the measured relative uncertainty on the model coefficients.

6.4.1 Effect of Perturbation Amplitude

This section examines the forward uncertainty on model coefficients with respect to the peak amplitude of the output voltage. Based on the transfer function measured by injecting five different perturbation amplitudes, the noise variability on the model coefficients is calculated for each experiment.

It is assumed that the first perturbation amplitude refers to an absolute amplitude of 1.0 and consecutively, the amplitude for the next perturbation is halved, and so on. The uncertainty of the transfer function propagates on the model coefficients as illustrated in Figure 6-8. Further, analysis of the above data reveals that relative uncertainty on all the model coefficients follows a power law (6-24) with exponent approximately -1.0 (refer to Table 6-2).

$$\sigma_{Model\ Coefficient}(\%) = \mathrm{w}.(v_o)^z \tag{6-24}$$

Model Coefficient	w	z
n_0	0.011	-1.12
n_1	0.013	-1.20
d_1	0.017	-1.19
d_2	0.010	-1.18

Table 6-2 Regression Coefficients of Relative Standard Deviation on Model Coefficients for Different Output Voltage Amplitudes

Conversely, the projection of model coefficients indicates inverse proportionality with the output voltage amplitude. Statistically, this behaviour establishes the characteristics of noise on model coefficients as white and Gaussian, as expected. This investigation also infers that the proposed methodology is robust to external noise injected in the system and is effective in detecting anomalies in the system.

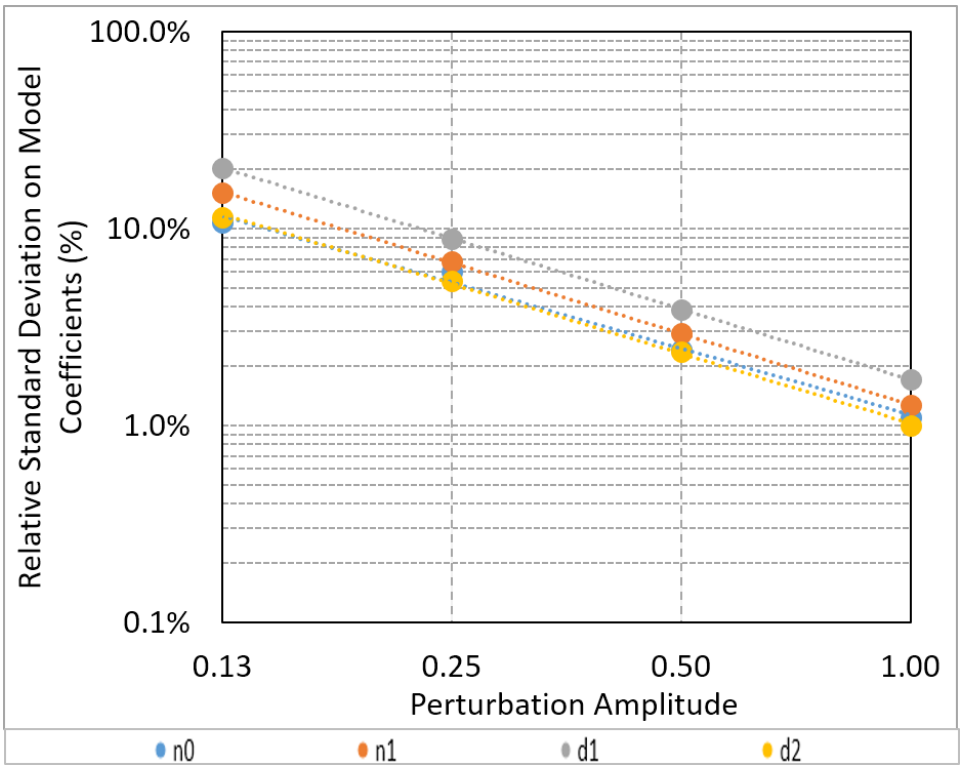

Figure 6-8 Relative Standard Deviation on Model Coefficients with respect to Perturbation Amplitude

6.4.2 Effect of Transfer Function

The uncertainty on the transfer function at each perturbation frequency influences uncertainty on the model coefficients. Mathematically, the relative uncertainty on a model coefficient can be defined as the quadratic mean of relative uncertainties of the transfer function at all frequencies of interest. Statistically, relative uncertainty on σ_{n_o} can be written as

$$\sigma_{n_0}(\%) = \sqrt{\sum_{p=1}^{F} \left(\sigma_{n_0 p}\right)^2} \quad ; \; p = 0,1,2 \ldots F \tag{6-25}$$

where $\sigma_{n_o p}$ is proportional to relative uncertainty on H(s) at each perturbed frequency. Similarly, relative uncertainty on other model coefficients can be written as

$$\sigma_{n_1}(\%) = \sqrt{\sum_{p=1}^{F} \left(\sigma_{n_1 p}\right)^2} \quad ; \; p = 0,1,2 \ldots F \tag{6-26}$$

$$\sigma_{d_1}(\%) = \sqrt{\sum_{p=1}^{F} \left(\sigma_{d_1 p}\right)^2} \quad ; \; p = 0,1,2 \ldots F \tag{6-27}$$

$$\sigma_{d_2}(\%) = \sqrt{\sum_{p=1}^{F} \left(\sigma_{d_2 p}\right)^2} \quad ; \; p = 0,1,2 \ldots F \tag{6-28}$$

Now, the uncertainty on each of the model coefficients can be predicted theoretically by estimating individual uncertainties due to perturbed frequencies.

If $Y(k)$ and $X(k)$ represent Discrete Fourier transformed complex output and input sequences of band-limited signals $y(t)$ and $x(t)$ and $N_Y(k)$ and $N_X(k)$ is a

discrete-time filtered white noise on $Y(k)$ and $X(k)$, then (Pintelon, et al., 1994) states $N_Y(k)$ represents a zero-mean circularly complex noise.

From the above definition, it follows that uncertainty on the transfer function (obtained from DFT) represents a zero-mean circularly complex Gaussian noise. Knowing the above characteristics, relative uncertainty on a model coefficient due to all the perturbed frequencies can be estimated through relative uncertainty on $H(s)$ at each perturbation frequency. In other words, the uncertainty on a model coefficient can be predicted from the SNR on the transfer function.

If $N_H(k)$ represents zero-mean circularly complex Gaussian noise on the transfer function, i.e.

$$N_H(k) \sim \mathcal{N}(0,1) e^{(\iota\, 2\pi\, Uniform(0,1))} \tag{6-29}$$

where $e^{(\iota\, 2\pi\, Uniform(0,1))}$ signifies uniformity of the complex random noise with zero mean and standard deviation equal to 1.0 on the unit circle, the transfer function with complex random noise can be described as

$$H_{noisy}(k) \sim \left(H_{theoretical}(k)\right)\,(1 + N_H(k)\,) \tag{6-30}$$

where $H_{theoretical}(k)$ is the theoretical Laplace rational fraction defined by power-train components. Subsequently, relative uncertainties on each model coefficient with respect to a percentage t of relative uncertainty on $H(s)$ can be defined as

$$H_{noisy}(k) \sim \left(H_{theoretical}(k)\right)\,(1 + (t\%)\, N_Y(k)\,) \tag{6-31}$$

Herein, the relative uncertainty on model coefficients is estimated by superimposing 1%, 2% and 4% complex random noise on the transfer function at each perturbation frequency individually. The prediction illustrated in Figure 6-9 and Figure 6-10 demonstrates increased uncertainty on model coefficients with percentage increase of complex noise on the transfer function.

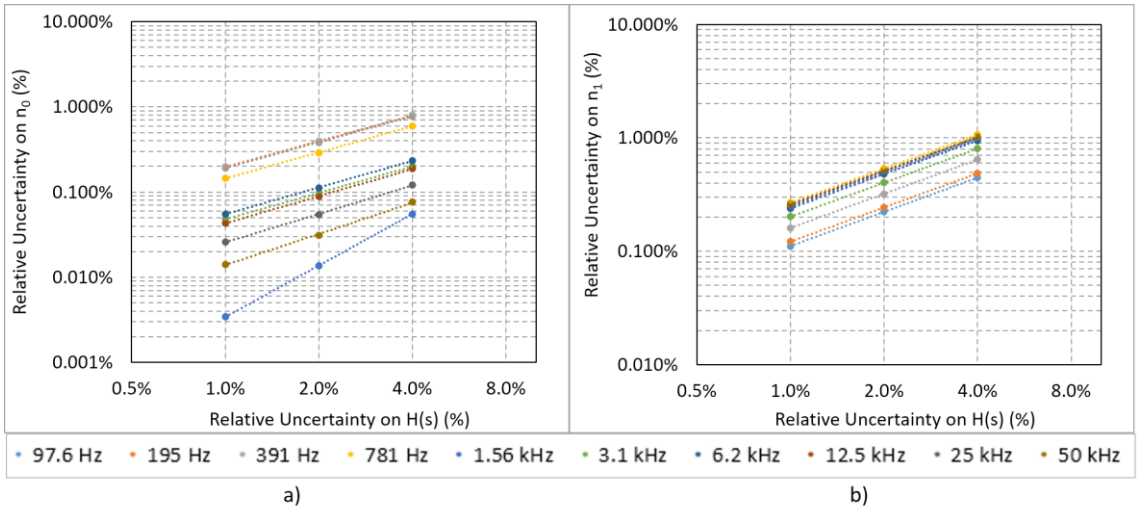

Figure 6-9 Relative Uncertainty based on Relative Uncertainty on H(s) at Each Perturbation Frequency

a) n_0 b) n_1

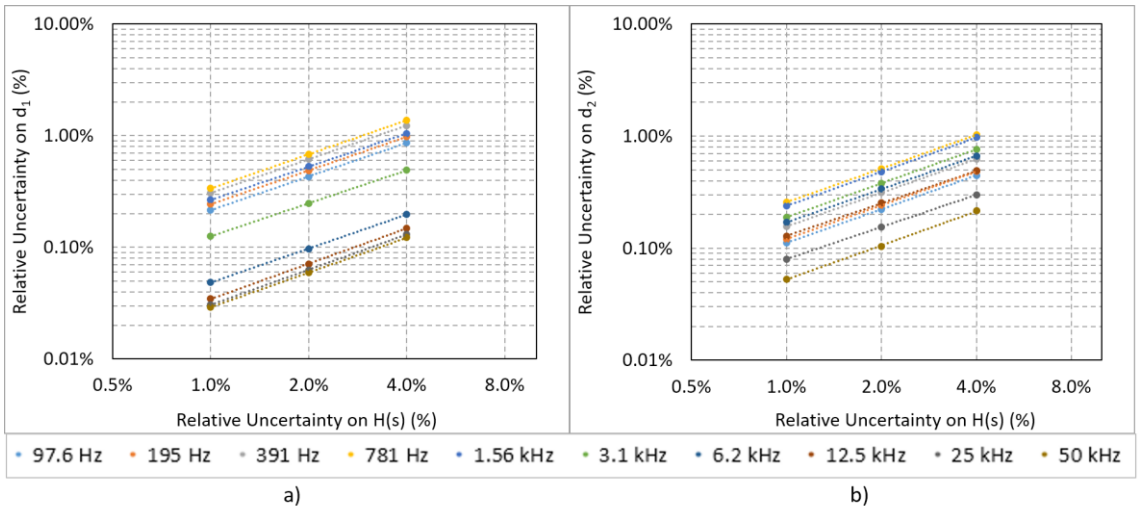

Figure 6-10 Relative Uncertainty based on Relative Uncertainty on H(s) at Each Perturbation Frequency

a) d_1 b) d_2

Mathematically, the noise sensitivity on each of the model coefficients portrays a power trend for each perturbation frequency of the form

$$\sigma_{n_{o_p}} = a' \left(\sigma_{\mathrm{H}_p}\right)^{b'} \tag{6-32}$$

and

$$\sigma_{n_{1_p}} = c' \left(\sigma_{\mathrm{H}_p}\right)^{d'}; \sigma_{d_{1_p}} = e' \left(\sigma_{\mathrm{H}_p}\right)^{f'}; \sigma_{d_{2_p}} = g' \left(\sigma_{\mathrm{H}_p}\right)^{h'} \tag{6-33}$$

providing a deterministic scaling and exponent factor tabulated in Table 6-3.

The results depict that relative uncertainty on every model coefficient is different with respect to a particular relative uncertainty on the transfer function.

Frequency (Hz)	a´	b´	c´	d´	e´	f´	g´	h´
97	0.20	1.00	0.11	1.00	0.22	1.00	0.11	1.00
195	1.99	1.00	0.12	1.00	0.25	1.00	0.12	1.00
391	0.20	1.00	0.16	1.00	0.31	1.00	0.16	1.00
781	0.16	1.02	0.27	1.00	0.36	1.02	0.26	1.00
1560	0.36	2.01	0.26	1.02	0.25	0.99	0.25	1.01
3100	0.06	1.03	0.20	1.00	0.12	0.98	0.20	1.01
6250	0.07	1.04	0.22	1.00	0.05	1.01	0.15	0.99
12500	0.06	1.06	0.24	0.98	0.04	1.05	0.11	0.97
25000	0.04	1.11	0.24	0.99	0.04	1.05	0.06	0.95
50000	0.04	1.22	0.26	1.00	0.03	1.03	0.06	1.01

Table 6-3 Regression Coefficients of Relative Standard Deviation on Model Coefficients at Frequencies of Interest

The relative uncertainty on each model coefficient is different according to Equation (3-32) at different frequencies of interest. In addition, the noise on the model coefficients approximates below 1% for 4% complex noise on the transfer function. This describes that circularly complex noise on the Fourier coefficients has less influence on the uncertainty of the model coefficients.

Using Equations (6-25) to (6-28) the noise sensitivity on each model coefficient can be predicted from the quadratic mean of noise sensitivities at all frequencies of interest.

It is calculated that the uncertainty on model coefficient (evaluated from Figure 6-3) based on the above statement match very closely to the predicted or theoretical uncertainties as shown in Figure 6-11 and Figure 6-12.

It is worth mentioning that the above calculation assumes that the 1% uncertainty on the measured transfer function refers to the measured relative uncertainty on the transfer function when the injected perturbation amplitude was 1.0. Similarly, 2% uncertainty is assumed when the perturbation amplitude is equal to 0.5, and so on.

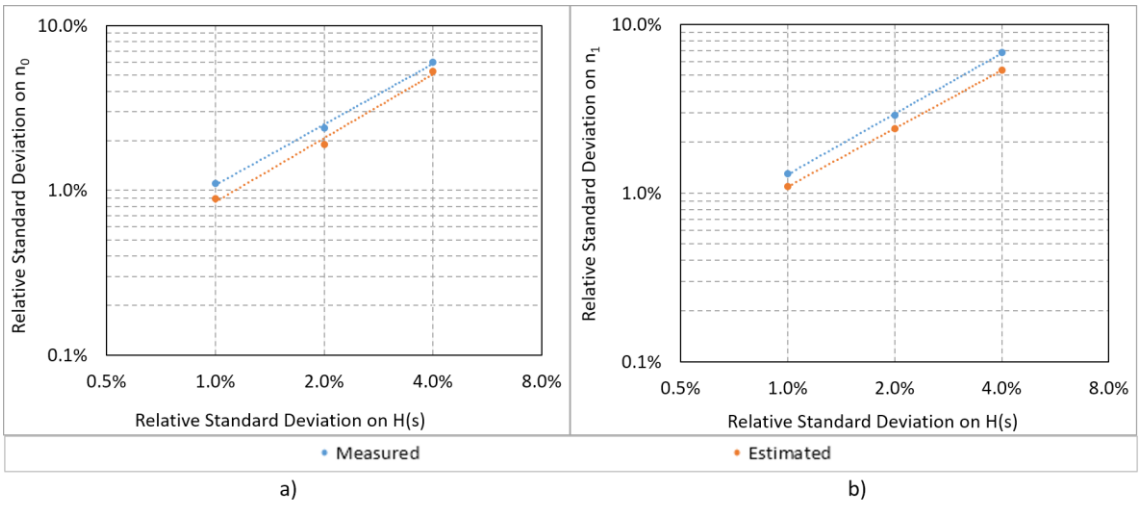

Figure 6-11 Measured vs Estimated Uncertainty Based on Uncertainty on the Transfer Function

a) n_0 b) n_1

The above investigation demonstrates that 1% circularly-complex random noise on the model coefficients introduces an approximate uncertainty of 1% on all the model coefficients, and so on. This also includes any modelling errors in the WLS algorithm.

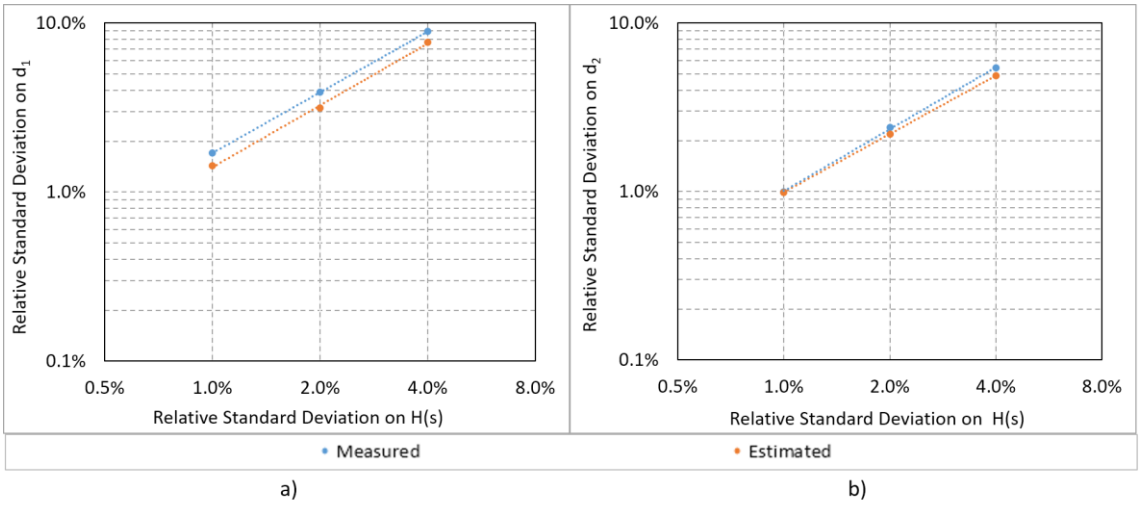

Figure 6-12 Measured vs Estimated Uncertainty Based on Uncertainty on the Transfer Function

a) d_1 b) d_2

6.5 Chapter Summary

The uncertainty analysis describes the effectiveness of the measurements and their uncertainties, including the robustness and ruggedness against different stimuli. The main objective of this chapter was to understand uncertainty on the system variables, including the transfer function and the identified model coefficients. The entire uncertainty analysis on the system led to the following contributions of this chapter.

- The uncertainty on measured system variables, i.e. the output voltage and the duty signal examined using the concept of simple Q-Q plots give a qualitative prediction that noise on these variables certainly is not uniformly distributed but is either a triangular or Gaussian distribution.
- The quantitative analysis of uncertainty on the measured transfer function, however, estimates an uneven SNR on the transfer function despite careful selection and injection of perturbation amplitude at different frequencies.
- The noise spectral characteristics of the ADC studied by superimposing 1% of the output voltage (12 mV) sinusoidal signal discovered a noise source with

a noise spectral density of the order of three times the variance of the quantisation noise of the ADC and a flicker noise source with a corner frequency of 3 kHz. The theoretical simulations of the above noise source in the system prove discontinuity in the SNR on the measured transfer function.

- Subsequently, given the uncertainty on the transfer function at different frequencies of interest, the theoretical estimate of uncertainty on the model coefficients reveals the expectation of uncertainty on all model coefficients. The approximation of the expected uncertainty with the measured uncertainty in the previous chapter indirectly proves the effectiveness of the estimator and how the propagation of uncertainty in the system.

7 Discussion and Conclusions

This chapter discusses the entire research work in a concise manner and highlights major findings and contributions to knowledge. The chapter concludes by describing the application of the above methodology in various fields of research and potential future research opportunities.

The first section describes how the research questions have been answered. The second section highlights the aim and objectives of the research and how they have been fulfilled. The subsequent section represents key contributions to existing knowledge. The fourth section reflects the strengths and limitations of the research work from the author's perspective. The fifth section provides future recommendations and potential advancements in this research. Finally, the chapter concludes by providing a summary of the research presented in this thesis.

7.1 Addressing the Research Question

The research question defined in the first chapter of this thesis was:

How can health monitoring of system performance metrics provide detection of anomalies in the system and/or the components?

The above research question was addressed in the following stages. The initial stage of the research detailed in Chapter 1 studied various health-monitoring frameworks that can enable detection of degradations and failures in passive electronic components and power converters. A system identification based health-monitoring method, among other techniques, reflects the capability of online health monitoring to detect anomalies in the system.

This resulted in a review of the system identification process in Chapter 2 and how it can be developed to address the research question. The second stage of the research, described in Chapters 3, 4, 5, and 6 developed and validated a set of algorithms that are robust and rugged enough to detect anomalies or degradations in the power converter and the passive electronic components.

The set of algorithms include a customised design of the perturbation/excitation signal to gain knowledge of specific features of the system, for example, the degradation in the ESR and the capacitance of the output filter capacitor. Subsequently, non-parametric measurement of response function through coherent/synchronous demodulation provided accurate measurement of the signal buried in the inherent analog noise and the digital noise of the quantisers. Finally, accurate parametric identification of the system model from non-parametric measurements minimising relative error function in the Weighted Least Squares approach proved the effectiveness of the proposed health-monitoring methodology and its use for degradation/anomaly detection.

Further, validation of the method was performed by external inclusion of filter capacitance in the system. The proximity of experimental results and the theoretical estimate of power-train component values in the presence of system uncertainties and non-linear characteristics of the system revealed that the method is feasible, useable, and consists of novel features that can be used to detect degradations/anomalies in the passive components.

Lastly, the research study has addressed, answered, and validated the research question in a systematic approach and provides evidence to support this.

7.2 Addressing the Aim and Objective

This section describes the aim and objectives of the research and provides the evidence of how research investigation has addressed each objective and finally, the aim of the research. The three objectives have been addressed.

Objective 1: Develop a health-monitoring tool on a basic DC-DC power converter topology

Evidence 1: This objective is met by developing proof of concept of the proposed health monitoring tool on a basic buck power converter. The process involved parametric identification of the system through non-parametric model identification (Chapter 3).

The non-parametric system identification involved a customised design of the perturbation/excitation signal to meet two objectives. The first design objective was to excite the control loop with an energy-rich perturbation signal designed to extract degrading patterns in passive electronic components. The second design objective was to inject the perturbation signal such that a constant SNR is maintained across the entire bandwidth of interest. The above design objectives were achieved by injecting a customised amplitude perturbation signal that excites the control loop at only ten frequencies of interest. The second step is accurate measurement/extraction of system response. This design objective is met by synchronous demodulation of system variables.

Finally, the parametric model identification is achieved by minimising the relative error between the non-parametric measurements and the estimated model. The developed proof of concept on a simple power converter topology directed towards its validation for anomaly detection.

Objective 2: Validate the developed capability for anomaly detection

Evidence 2: This objective is met by introducing an additional component in the power stage that reflects the manifestation of anomalies in the passive electronic components. The developed methodology is verified from the theoretical system model and the experimental system. The theoretical model is built in SIMPLIS while the weighted least square model identification and parametric extraction is done in MathCAD. Similarly, the model identification extraction of power-train component values from the experimental system is done in MathCAD.

The accurate extraction of power stage component values from the theoretical model in addition to the experimental system clearly portrays that the developed system identification technique is suitable for anomaly or degradation detection in passive electronic components in switch-mode power supplies.

Objective 3: Examine robustness and ruggedness of the tool despite uncertainties in the system and the monitoring tool

Evidence 3: This objective is met in Chapter 6 wherein uncertainty analysis is used to estimate the effectiveness of the proposed and developed health-monitoring capability.

The uncertainty on the measured system variables, the transfer function, and the model coefficients is addressed taking into consideration the external stimulus, i.e. the perturbation amplitude and the inherent noise in the system. The qualitative analysis of uncertainty on the measured system parameters depicts a Gaussian or triangular distribution, compared to uniform distribution of the quantisers. The quantitative uncertainty on the non-parametric FRF measurements, on the other hand, describes that despite careful selection of perturbation amplitude, the SNR is not constant across the bandwidth of interest. The research thereafter identifies this unknown source of uncertainty as a combination of flat band quantisation noise and resistive flicker noise. The uncertainty on the model coefficients represents the presence of circularly-complex Gaussian noise. This is verified through theoretical model in addition to the experimental uncertainty estimates. The entire uncertainty analysis corroborates the robustness and ruggedness of the method to detect anomalies in the system besides the presence of analog and digital noise in the system.

The aim of the research is to develop a health-monitoring capability that monitors and evaluates system parameters/metrics to detect system and/or component anomalies taking into account the system noise. This aim is accomplished by the fulfilment of the three objectives.

7.3 Contribution to Knowledge

The contribution to knowledge by this research is established through the development, implementation, and validation of the research methodology and through the findings of the research created during the research itself. The execution of the research aim through its objectives amalgamated two diverse research fields: power electronics and system identification. This unification resulted in the recognition of novel aspects of this research. Since a similar study that captures the degradation detection in passive electronic components has not

been acknowledged prior to the research, a substantial contribution to knowledge has been indicated.

The main contributions of this research are summarised as follows:

- Shows the necessity to detect existing failures and degradation in power converter systems and passive electronic components.
- Shows that the proposed system identification based health monitoring has additional capability compared to existing health-monitoring techniques.
- Shows how system identification based health monitoring designed to identify a parametric system model from non-parametric FRF measurements can be utilised to extract power stage component values accurately.
- Shows the systematic approach of techniques necessary to capture and measure the degradation or anomalies in electronic components in the case of power supplies.
- Shows how uncertainty analysis measures the effectiveness of the health-monitoring methodology while demonstrating the capability of the method for anomaly detection.

The proposed health-monitoring capability highlights key contributions of the research.

The implementation and validation of methodology on a low-voltage power converter with a tight voltage tolerance constraint proves the ruggedness of the method regardless of uncertainties in the system and the model itself.

Primarily, the correct choice of the experimental setup, including the selection of sensors and acquisition systems, decisions for system synchronisation, and the choice of inter-sample behaviour played a vital role in the accomplishment of the research. The band-limited assumption of the inter-sample behaviour instead of Zero-Order-Hold distinguishes this research work from others because the above hypothesis provides knowledge of the system behaviour, compared to digital control or simulation of a system.

The custom design of the perturbation signals specifically to meet the design objectives has proved that the selection of perturbation signal amplitude and frequency of interest is imperative for system identification based health monitoring. In addition, the coherent demodulation of system response using only 10 perturbation frequencies has demonstrated the capability of the method against existing measurement techniques. Finally, the parametric identification of the system model through relative minimisation of the cost function across the logarithmic frequency range acknowledged accurate extraction of the power-train component values of the power converter.

7.4 Reflection upon the Research

This section echoes upon the limitations encountered during the research and the challenges in the implementation of the research objectives.

Identifying suitable health-monitoring techniques for anomaly detection

- Details on health-monitoring techniques are usually published in the prognostic and health management research community that focuses on the use of dedicated sensors and model-based prognosis. However, there was a lack of availability of system identification based techniques in the wider prognostic research community. This limitation was addressed by redirecting the focus towards power electronic system identification methods.
- Consequently, several model identification techniques available in the literature have been reviewed. However, the majority of the methods are developed to control or simulate the digital controller and none of the methods focus on anomaly detection. This revelation stirred the research investigation to develop a system identification based health monitoring tool that addresses the concern of degradation or anomaly detection in passive electronic components within aircraft power supplies.

Validating the methodology of anomaly detection

- The main limitation associated with the validation of the proposed methodology for anomaly detection is the constrained time scale of the research project. Therefore, the author verified the experimental outcome of the method by introducing system change that reflects an anomaly or degradation in the system. The above result is further validated by simulating a theoretical model of the system.

Examining the effectiveness of the methodology

- The author encountered a number of limitations in examining the effectiveness of the health-monitoring methodology. The uncertainty analysis is a diverse field that uses complex probabilistic approaches to understand the characteristic of the system. However, the author's work is limited to simple concepts to understand the uncertainty/sensitivity of the system despite directing focus on complex methods at the initial stage. This decision has revealed several features of the system and the experimental setup itself, which clearly depicts the nature of the inherent and external uncertainties in the system and the models.

7.5 Future Recommendations

The research herein, describes robust and rugged methodology besides several development opportunities in system identification based health monitoring of power electronic systems. This include the use of advanced estimation algorithms, complex power electronics systems, computational efficient digital controllers and lastly consideration of environmental factors.

The proposed modus operandi provide foundation to health monitoring of avionic power supply architecture including front-end 115 V AC/28 V DC power converters, in addition to, different topologies including boost, buck-boost, flyback and other DC-DC power conversion systems.

A single feedback loop, easy design, but complex compensation network voltage mode control of power converter could be replaced by two feedback loop, complex but simple compensation network current controlled power converter. Nevertheless, the benefits of current control scheme are swamped by certain issues that can be resolved during the design process.

The neural network based estimators such as Particle filter, Kalman filter plus Bayesian statistics introduce advanced knowledge to sources of uncertainty, data patterns, diagnosis, prognosis, compared to rugged Recursive weighted least square estimator.

The programmable Control Law Accelerator, CLA, within 32-bit F28069 digital controller, provides the capability to execute complex mathematical calculations independent of the main CPU, while alleviating computational performance of the controller, could be implemented in the future.

Lastly, the acknowledged effect of temperature on the performance of electronic components, could be realised with the developed system identification based health monitoring.

APPENDICES

Appendix A Analog and Digital Control of Power Converters

A power converter consists of a power stage network and a feedback network as shown in

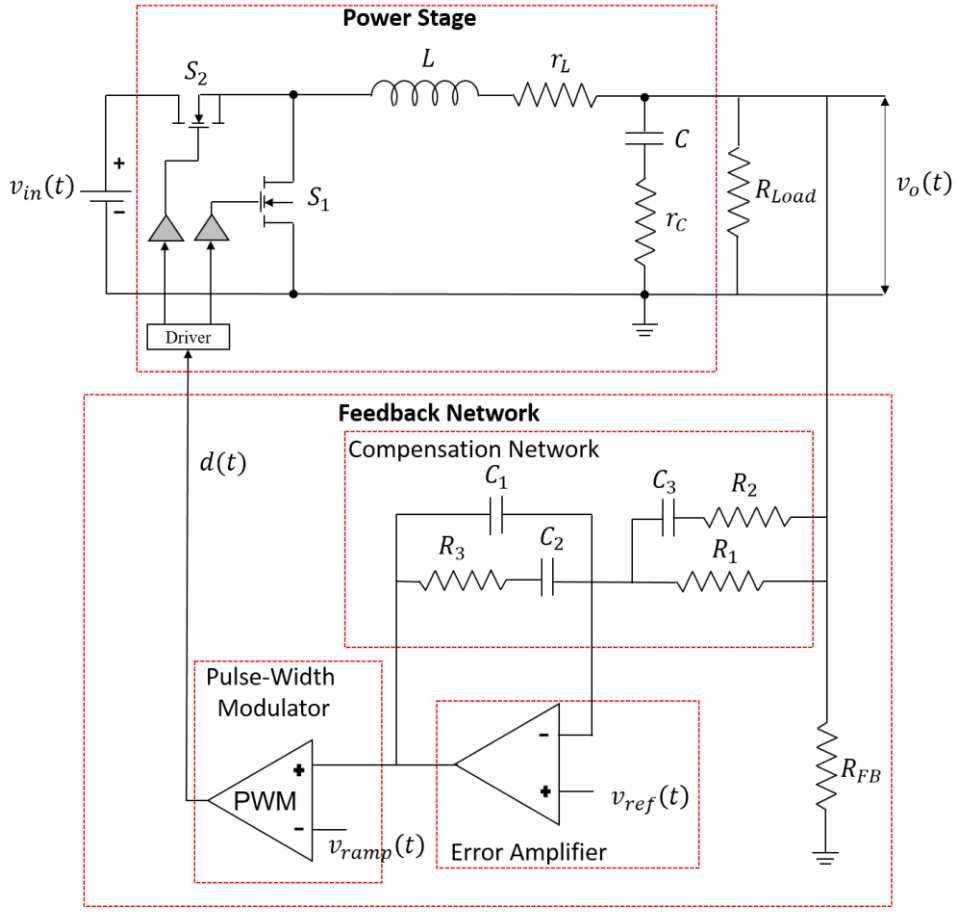

Figure A-1. The power stage network involves a power switch S_1 and S_2 and, an output LC filter that converts a high input voltage $v_{in}(t)$ to a low output voltage $v_o(t)$, in the case of a POL converter. The feedback network regulates the output voltage by modulating the power switch duty cycle $d(t)$.

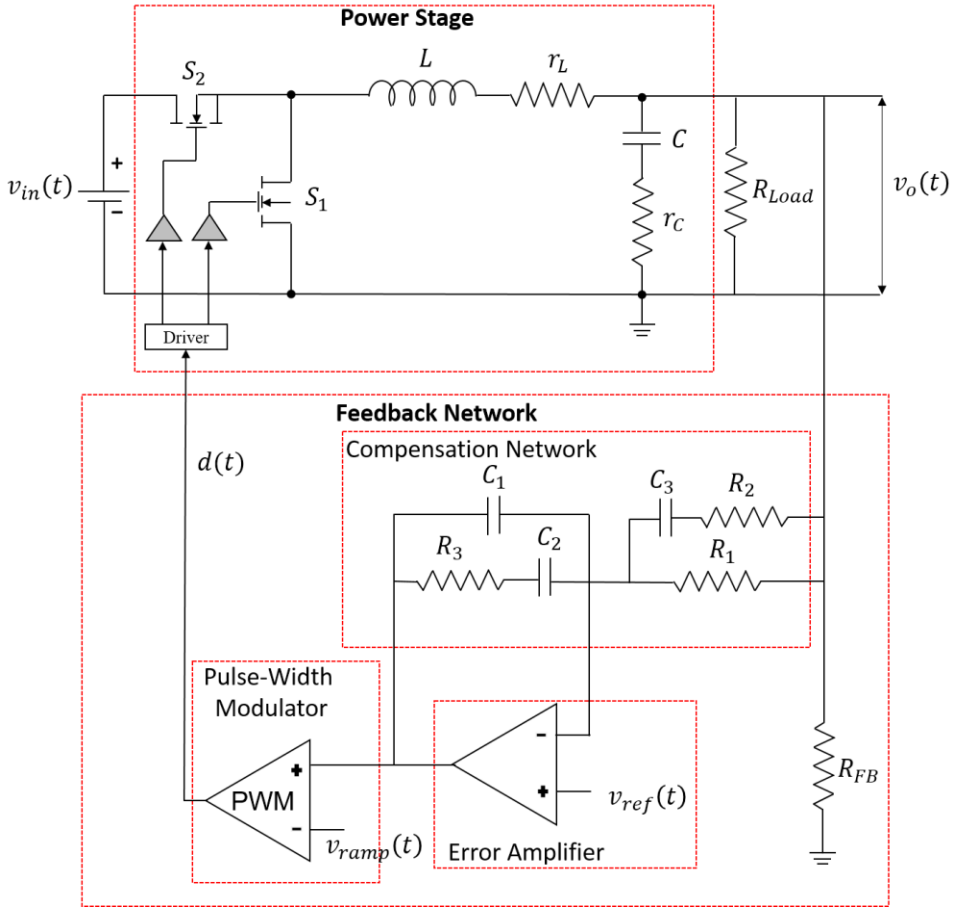

Figure A-1 Analog POL Converter

The feedback network includes an error amplifier, a compensation network, and a Pulse-Width Modulator (PWM). The function of the error amplifier is to generate a control voltage for the pulse width modulator. This is achieved by comparing a fraction of the output voltage $v_o(t)$ with a user-defined reference voltage $v_{Ref}(t)$. $v_o(t)$ is fed to the inverting input of the error amplifier with the intention that if the output voltage $v_o(t)$ increases, the output of the error amplifier decreases thereby regulating the output voltage.

The compensation network involves a network of passive electronic components generally in Type I, Type II, or Type III network that stabilises the feedback loop and optimises the transient response to dynamic load conditions [99]. The pulse width modulator is a comparator which evaluates the difference between the control voltage and fixed-frequency external ramp voltage $v_{ramp}(t)$. The external

ramp voltage is either fixed to a particular peak value or is varied depending on the input voltage $v_{in}(t)$.

Generally, the feedback network is designed using analog techniques as described. However, with advancements in digital control, digital systems have replaced analog circuits.

A digital power controller equivalent or a digitally-controlled power converter, as shown in Figure A-2, consists of a power stage network and a digital controller, which incorporates an error amplifier, a compensator network, and a PWM. The ADC, the digital filter and a digital pulse width modulator (DPWM) replace the function of the error amplifier, the compensation network, and the modulator in the digital controller. The COTS microcontrollers and the DSP integrate all the features of the feedback network. However, a FPGA can also provide the same capability with additional acquisition systems.

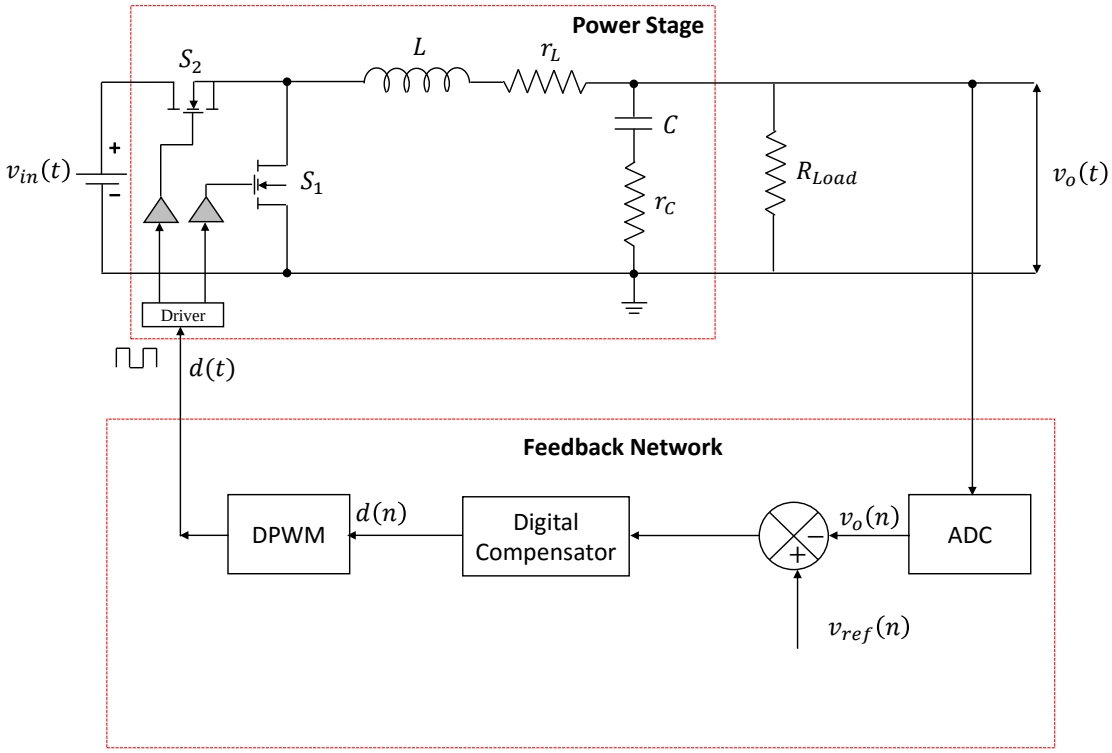

Figure A-2 Digital POL Converter

In digital control of power converters, the ADC discretises the output voltage $v_o(t)$ into sequences of n samples $v_o(n)$ and computes the error between the digital

reference and the digital signal. The digital corrector/filter, usually a Proportional-Integral-Derivative (PID) controller, compensates the error to provide a digital sequence $d(n)$. The Digital Pulse-Width Modulator (DPWM) then commands a PWM signal $d(t)$, duty signal, to regulate the control loop.

Appendix B Weighted Recursive Least Square Algorithm

The identification process states the system model as a solution to the normal equation of the form

$$\hat{\beta}_{W_i} = \sum_i \left[\left(\sum_{k=0}^{F} \overline{(S_{\iota_k} W_\iota)^T} . (S_{i_k} W_i) \right)^{-1} \left(\sum_{k=0}^{F} (W_i \, H_{NP_k}) . \overline{(S_{\iota_k} W_\iota)^T} \right) \right]$$

where $\hat{\beta}_W$ represents the best model fit of the model coefficients, W states the real-value diagonal weighing matrix. The individual weights of the weighing matrix are strictly positive $w_{ij} \geq 0$. S represents the state variable vector containing bias function and coefficients as its elements. The '·' denotes the dot product, $\overline{\ }$ denotes the complex conjugate, and T denotes the transpose. $H_{NP_k}$is a column vector containing non-parametric FRF measurements.

In steps 1 and 2, the algorithm defines and initialises the denominator, the numerator, and the frequency vectors. The elements of the weighing matrix, the numerator and denominator vectors are initialised to zero except d_0 is constrained to 1.0 in the next step. The WLS estimator takes the non-parametric FRF measurement column vector and denominator vector as the input to evaluate the weighing matrix, i.e. for i = 0, the unknown weighing function is defined based on prior analysis of the measured transfer function in step 4.

Step	Equation
1	Define numerator and denominator vectors $D = [d_0 \quad d_1 \quad d_2]^T$, $N = [n_0 \quad n_1]^T$
2	Define frequency column vector $freq_k = [freq_0 \quad \dots \quad freq_k]^T$ where k = 0,1,2 …F

3	Initialise i = 0…20, W = 0, $d_0 = 1$, d_1, d_2, … $d_d = 0$, N = 0
4	Calculate weighing matrix $$W_{i_k} = \frac{1}{\lvert D_{i_k} \rvert \lvert H_{NP_k} \rvert}$$
5	Calculate state variable vector $$S_{i_k} = N_{i_k} - D_{i_k} H_{NP_k}$$ where N_{i_k} and D_{i_k} define the column vector based on the order of numerator and denominator vectors $$N_{i_k} = [s^0 \quad s^1]^T,\ D_{i_k} = s^0 \quad s^1 \quad s^2]^T$$
6	Relative error function is estimated $$V_{i_k} = S_{i_k} W_i$$
7	$$P_{i_k} = \sum_{k=0}^{F} \overline{V_{\iota_k}^T} . V_{i_k}$$
8	$$Q_{i_k} = W_i \, H_{NP_k}$$
9	$$\hat{\beta}_{W_i} = \sum_i \left[\left(\sum_{k=0}^{F} \overline{V_{\iota_k}^T} . V_{i_k} \right)^{-1} \left(\sum_{k=0}^{F} Q_{i_k} \overline{V_{\iota_k}^T} \right) \right]$$ or $$\hat{\beta}_{W_i} = \sum_i \left[\left(\sum_{k=0}^{F} \overline{(S_{\iota_k} W_\iota)^T} . (S_{i_k} W_i) \right)^{-1} \left(\sum_{k=0}^{F} (W_i \, H_{NP_k}) . \overline{(S_{\iota_k} W_\iota)^T} \right) \right]$$
10	Go back to step 1

Table B-1 Steps to Implement Recursive WLS Algorithm

Consequently, the algorithm estimates the state variable vector and the cost function based on the selected order of the numerator and the denominator vectors in step 5. The next step entails estimating the relative error function. This modifies to matrix P to obtain the first part of the said normal equation. In step 8, the second part of the normal equation is approximated by weighing the individual experimental data points. Finally, the system model is estimated in step 9. The entire process recursively minimises the relative error instead of the absolute error on the model estimates for a number of iterations.

Appendix C Parametric Extraction

For a basic DC-DC buck converter, second-order system, the equivalent Laplace model is defined by

$$\mathrm{H}(\mathrm{s_k}) = \frac{\mathrm{n_0} + \mathrm{s_k}\,\mathrm{n_1}}{\mathrm{d_0} + \mathrm{s_k d_1} + \mathrm{s_k^2 d_2}}$$

Where the model coefficients can be evaluated from the transfer function equivalent to

$$\mathrm{H(s)} = \frac{\mathrm{v_o}(s)}{d(s)}$$

$$\mathrm{H}(s) = \mathrm{K}\left(\frac{\mathrm{Z_{out}}}{\mathrm{Z_{out}} + \mathrm{Z}}\right)$$

where $\mathrm{K} = v_{in} + v_{S2(Knee)}$

$$\mathrm{Z_{out}} = \frac{\mathrm{R}_{Load} \times \left(r_C + \frac{1}{sC}\right)}{\mathrm{R}_{Load} + \left(r_C + \frac{1}{sC}\right)} = \frac{sC\mathrm{R}_{Load} r_C + \mathrm{R}_{Load}}{s\mathrm{R}_{Load} C + sCr_C + 1}$$

and

$$Z = sL + r_{L+S}$$

where the combined resistance of r_L, r_{S1}, r_{S2} and the shunt resistance r_{Shunt} is defined by

$$\mathrm{r_{L+S}} = \mathrm{r_L} + \mathrm{D}\,\mathrm{r_{S1}} + (1 - \mathrm{D})\mathrm{r_{S2}} + \mathrm{r_{Shunt}}$$

And $v_{S2(Knee)}$ defines the knee voltage of the switch S_2.

$$\mathrm{H}(s) = \frac{\frac{sC\mathrm{R}_{Load} r_C + \mathrm{R}_{Load}}{s\mathrm{R}_{Load} C + sCr_C + 1}}{\frac{sC\mathrm{R}_{Load} r_C + 1}{s\mathrm{R}_{Load} C + sCr_C + 1} + sL + r_{L+S}}$$

$$\mathrm{H}(s) = \frac{sC\mathrm{R}_{Load} r_C + \mathrm{R}_{Load}}{\frac{sC\mathrm{R}_{Load} r_C + \mathrm{R}_{Load}}{s\mathrm{R}_{Load} C + sCr_C + 1} + sL + r_{L+S}}$$

$$H(s) = K\frac{sCR_{Load}r_C + R_{Load}}{sCR_{Load}r_C + 1 + s^2LR_{Load}C + s^2LCr_C + sL + sr_{L+S}R_{Load}C + sr_{L+S}Cr_C + r_{L+S}}$$

$$H(s) = K\frac{sCR_{Load}r_C + R_{Load}}{s^2LR_{Load}C + s^2LCr_C + sCR_{Load}r_C + sL + sr_{L+S}R_{Load}C + sr_{L+S}Cr_C + R_{Load} + r_{L+S}}$$

$$H(s) = K\frac{sCR_{Load}r_C + R_{Load}}{s^2LC(R_{Load} + r_C) + s(C(R_{Load}r_C + r_{L+S}R_{Load}) + r_{L+S}r_C + L) + (R_{Load} + r_{L+S})}$$

$$H(s) = K\frac{\frac{sR_{Load}r_CC}{R_{Load} + r_{L+S}} + \frac{R_{Load}}{R_{Load} + r_{L+S}}}{s^2\frac{LC(R_{Load} + r_C)}{R_{Load} + r_{L+S}} + s\frac{(C(R_{Load}r_C + r_{L+S}R_{Load} + r_{L+S}r_C) + L)}{R_{Load} + r_{L+S}} + 1}$$

$$H(s) = K\frac{\frac{R_{Load}}{R_{Load} + r_{L+S}} + s\left(\frac{R_{Load}r_CC}{R_{Load} + r_{L+S}}\right)}{1 + s\left(\frac{(C(R_{Load}r_C + r_{L+S}R_{Load} + r_{L+S}r_C) + L)}{R_{Load} + r_{L+S}}\right) + s^2\left(\frac{LC(R_{Load} + r_C)}{R_{Load} + r_{L+S}}\right)}$$

Therefore,

$$n_0 = K\frac{R_{Load}}{(R_{Load} + r_{L+S})})$$

$$n_1 = K\frac{R_{Load}}{(R_{Load} + r_{L+S})}\,C\,r_c$$

$$d_0 = 1$$

$$d_1 = \frac{r_{L+S}\,C\,(R_{Load} + r_C) + CR_{Load}r_C + L}{(R_{Load} + r_{L+S})}$$

$$d_2 = L\,C\frac{(R_{Load} + r_C)}{(R_{Load} + r_{L+S})}$$

APPENDIX D QUANTILE FUNCTION

Symmetric Triangular Distribution

For a continuous random variable X with probability distribution function $f(x)$ as shown below; mean m, variance σ^2, cumulative distribution function $p(x)$ can be defined as

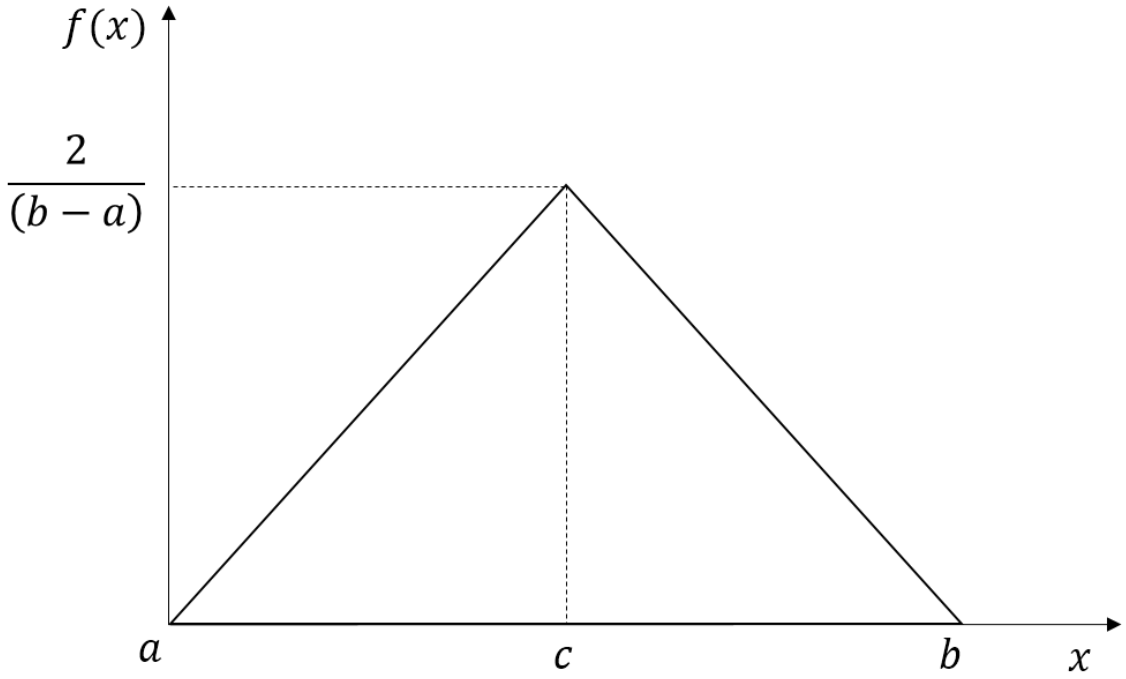

Figure D-1 Probability density function for symmetric Triangular distribution

$$m = \frac{a + b + c}{3}$$

$$\sigma^2 = \frac{a^2 + b^2 + c^2 - ab - bc - ca}{18}$$

$$p(x) = \begin{cases} 0, & x \le a \\ \dfrac{(x-a)^2}{(b-a)(c-a)}, & a < x \le c \\ 1 - \dfrac{(b-x)^2}{(b-a)(b-c)}, & c < x < b \\ 1, & b \le x \end{cases}$$

and, for a symmetrical triangular distribution,

$$c = \frac{a+b}{2}$$

holds true. Substituting, the above, in mean and variance equations; variables a and b can be expressed as

$$a = m - \sqrt{6}\sigma \ , \ b = m + \sqrt{6}\sigma, \ c = m$$

Therefore, cumulative distribution function can be re-defined in terms of mean and standard deviation as

$$p(x) = \begin{cases} 0, & x \leq (m - \sqrt{6}\sigma) \\ \dfrac{\left(x - m + \sqrt{6}\sigma\right)^2}{12\,\sigma^2}, & (m - \sqrt{6}\sigma) < x \leq m \\ 1 - \dfrac{\left(m + \sqrt{6}\sigma - x\right)^2}{12\,\sigma^2}, & m < x < (m + \sqrt{6}\sigma) \\ 1, & (m + \sqrt{6}\sigma) \leq x \end{cases}$$

The quantile function $F^{-1}(p)$, inverse of cumulative distribution function can be calculated

$$F^{-1}(p) = inf\{x : F(x) \geq p\}.$$

iff F is continuous and strictly increasing. From cumulative distribution function,

Case 1: For $(m - \sqrt{6}\sigma) < x \leq m$

$$p = \frac{\left(x - m + \sqrt{6}\sigma\right)^2}{12\,\sigma^2} = \frac{x^2 + m^2 + 6\sigma^2 - 2xm - 2\sqrt{6}m\sigma + 2\sqrt{6}x\sigma}{12\,\sigma^2}$$

Solving for x, from the quadratic equation yields

$$x = \begin{cases} 12\,\sigma^2\left(\dfrac{\sqrt{\dfrac{p}{3}}}{2\sigma} + \dfrac{2m - 2\sqrt{6}\sigma}{24\sigma^2}\right) \\ -12\,\sigma^2\left(\dfrac{\sqrt{\dfrac{p}{3}}}{2\sigma} - \dfrac{2m - 2\sqrt{6}\sigma}{24\sigma^2}\right) \end{cases}$$

The quantile function $F^{-1}(p)$ holds true for single value of x, i.e.

$$F^{-1}(p) = 12\,\sigma^2\left(\frac{\sqrt{\frac{p}{3}}}{2\sigma} + \frac{2m - 2\sqrt{6}\sigma}{24\sigma^2}\right) = m - \sqrt{6}\sigma\left(1 - \sqrt{2p}\right)$$

$$F^{-1}(p) = m - \sqrt{6}\sigma\left(1 - \sqrt{2p}\right) \qquad for\ (m - \sqrt{6}\sigma) < x \leq m$$

Similarly, quantile function for $m < x < (m + \sigma\sqrt{6})$, define

$$F^{-1}(p) = m + \sqrt{6}\sigma\left[1 - \sqrt{2(1-p)}\right] \qquad for\ \left(m - \sqrt{6}\sigma\right) < x \leq m$$

Uniform Distribution

For Uniform distribution, mean m, variance σ^2, cumulative distribution function $p(x)$, is defined as

$$m = \frac{a+b}{2}$$

$$\sigma^2 = \frac{(b-a)^2}{12}$$

$$p(x) = \begin{cases} 0, & x < a \\ \dfrac{(x-a)}{(b-a)}, & x \in [a,b) \\ 1, & x \geq b \end{cases}$$

Solving for a and b yields using above equations,

$$a = m - \sqrt{3}\sigma \text{ and } b = m + \sqrt{3}\sigma$$

defines the quantile function for uniform distribution,

$$F^{-1}(p) = m + \sqrt{3}\sigma(2p-1)$$

Normal Distribution

The inverse of normal cumulative distribution function, available in Microsoft Excel: Statistical formulas, defined by NORM.INV, is used to calculate the normal distribution quantile function.

REFERENCES

[1] Jennions, I. K. (2011) *Integrated Vehicle Health Management: Perspectives on an Emerging Field,* 1st ed., SAE International, Pennsylvania, USA.

[2] Pecht, M. G. (2008) *Prognostics and Health Management of Electronics,* 1st ed., John Wiley & Sons, Inc., Hoboken, NJ.

[3] Babbar, A., Syrmos, V. L., Ortiz, E. M. and Arita, M. M. (2009) "Advanced diagnostics and prognostics for engine health monitoring", *IEEE Aerospace Conference,* 7-14 March, Big Sky, MT, pp. 1-10.

[4] Janvier, A. (2008) "Engine Health Monitoring", *IET Seminar on Aircraft Health Management for New Operational and Enterprise Solutions,* 25-26 June, London, United Kingdom.

[5] Kacprzynski, G. J., Roemer, M. J., Modgil, G., Palladino, A. and Maynard, K. (2002) "Enhancement of physics-of-failure prognostic models with system level features", *Proc. IEEE Aerospace Conf.*, vol. 6, 9-16 March, Big Sky, Montana, pp. 2919-2925.

[6] Xie, J. and Pecht, M. G. (2004) "Application of in-situ health monitoring and prognostic sensors", *Proc. 9th Pan Pacific Microelectron. Symp. Exhibits Conf.* 10-12 February, Oahu, HI, pp. 334-339.

[7] Pecht, M. (2006) "Prognostics and health monitoring of electronics", *International Conference on Electronic Materials and Packaging (EMAP),* 11-14 December, IEEE, pp. 1-10.

[8] Vichare, N. M. and Pecht, M. G. (2006) "Prognostics and health management of electronics", *IEEE Trans. Components and Packaging Technologies,* vol. 29, no. 1, pp. 222-229.

[9] Scanff, E., Feldman, K. L., Ghelam, S., Sandborn, P., Glade, M. and Foucher, B. (2007) "Life cycle cost impact of using prognostic health management (PHM) for helicopter avionics", *Microelectronics Reliability,* vol. 47, no. 12, pp. 1857-1864.

[10] Saxena, A., Roychoudhury, I., Celaya, J., Saha, S., Saha, B. and Goebel, K. (2010) "Requirements specification for prognostics performance - an

overview", *American Institute of Aeronautics and Astronautics Infotech,* 20-22 April, Atlanta, Georgia, pp. 1-16.

[11] Department of Defense (1981) *Definition of Terms for Reliability and Maintainability,* MIL-STD-721C, Department of Defense, Washington, DC.

[12] International Electrotechnical Commission (1990) *Chapter 191 - Dependability and Quality of Service,* IEC 60050, International Electrotechnical Vocabulary, Geneva, Switzerland.

[13] ISO/IEC/IEEE (2010) *Systems and Software Engineering -- Vocabulary,* 24765, Institute of Electrical and Electronics Engineering, NY, US.

[14] Pressman, A. I., Billings, K. and Morey, T. (2009) *Switching Power Supply Design,* 3rd ed., McGraw-Hill Professional, NY, USA.

[15] Steigerwald, R. L., Ludwig, G. W. and Kollman, R. (1995) "Investigation of power distribution architectures for distributed avionics loads", *Proc. IEEE 26th Annual Power Electronics Specialists Conf.*, Vol. 1, 18-22 June, Atlanta, GA, pp. 231-237.

[16] White, R. V. (2003) "Emerging on-board power architectures", *Proc. IEEE 18th Annual Applied Power Electronics Conf. and Exposition,* Vol. 2, 9-13 February, Miami Beach, FL, USA, pp. 799-804.

[17] Erickson, R. and Maksimović, D. (2004) *Fundamentals of Power Electronics,* 2nd ed., Kluwer, Norwell, MA.

[18] Balocco, D., Derory, E., Ploquin, D. and Zardini, C. (1996) "A new single-stage isolated power factor preregulator for avionics distributed power supply systems", *Proc. IEEE 27th Annual Power Electronics Specialists Conf.*, Vol. 2, 23-27 June, Baveno, pp. 1717-1723.

[19] ITRS (2007) *International Technology Roadmap for Semiconductors Executive Summary,* Overall Roadmap Technology Characteristics, ITRS.

[20] ITRS (2012) *International Technology Roadmap for Semiconductors: Executive Summary,* Power Supply and Power Dissipation, ITRS.

[21] Thottuvelil, V. J. (2013) *Optimizing POL Transient Response with the Tunable Loop Feature,* TunableLoop, General Electric Corporation.

[22] Hicks, J., Bergstrom, D., Hattendorf, M., Jopling, J., Maiz, J., Pae, S., Prasad, C. and Wiedemer, J. (2008) "45nm transistor reliability", *Intel Technology Journal,* vol. 12, no. 2, pp. 131-144.

[23] Constantinescu, C. (2008) "Intermittent faults and effects on reliability of integrated circuits", *Proc. IEEE Annual Reliability and Maintainability Symp.* 28-31 January, Las Vegas, NV, pp. 370-374.

[24] Gregory, J. C., Hafner, M. A. and Vian, J. (2004) "Electronic Systems Health Monitoring using Electromagnetic Emissions", *SAE Technical Paper No. 2004-01-3161*.

[25] Orsagh, R., Brown, D., Roemer, M., Dabnev, T. and Hess, A. (2005) "Prognostic health management for avionics system power supplies", *Proc. IEEE Aerosp. Conf.,* 5-12 March, Big Sky, MT, pp. 3585-3591.

[26] Saha, B., Celaya, J. R., Wysocki, P. F. and Goebel, K. (2009) "Towards prognostics for electronics components", *Proc. IEEE Aerospace Conf.*, 7-14 March, Big Sky, MT, pp. 1-7.

[27] Kulkarni, C., Biswas, G., Koutsoukos, X., Celaya, J. and Goebel, K. (2010) "Integrated diagnostic/prognostic experimental setup for capacitor degradation and health monitoring", *Proc. IEEE AUTOTESTCON,* 13-16 September, Orlando, FL, pp. 1-7.

[28] Yang, S., Xiang, D., Bryant, A., Mawby, P., Ran, L. and Tavner, P. (2010) "Condition monitoring for device reliability in power electronic converters - a review", *IEEE Trans. Power Electron.,* vol. 25, no. 11, pp. 2734 - 2752.

[29] Goodman, D., Vermeire, B., Spuhler, P. and Venkatramani, H. (2005) "Practical application of PHM/Prognostics to COTS power converters", *Proc. IEEE Aerospace Conf.*, 5-12 March, Big Sky, MT, pp. 3573-3578.

[30] Bagul, Y. G., Zeid, I. and Kamarthi, S. V. (2008) "A framework for prognostics and health management of electronic systems", *Proc. IEEE Aerospace Conf.*, 1-8 March, Big Sky, MT, pp. 1 - 9.

[31] Huang, Y., Ross, M., Amor-Segan, M., Dhadyalla, G., Jones, R. P., Bennett, P., Mouzakitis, A. and Kieloch, J. (2010) "Development of an automated testing system for vehicle infotainment system", *International Journal of Advanced Manufacturing Technology,* vol. 51, no. 1-4, pp. 233-246.

[32] EPRI (2005) *Evaluating the Effects of Aging on Electronic Instrument and Control Circuit Boards and Components in Nuclear Power Plants,* 1011709, U.S. Department of Energy, Palo Alto, CA, and U.S. Department of Energy.

[33] Mayper, V. and Goodman, D. M. (1967) "Problems and pitfalls in automatic test computer programming", *Automation in Test Equipment, vol. III.* pp. 41-85.

[34] Bardell, P., McAnney, W. and Savir, J. (1987) *Built-In Test for VLSI: Pseudorandom Techniques,* 1st ed., Wiley-Interscience, New York.

[35] Veillette, B. R. and Roberts, G. W. (1995) "A built-in self-test strategy for wireless communication systems", *Proc. IEEE International Test Conference,* 21-25 October, Washington, DC, pp. 930-939.

[36] Stroud, C. E. (2002) *A Designer's Guide to Built-In Self-Test,* 1st ed., Springer US, USA.

[37] Gao, R. X. and Suryavanshi, A. P. (2001) "BIT for intelligent system design and condition monitoring", *Proc. 18th IEEE Instrumentation and Measurement Technology Conf.*, Vol. 3, 21-23 May, Budapest, pp. 1519-1524.

[38] Kulkarni, C. (2013) *A Physics-Based Degradation Modeling Framework for Diagnostic and Prognostic Studies in Electrolytic Capacitors* (Doctor of Philosophy thesis), Graduate School of Vanderbilt University, Nashville, Tennessee.

[39] Butler, W. (2012) *A Primer on Architectural Fault Tolerance,* NASA/TM-2008-215108, NASA, Langley Research Center, Hampton, Virginia.

[40] Konemann, B., Zwiehoff, G. and Mucha, J. (2002) "Built-in test for complex digital integrated circuits", *IEEE J. Solid-State Circuits,* vol. 15, no. 3, pp. 315-319.

[41] Kim, I., Zorian, Y., Komoriya, G., Pham, H., Higgins, F. P. and Lewandowski, J. L. (1998) "Built in self repair for embedded high density SRAM", *Proc. IEEE International Test Conf.*, 18-23 October, Washington, DC, pp. 1112-1119.

[42] Wibbenmeyer, J. and Chen, C. -. H. (2007) "Built-in self-Test for low-voltage high-speed analog-to-digital converters", *IEEE Trans. Instrumentation and Measurement,* vol. 56, no. 6, pp. 2748-2756.

[43] Rosenthal, D. and Wadell, B. C. (2002) "Predicting and eliminating built-in test false alarms", *IEEE Trans. Reliability,* vol. 39, no. 4, pp. 500-505.

[44] Pecht, M. G., Dube, M., Natishan, M., Williams, R., Banner, J. and Knowles, I. (2001) "Evaluation of built-in test", *IEEE Trans. Aerospace and Electron. Systems,* vol. 37, no. 1, pp. 266-271.

[45] Goodman, D., Vermeire, B., Ralston-Good, J. and Graves, R. (2006) "A board-level prognostic monitor for MOSFET TDDB", *Proc. IEEE Aerospace Conf.*, 4-11 March, Big Sky, MT, pp. 1-6.

[46] Kim, K. K., Wang, W. and Choi, K. (2010) "On-chip aging sensor circuits for reliable nanometer MOSFET digital circuits", *IEEE Trans. Circuits and Systems II: Express Briefs,* vol. 57, no. 10, pp. 798-802.

[47] Nan, H. and Choi, K. (2013) "TDDB monitoring and compensation circuit design for deeply scaled CMOS technology", *IEEE Trans. Device and Materials Reliability,* vol. 13, no. 1, pp. 18-25.

[48] Pecht, M. G. and Dasgupta, A. (2002) "Physics-of-failure: an approach to reliable product development", *Proc. IEEE Final Report International Integrated Reliability Workshop,* 22-25 October, Lake Tahoe, CA, USA, pp. 1-4.

[49] Vichare, N., Rodgers, P., Eveloy, V. and Pecht, M. G. (2007) "Monitoring environment and usage of electronic products for health assessment and product design", *Quality Technology & Quantitative Management,* vol. 4, no. 2, pp. 235-250.

[50] Mishra, S., Ganesan, S., Pecht, M. G. and Xie, J. (2004) "Life consumption monitoring for electronics prognostics", *Proc. IEEE Aerospace Conf.*, Vol. 5, 6-13 March, Big Sky, MT, pp. 3455-3467.

[51] Pecht, M. G. (1995) *Product Reliability, Maintainability, and Supportability Handbook,* 2nd ed., CRC Press, USA.

[52] Gu, J. and Pecht, M. G. (2008) "Prognostics and health management using physics-of-failure", *Proc. Annu. Rel. and Maintainability Symp.*, 28-31 January, Las Vegas, NV, pp. 481-487.

[53] S. Kumar, E. Dolev and M. Pecht (2010) "Parameter selection for health monitoring of electronic products", *Microelectronics Reliability,* vol. 50, no. 2, pp. 161-168.

[54] Li, F., Pecht, M., Lau, D. and Niu, G. (2010) "The research and application of the method of life consumption monitoring based on physics of failure", *11th International Conference on Electronic Packaging Technology & High Density Packaging (ICEPT-HDP),* pp. 1027-1033-.

[55] Goodman, D., Hofmeister, J. and Judkins, J. (2007) "Electronic prognostics for switched mode power supplies", *Microelectronics Reliability: Electronic System Prognostics and Health Management,* vol. 47, no. 12, pp. 1902-1906.

[56] Kulkarni, C., Biswas, G. and Koutsoukos, X. (2009) "A prognosis case study for electrolytic capacitor degradation in DC-DC converters", *Proc. Prognostics and Health Management Society Conf.,* 27 September - 1 October, San Diego, CA, pp. 1-10.

[57] Nasser, L. and Curtin, M. (2006) "Electronics reliability prognosis through material modeling and simulation", *Proc. IEEE Aerospace Conf.*, 4-11 March, Big Sky, MT, pp. 1-7.

[58] Saha, B. and Goebel, K. (2008) "Uncertainty management for diagnostics and prognostics of batteries using Bayesian techniques", *Proc. IEEE Aerospace Conf.*, 1-8 March, Big Sky, MT, pp. 1-8.

[59] Cheng, S. and Pecht, M. G. (2007) "Multivariate state estimation technique for remaining useful life prediction of electronic products", *AAAI Fall Symp. on Artificial Intelligence for Prognostics,* 9-11 November, Arlington, Virginia, pp. 26-32.

[60] Pecht, M.G. and Chen, S. (2010) *Prognostics and Health Management Method for Aging Systems*, Patent No. 8,423,484, US.

[61] Jaai, R., Pecht, M. G. and Cook, J. (2009) "Detecting failure precursors in BGA solder joints", *Proc. IEEE Annual Reliability and Maintainability Symp.*, 26-29 June, Fort Worth, TX, pp. 100-105.

[62] Mathew, S., Das, D., Osterman, M., Pecht, M. G. and Ferebee, R. (2006) "Prognostics assessment of aluminium support structure on a printed circuit board", *J. Electron. Packag.,* vol. 128, no. 4, pp. 339-345.

[63] Orsagh, R., Brown, D., Kalgren, P., Byington, C. S., Hess, A. and Dabney, T. (2006) "Prognostic health management for avionic systems", *Proc. IEEE Aerospace Conf.*, 4-11 March, Big Sky, MT, pp. 1-7.

[64] Morroni, J., Dolgov, A., Shirazi, M., Zane, R. and Maksimovic, D. (2007) "Online health monitoring in digitally controlled power converters", *Proc. IEEE Power Electron. Specialists Conf.*, 17-21 June, Orlando, FL, pp. 112-118.

[65] Miao, B., Zane, R. and Maksimovic, D. (2005) "System identification of power converters with digital control through cross-correlation methods", *IEEE Trans. Power Electron.,* vol. 20, no. 5, pp. 1093-1099.

[66] Roinila, T., Helin, T., Vilkko, M., Suntio, T. and Koivisto, H. (2009) "Circular correlation based identification of switching power converter with uncertainty analysis using fuzzy density approach", *Simulation Modelling Practice and Theory,* vol. 17, no. 6, pp. 1043-1058.

[67] Shirazi, M., Morroni, J., Dolgov, A. and Maksimovic, D. (2008) "Integration of frequency response measurement capabilities in digital controllers for DC–DC converters", *IEEE Trans. Power Electron.,* vol. 23, no. 5, pp. 2524-2535.

[68] Gu, J., Barker, D. and Pecht, M. G. (2007) "Uncertainty assessment of prognostics of electronics subject to random vibration", *Proc. AAAI Fall Symp. Artificial Intelligence for Prognostics,* 9-11 November, Arlington, VA, USA, pp. 50-57.

[69] Zhang, H., Kang, R., Luo, M. and Pecht, M. G. (2009) "Precursor parameter identification for power supply prognostics and health management", *Proc. IEEE 8th International Conf. Reliability, Maintainability and Safety,* 20-24 July, Chengdu, pp. 883 - 887.

[70] Vichare, N.M. and Pecht, M.G. (2010) *Method to Extract Parameters from In-Situ Monitored Signals for Prognostics*, US Patent No. 8521443 ed., San Francisco, CA.

[71] Kornecki, A. J. and Zalewski, J. (2010) "Hardware certification for real-time safety-critical systems: state of the art", *Annual Reviews in Control,* vol. 34, no. 1, pp. 163-174.

[72] Sun, B., Zeng, S., Kang, R. and Pecht, M. G. (2012) "Benefits and challenges of system prognostics", *IEEE Trans. Reliability,* vol. 61, no. 2, pp. 323-335.

[73] Feldman, K., Jazouli, T. and Sandborn, P. A. (2009) "A methodology for determining the return on investment associated with prognostics and health management", *IEEE Trans. Reliability,* vol. 58, no. 2, pp. 305-316.

[74] Bin Zhang, Liang Tang, DeCastro, J. and Goebel, K. (2010) "A verification methodology for prognostic algorithms", *Proc. IEEE AUTOTESTCON,* 13-16 September, Orlando, FL, pp. 1--8.

[75] Cheng, S., Azarian, M. H. and Pecht, M. G. (2010) "Sensor systems for prognostics and health management", *Sensors,* vol. 10, no. 6, pp. 5774-5797.

[76] Zhang, G. (2005) *Optimum Sensor Localization/Selection in a Diagnostic/Prognostic Architecture* (Doctor of Philosophy thesis), Georgia Institute of Technology, Atlanta, GA, USA.

[77] Ljung, L. (1999) *System identification: Theory for the User,* 2nd ed., Prentice-Hall, NJ.

[78] Algreer, M., Armstrong, M. and Giaouris, D. (2012) "Active online system identification of switch mode DC–DC power converter based on efficient recursive DCD-IIR adaptive filter", *IEEE Trans. Power Electron.,* vol. 27, no. 11, pp. 4425-4435.

[79] Patella, B., Prodic, A., Zirger, A. and Maksimovic, D. (2003) "High-frequency digital PWM controller IC for DC-DC converters", *IEEE Trans. Power Electron.,* vol. 18, no. 1, pp. 438-446.

[80] Pintelon, R. and Schoukens, J. (2012) *System Identification: A Frequency Domain Approach,* 2nd ed., John Wiley & Sons, Inc., New Jersey.

[81] Schoukens, J., Pintelon, R., van der Ouderaa, E. and Renneboog, J. (1988) "Survey of excitation signals for FFT based signal analyzers", *IEEE Trans. Instrumentation and Measurement,* vol. 37, no. 3, pp. 342-352.

[82] Gonzalez-Espi, F., Figueres, E., Garcera, G., Gonzalez-Medina, R. and Pascual, M. (2010) "Measurement of the loop gain frequency response of digitally controlled power converters", *IEEE Trans. Industrial Electron.,* vol. 57, no. 8, pp. 2785-2796.

[83] Roinila, T., Vilkko, M. and Suntio, T. (2009) "Fast frequency response measurement of switched-mode Converters in the presence of nonlinear distortions", *Proc. IEEE Energy Conversion Congress and Exposition,* 20-24 September, San Jose, CA, pp. 3014-3020.

[84] Miao, B., Zane, R. and Maksimovic, D. (2004) "A modified cross-correlation method for system identification of power converters with digital control", *Proc. Power Electron. Spec. Conf.*, Vol. 5, 20-25 June, Aachen, Germany, pp. 3728-3733.

[85] Barkley, A. and Santi, E. (2008) "Improved online identification of switching converters using digital network analyzer techniques", *Proc. Power Electron. Spec. Conf.*, 15-19 June, Rhodes, pp. 891-896.

[86] Barkley, A. and Santi, E. (2009) "Online monitoring of network impedances using digital network analyzer techniques", *Proc. 24th Annual IEEE Applied Power Electronics Conf. and Exposition,* 15-19 February, Washington, DC, pp. 440-446.

[87] Barkley, A. and Santi, E. (2009) "Improved online identification of a dc–dc converter and its control loop gain using cross-correlation methods", *IEEE Trans. on Power Electron.,* vol. 24, no. 8, pp. 2021-2031.

[88] Roinila, T., Vilkko, M. and Suntio, T. (2009) "Fast Loop gain measurement of a switched-mode converter using a binary signal with a specified fourier amplitude spectrum", *IEEE Trans. Power Electron.,* vol. 24, no. 12, pp. 2746-2755.

[89] Roinila, T., Vilkko, M. and Suntio, T. (2010) "Frequency-response measurement of switched-mode power supplies in the presence of nonlinear distortions", *IEEE Trans. Power Electron.,* vol. 25, no. 8, pp. 2179-2187.

[90] Schoukens, J., Pintelon, R. and Van Hamme, H. (1994) "Identification of linear dynamic systems using piecewise constant excitations: use, misuse and alternatives", *Automatica,* vol. 30, no. 7, pp. 1153-1169.

[91] Huynh, P. and Cho, B. H. (1995) "Empirical small-signal modeling of switching converters using Pspice", *Proc. IEEE Power Electron. Spec. Conf.*, Vol. 2, 18-22 June, Atlanta, GA, pp. 809-815.

[92] Maksimovic, D. (2000) "Computer-aided small-signal analysis based on impulse response of DC/DC switching power converters", *IEEE Trans. Power Electron.,* vol. 15, no. 6, pp. 1183-1191.

[93] Pitel, G. E. and Krein, P. T. (2008) "Real-time system identification for load monitoring and transient handling of DC-DC supplies", *Proc. IEEE Power Electron. Spec. Conf.*, 15-19 June, Rhodes, pp. 3807-3813.

[94] MacCleery, B., Trescases, O., Mujagic, M., Bohls, D. M., Stepanov, O. and Fick, G. (2012) "A new platform and methodology for system-level design of next-generation FPGA-based digital SMPS", *Proc. IEEE Energy Conversion Congress and Exposition,* 15-20 September, Raleigh, NC, pp. 1599-1606.

[95] Texas Instruments (2014) *TMS320F2806x Piccolo™ MCUs Datasheet,* SPRS698E, TI, Dallas, Texas.

[96] Texas Instruments (2014) *Code Composer Studio (CCS) Integrated Development Environment (IDE)*, available at: http://www.ti.com/tool/CCSTUDIO (accessed 2011,06/06).

[97] Texas Instruments (2014) *TMS320x2806x Piccolo Technical Reference Manual,* SPRUH18E, TI.

[98] Peterchev, A. and Sanders, S. (2001) "Quantization resolution and limit cycling in digitally controlled PWM converters", *Proc. 32nd IEEE Annu. Power Electron. Specialists Conf.* Vol. 2, 17-21 June, Vancouver, BC, pp. 465-471.

[99] Vasca, F. and Iannelli, I. (2012) *Dynamic and Control of Switched Electronic Systems: Advanced Perspectives for Modeling, Simulation and Control of Power Converters,* 1st ed., Springer Science & Business Media, London.